J-integral Computations for Linear Elastic Fracture Mechanics in *h,p,k* Mathematical and Computational Framework

by

C2007
Daniel Nunez

B.S. (Aerospace Engineering), The University of Kansas, Lawrence, KS, 2003

A thesis submitted to the Department of Aerospace Engineering and the faculty of the graduate school of the University of Kansas in partial fulfillment of the requirements for the degree of Master of Science

Dr. Karan Surana ______________________
Thesis Advisor

Dr. Mark Ewing ______________________
Committee-Chairman

Dr. Ray Taghavi ______________________
Committee Member

Dr. Richard Hale ______________________
Committee Member

Date defended: ______________________

Acknowledgments

I would like to thank Dr. Surana (Deane E. Ackers Distinguished Professor of Mechanical Engineering) for his patience, supervision and encouragement throughout my studies here at KU. His guidance and advice have been invaluable throughout the course of this work. It has been a tremendous learning experience and I am grateful for it. I would also like to thank the other members of my thesis committee, Dr. Mark Ewing, Dr. Ray Taghavi and Dr. Richard Hale for their support and their time to serve on my committee. I also extend my thanks to the department of Mechanical Engineering for awarding me the Strobel Scholarship.

The financial support provided by DEPSCoR/AFOSR and AFOSR through grant numbers F49620-03-01-0298, F49620-03-1-0201 to the University of Kansas, department of Mechanical Engineering and Texas A & M University, College Station, department of Mechanical Engineering is gratefully acknowledged. The seed grand provided by ARO through grant number FED46680 to the University of Kansas, department of Mechanical Engineering is also acknowledged. The financial support from the Department of Mechanical Engineering of the University of Kansas to support this work is much appreciated. The computational facilities provided by the Computational Mechanics Laboratory (CML) of the Mechanical Engineering department and the software development infrastructure in CML have been instrumental in conducting the numerical studies.

Finally, I would like to thanks my parents, Dr. Candido Nunez Leon and Arch. Felicita Irrazabal de Nunez, for their constant support and encouragement

Abstract

This thesis presents an infrastructure for computations of the J-integral for mode I linear elastic fracture mechanics in *h,p,k* mathematical and computational framework using finite element formulations based on the Galerkin method with weak form and the least squares process. Since the differential operators in this case are self-adjoint, both the Galerkin method with weak form and the least square processes yield unconditionally stable computational processes. The use of *h,p,k* frameworks permits higher order global differentiability approximations in the finite element processes which are necessitated by physics, calculus of continuous and differentiable functions and higher order global differentiability features of the theoretical solutions. The significant aspect of this research is that with the proposed methodology very accurate J-integral computations are possible for all paths including those in very close proximity of the crack without use of special crack tip or quarter point elements at the crack tip. A center crack panel under isotropic homogeneous plane strain linear elastic behavior, subjected to uniaxial tension (mode I) is used as model problem for all numerical studies. The investigations presented in this thesis are summarized here: (i) J-integral expression is derived and it is shown that its path independence requires the governing differential equations (GDEs) to be satisfied in the numerical process used for its computations (ii) It has been shown that the J-integral path Γ must be continuous and differentiable (iii) The integrand in the J-integral must be continuous along the path as well as normal to the path (iv) Influence of the higher order global differentiability approximations on the accuracy of the J-integral is demonstrated (v) Stress intensity correction factors are computed and compared with published data.

The work presented here is a straight-forward finite element methodology in *h,p,k* framework is presented in which all mathematical requirements for J-integral computations are satisfied in the computational process and as a result very accurate computations of J-integral are possible for any path surrounding the crack tip without using any special treatments. Both the Galerkin method with weak form and the least square processes perform equally well.

Contents

List of Figures

List of Tables

Nomenclature

p	= Degree of Local Approximation
h	= Discretization Parameter
k-1	= Global Differentiability of Local Approximation
Γ	= Contour Along which the J-integral is Evaluated
$d\Gamma$	= Infinitesimal Arc Length Segment of Γ
Γ^*	= Closed Path
A^*	= Area Enclosed by Γ^*
a	= Half the Crack Length
b	= Half the Width of the Panel
h	= Half the Height of the Panel
E	= Young's Modulus
ν	= Poisson's Ratio
K_I	= Stress Intensity Factor for an Infinite Medium
K_I^f	= Stress Intensity Factor for a Finite Medium
C_f	= Correction Factor Applied to K_I to Account for Finite Sized Medium
J^f	= J-integral for a Finite Medium
J	= J-integral for an Infinite Medium
$[J]$	= Jacobian Matrix
W	= Strain Energy Density Function

A_J = Integration of Equations of Equilibrium over a Closed Area A^*

$\{\bar{x}\}$ = Deformed Coordinates

$\{x\}$ = Undeformed Coordinates

x = x-coordinate

y = y-coordinate

$\{\vec{n}\}$ = Normal Unit Vector

T = Traction Vector

u = Displacement Vector of a Material Particle

v = Velocity Vector of a Material Particle

$\vec{F}^b$ = Body Force per Unit Mass Vector

ρ = Mass Density in the Undeformed Configuration

$\bar{\rho}$ = Mass Density in the Deformed Configuration

c_{ijkl} = Fourth Order Tensor Containing Material Behavior

$[C]$ = Material Matrix

D_{ik} = Components of $[D]=[C]^{-1}$

σ = Applied Uniform Tensile Stress

σ_{ij} = Cauchy Stresses

ε_{ij} = Cauchy Strains

e = Element

M = Number of Elements

Ω	= Domain
Γ	= Closed Boundary of Ω
$\bar{\Omega}$	= Union of Ω and Γ
$\bar{\Omega}^T$	= Discretization of $\bar{\Omega}$
Γ^e	= Closed Boundary of the Element
$\bar{\Omega}^e$	= Union of Ω_e and Γ_e
Φ	= Vector of Dependent Variables
Φ_h	= Global Approximation of Φ over $\bar{\Omega}^T$
Φ_h^e	= Local Approximation of Φ over $\bar{\Omega}^e$
u	= Displacement in the x-direction
v	= Displacement in the y-direction
σ_{xx}	= Normal Stress in the x-direction
σ_{yy}	= Normal Stress in the y-direction
σ_{xy}	= Shear Stress
ε_{xx}	= Normal Strain in the x-direction
ε_{yy}	= Normal Strain in the y-direction
γ_{xy}	= Engineering Shear Strain $= 2\varepsilon_{xy}$
u_h	= Global Approximation of u over $\bar{\Omega}^T$
v_h	= Global Approximation of v over $\bar{\Omega}^T$
$(\sigma_{xx})_h$	= Global Approximation of σ_{xx} over $\bar{\Omega}^T$

$(\sigma_{yy})_h$ = Global Approximation of σ_{yy} over $\bar{\Omega}^T$

$(\sigma_{xy})_h$ =Global Approximation of σ_{xy} over $\bar{\Omega}^T$

u_h^e = Local Approximation of u over $\bar{\Omega}^e$

v_h^e = Local Approximation of v over $\bar{\Omega}^e$

$(\sigma_{xx})_h^e$ = Local Approximation of σ_{xx} over $\bar{\Omega}^e$

$(\sigma_{yy})_h^e$ = Local Approximation of σ_{yy} over $\bar{\Omega}^e$

$(\sigma_{xy})_h^e$ = Local Approximation of σ_{xy} over $\bar{\Omega}^e$

ne = Number of Equations

w_1 = Test Function

w_2 = Test Function

$B_1(\ ;\ )$ = Self-adjoint Functional Corresponding to Φ_h and w_1

$B_2(\ ;\ )$ = Self-adjoint Functional Corresponding to Φ_h and w_2

$I(\Phi_h)$ = Error Functional in Least Squares Finite Element Formulation

E_i^e = Element Error (Residual) Equation for an Element e

V_h = Approximation Space

U = Total Energy of the System

U_0 = Elastic Energy of the Loaded Uncracked Plate

U_a = Change in Elastic Energy Caused by Introducing a Crack

U_γ = Change in Elastic Surface Energy Caused by Crack Surface Formation

U_p = Potential Energy

F = The Work Performed by External Forces

R = Crack Resistance per Unit Thickness

G = Elastic Energy Release Rate per Unit Thickness

G_C = Critical Energy Release Rate per Unit Thickness

q_1 = Displacement Field due to a Virtual Crack Extension

Dofs = Degrees of Freedom

LEFM = Linear Elastic Fracture Mechanic

EPFM = Elastic Plastic Fracture Mechanics

BVP = Boundary Value Problems

CTOD = Crack Tip Opening Displacement

VC = Variationally Consistent

VIC = Variationally Inconsistent

GAL/WF = Galerkin Method with Weak Form

LSP = Least Square Processes

PDEs = Partial Differential Equations

GDEs = Governing Differential Equations

Chapter 1
EQUATION CHAPTER 1 SECTION 1
Introduction and Scope of Work

1.1 Introduction

The experimental fracture strength (load at which failure occurs) of flawed solid materials is 10 to 1000 times below the fracture strength of unflawed ones, due to the fact that tiny internal and external surface cracks, originated during production or service, create higher stresses near these cracks. This observation lead English aeronautical engineer A. A. Griffith to the conception of fracture mechanics. In the 1920s, he showed that the total energy of the system U is equal to the sum of: the elastic energy of the loaded uncracked plate (a constant) U_0; the change in the elastic energy caused by introducing the crack in the plate U_a; the change in the elastic surface energy caused by the formation of the crack surfaces U_γ; minus the work performed by external forces F [1]. He formulated the concept that crack growth instability will occur as soon as U no longer increases with increasing crack length a. Due to the fact that U_0 is a constant, crack growth instability will occur as soon as the change of F minus U_a due to crack propagation (crack driving force) is greater than the change of U_γ due to crack propagation (crack resistance to growth). This crack driving force is referred to as elastic energy release rate per unit thickness G, and the crack resistance to growth as critical energy release rate per unit thickness G_C. Therefore, crack growth instability will occur as soon as G is greater than G_C. Griffith's theory was developed for brittle materials under elastic behavior. Griffith finally showed that for a center crack in a plate with infinite width, G is equal to $\pi\sigma^2 a / E$ for isotropic, homogeneous, plane stress linear elastic behavior and $(1-\nu^2)\pi\sigma^2 a / E$ for isotropic, homogeneous, plane strain linear elastic behavior, where σ, E and ν are the applied uniform tensile stress, Young's Modulus, and Poisson's ratio respectively [1-3].

In the mid-1950s, Irwin showed that the local stress field near the crack tip of an isotropic linear elastic material can be expressed as a product of $1/\sqrt{r}$ and a function $f_{ij}(\theta)$ with a scaling factor K, which he called stress intensity factor [1]. When $r \to 0$, τ_{xy} equals zero and singularity is introduced in σ_{xx} and σ_{yy}. Irwin further showed that the energy approach developed by Griffith is equivalent to the stress intensity approach, in the sense that crack growth instability will occur as soon as K is greater than the critical stress intensity factor K_C. In addition, he distinguished three different modes that describe different crack surface displacement and applied loading (mode I, II and III), where each of these three modes has a specific stress intensity factor represented as K_I, K_{II} and K_{III} respectively [1-3]. He finally connected Griffith energy approach and the stress intensity factor approach deriving an expression relating G and the stress intensity factors K_I, K_{II} and K_{III} [3]. This direct relation between G and K means that under linear elastic fracture mechanic conditions (LEFM), the achievement of a critical stress intensity factor, K_C, is exactly equivalent the achievement of critical energy release rate per unit thickness G_C. For the specific case of Mode I (the most common load type in engineering design), the expression is reduced to $G = K_I^{\,2} / E$ for isotropic, homogeneous plane stress linear elastic behavior and $G = \left(1-\nu^2\right) K_I^{\,2} / E$ for isotropic, homogeneous plane strain linear elastic behavior [1-3].

The value of the stress intensity factor K is a function of the applied stress, the size and the position of the crack as well as the geometry of the specimen in which cracks are detected. In the last few decades, many closed-form solutions of the stress intensity factor K for simple configurations have been derived, while the critical stress intensity factor K_C is obtained experimentally [1-2]. Also because K_C is unique for a particular material, engineers can use this variable for selecting appropriate materials for a range of different applications. This critical information helps engineers to optimize the design and ensure the safety on the operations and to prevent or minimize possible accidents. This is extremely important for the design of aircraft components, where there are a lot of rivet holes and small cracks.

Based on Irwin's theory, the stresses σ_{xx} and σ_{yy} are infinity at the crack tip, but in reality, since materials plastically deform as the yield stress is reached, a plastic zone will form near the crack tip, which limits the stresses to finite values. Irwin showed that LEFM concepts could be slightly altered in order to cope with limited plasticity in the crack tip region by treating the crack length longer than its physical size [1-3]. Nevertheless, there are many important classes of materials that are too ductile to describe their behavior by LEFM: the crack tip plastic zone is simply too large. Then the problem has to be treated elasto-plastically by considering elastic plastic fracture mechanics (EPFM) [1].

In 1968, Rice introduced a line integral called the J-integral [31, 38], which has the same value for all integration paths surrounding the tip of a notch in two-dimensional deformation fields of materials exhibiting linear or nonlinear elastic behavior (reversible process). If G is the strain energy release rate per unit thickness, then $J = G$ by definition, thus the J-integral concept is compatible with linear elastic fracture mechanics. The path independency of the J-integral expression allows calculation along a contour remote from the crack tip. This is what makes the J-integral concept so attractive. Further we note that since J equals G, we may write $J = G = K_I^{\,2} / E$ for isotropic, homogeneous plane stress and $J = G = \left(1-\nu^2\right) K_I^{\,2} / E$ for isotropic, homogeneous plane strain linear elastic behavior [1-3]. Obtaining solutions for the J-integral in actual specimens turns out to be difficult and it is generally necessary to use computational methods such as finite element techniques. Using finite element processes, the J-integral concept can be used in LEFM to calculate stress intensity factors in structures that do not posses a closed form solution for K, and compare them with critical stress intensity factors K_C. The primary interest in discussing nonlinear materials lies with elastic-plastic behavior, particularly in relation to elasto-plastic fracture mechanics (EPFM). Therefore, the J-integral concept can also be used in EPFM to calculate J values and compare them with critical J_C values determined empirically [1-2]. However, the extension of non-linear elastic to elasto-plastic behavior is beyond the scope of this work.

Finite element computations of J-integral values for linear elastic fracture mechanics involve numerically simulating the solutions of boundary value problems (BVP) that contain a singularity of the solution derivatives at some point(s) in the domain of definition of the BVP. Such point(s) are referred to as singular points and hence the name singular BVP. The theoretical solutions of such boundary value problems are not analytic at the singular points but analytic everywhere else. In attempting to solve such singular BVP numerically, many difficulties arise: in the currently published literature [5-7,12,13,15]:

(a) A major constraint is the use of C^0 low degree *p*-version local approximation such as C^0 linear displacement local approximation finite elements due to the fact that use of C^0 higher degree *p*-version local approximations resulted in solutions with wild oscillations in the vicinity of the crack tip. Furthermore, these oscillations increased with increasing *p*-levels and mesh refinements [33, 39, 40]. In view of this, the use of C^0 linear displacement local approximation finite elements became popular since solutions without oscillations were possible with excessive mesh refinement. This improvement is an illusion due to the fact that it is the gradients of the solution that determine the accuracy of the J-integral values, and when using C^0 linear displacement local approximation, the solution gradients become highly diffused [33, 37].

(b) In a different approach, attempts are made to incorporate the singularity of the solution in the computational process [18-23, 25-29, 36]. Use of quarter point singular elements and special basis functions incorporating the strength of the singularity are among such approaches. It is important to remark that these approaches are not general because their use requires a priori knowledge of the strength of singularity. In such approaches, correct integration of the coefficients of the element matrices is not possible and hence, accuracy of the solution becomes questionable.

(c) A main limitation of currently used finite element methodologies in J-integral computations is the lack of required global differentiability of local approximations, which arises from employing *h,p* mathematical framework with C^0 local approximations when designing the finite element and computational processes.

(d) Non-differentiable paths are used when computing J-integral values, which is generally a consequence of using quadrilateral or triangular elements with linear sides that cannot be avoided if the local approximation for the displacement field is linear.

(e) Another serious problem is the discontinuity of the integrand in the J-integral expression along the path as well as normal to the path due to the use of C^0 local approximation for displacements. Because of these, special treatments and modifications to Rice's original J-integral expression are being employed in the currently used computations to circumvent or alleviate the errors introduced in the J-integral computations [13, 16, 17, 34, 37].

1.2 Scope of Work

In this work, linear elastic fracture mechanics with isotropic material behavior is used as a model problem to address all of the issues discussed above. It is shown that quarter point singular elements and special basis functions incorporating the strength of the singularity are unnecessary, and that *h,p,k* framework permits higher order global differentiability local approximations that are necessitated by the higher order global differentiability characteristics of the theoretical solution, and that J-integral can be maintained in Riemann sense as opposed to Lebesgue. This results in significantly accurate computations of the integrals. The J-integral paths are always differentiable which is essential for the J-integral computations to be valid along the chosen path. It is shown that in *h,p,k* framework, by employing differentiable J-integral paths and maintaining integrals in the Riemann sense, the numerically computed J-integral values remain virtually path independent regardless of the proximity of the path to the crack tip and match extremely well with the theoretical values.

The research presented in this thesis demonstrates the need for proper choice of approximation spaces. The *h,p,k* framework is essential in this regard. Higher order and degree global differentiability approximations result in improved accuracy and hence are meritorious in the J-integral computations. Maintaining J-integrals in Riemann sense along differentiable path is essential for correct and accurate computations of J-integrals. The approach presented here in *h,p,k* framework is a straight forward finite element computational methodology that is free of any and all special treatments. The finite element formulation based on the Galerkin method with weak form and the least square processes are considered in the computations of J-integrals. Stress intensity factors and correction factors obtained from the numerical studies presented here are compared with those obtained using analytical expressions available in literature [46].

Chapter 2

EQUATION CHAPTER 2 SECTION 1

Theoretical Aspects of the J-integral for Two Dimensional Elasticity and Presently Used Methodologies

2.1 Theoretical derivations

The original derivation of the J-integral was presented by Rice in 1968 [38]. In this derivation, Rice considered the variation of the potential energy inside a fixed arbitrary region containing the crack tip [38]. A few alternative derivations have been presented in the literature. In 1984, Ewarlds and Wanhill provided a simpler derivation starting with Griffith's energy balance [1]. In 1985, Kanninen and Popelar [41] presented a different derivation starting with the statement of total potential energy [41]. In 1995, the same derivation was presented also by Anderson [42]. In 2004, it was pointed by Jin and Sun [42] that such derivation applies the divergence theorem in a region containing the crack tip, and that it is flawed because of the crack tip stress singularity. They mentioned that it has been ignored that the stress singularity at the crack tip invalidates the direct treatment of such theorem. Furthermore, Jin and Sun provided a mathematically rigorous and physically straightforward derivation of the J-integral applying the divergence theorem properly. Having this in mind, it is important to notice that Ewarlds and Wanhill derivation [1] uses Green's theorem in a region enclosing the crack tip. Therefore, this derivation is also flawed. The J-integral, with units of force per unit thickness, is given by (2.1), the strain energy density by (2.2) and traction by (2.3).

$$J = \int_{\Gamma} W dy - \int_{\Gamma} T_i \frac{\partial u_i}{\partial x} ds \tag{2.1}$$

$$W = W(\varepsilon) = \int_{0}^{\varepsilon} \sigma_{ij} d\varepsilon_{ij} \tag{2.2}$$

$$T_i = \sigma_{ij} n_j \tag{2.3}$$

As stated above, derivations presented by Ewarlds and Wanhill [1] and Kanninen and Popelar [41] are flawed. Nevertheless, both derivations are presented to illustrate the fact that different approaches can be taken in deriving the J-integral expression. Furthermore, what these derivations have in common is that they all start with an expression for the strain energy release rate, G, per unit thickness, which after manipulations becomes the J-integral. It is also important to specifically identify the problems associated with the flawed derivations, and that the derivation proposed by Jin and Sun [42] is based on the same general idea than Kanninen and Popelar's work, but departs into a different approach to address the effect of the crack tip singularity.

2.1.1 H. L. Ewarlds and R. J. H. Wanhill (derivation of J-integral)

H. L. Ewarlds and R. J. H. Wanhill [1] presented a derivation starting with Griffith's energy balance approach for elastic behavior by consider an infinite plate of unit thickness that contains a through-thickness crack of length $2a$ and that is subjected to uniform tensile stress, σ, applied at infinity. Figure 2.1 represents an approximation to such a plate.

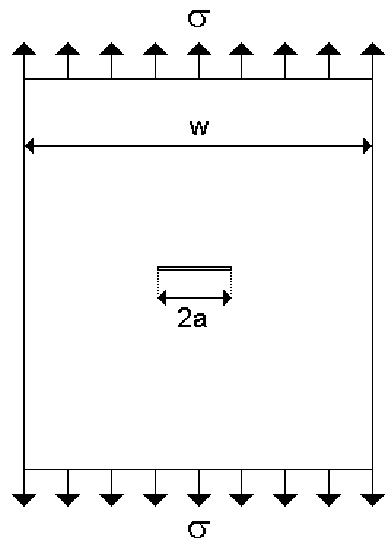

Figure 2.1: Infinite plate of unit thickness with a through-thickness crack (2a<<w)

The total energy U of the cracked plate for elastic behavior may be written as,

$$U = U_0 + U_a + U_\gamma - F \tag{2.4}$$

where U_0 is the elastic energy of the loaded uncracked plate (a constant), U_a is the change in the elastic energy caused by introducing the crack in the plate, U_γ is the change in the elastic surface energy caused by the formation of the crack surfaces, and F is the work performed by external forces (this must be subtracted in equation (2.1), since it is not part of the internal potential energy of the plate). Crack growth instability will occur as soon as U no longer increases with increasing crack length a. Thus instability will occur if,

$$\frac{dU}{da} \leq 0 \tag{2.5}$$

Since U_0 is a constant, instability will occur if,

$$\frac{d}{da}\left(F-U_a\right)\geq\frac{dU_\gamma}{da} \tag{2.6}$$

The elastic energy release rate, G, per unit thickness is defined by equation (2.7) and the crack resistance, R, per unit thickness is defined by equation (2.8). Thurs instability will occur if equation (2.9) is met.

$$G=\frac{d}{da}\left(F-U_a\right) \tag{2.7}$$

$$R=\frac{dU_\gamma}{da} \tag{2.8}$$

$$G\geq R \tag{2.9}$$

An equivalent of G can be defined by equation (2.10). The potential energy U_p is defined by equation (2.11). Therefore equation (2.4) becomes equation (2.12).

$$J=\frac{d}{da}\left(F-U_a\right) \tag{2.10}$$

$$U_p=U_0+U_a-F \tag{2.11}$$

$$U=U_p+U_\gamma \tag{2.12}$$

Thus U_p contains all the energy terms that may contribute to nonlinear elastic behavior, while U_γ is generally irreversible. Since U_0 is a constant, differentiation of U_p is given by equation (2.13). Therefore, it is seen that by definition, J is specified by equation (2.14). Now since dF/da represents the energy provided by the external force

F per increment of crack extension and dU_a / da is the increase of elastic energy owing to the external work dF / da, the quantity dU_p / da is the change in stored energy.

$$\frac{dU_p}{da} = \frac{d}{da}(U_a - F) = -\frac{d}{da}(F - U_a) \quad (2.13)$$

$$J = -\frac{dU_p}{da} \quad (2.14)$$

Now, consider a cracked body of unit thickness as shown in Figure 2.2. The body has a perimeter Γ and a surface A. A traction $\overline{T}$ acts on a part S_0 of the perimeter and performs external work of an amount ΔF. Thus parts of the body undergo a displacement represented as a displacement vector $\overline{u}$. Let U_{01} be the energy contained in the plate before the traction is applied. Note that U_{01} has the same meaning as U_0 in equation (2.4), except that this time we start with a plate that already contains a crack. Thus U_{01} represents the energy contained in the cracked plate owing to any previous history. The effect of applying the traction may now be considered for two cases; for crack growth and for no crack growth.

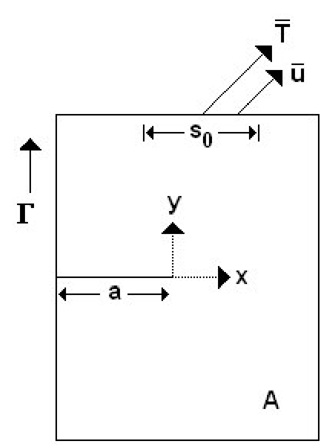

Figure 2.2: A cracked body of unit thickness loaded by a traction T

For no crack growth, the potential energy is,

$$U_{p1} = U_{01} + \Delta F \quad (2.15)$$

For crack growth Δa, ΔF is given by equation (2.16), and the potential energy by equation (2.17).

$$\Delta F = \Delta U_a + \Delta U_\gamma \, \Delta F \quad (2.16)$$

$$U_{p2} = U_{01} + \Delta U_a \quad (2.17)$$

Note that the change in surface energy ΔU_γ is irreversible and cannot be part of U_{p2}. It follows that the change in potential energy ΔU_p due to a crack extension Δa is,

$$\Delta U_p = U_{p2} - U_{p1} \quad (2.18)$$

Using equation (2.15) and (2.17), equation (2.18) can be rewritten as,

$$\Delta U_p = \Delta U_a - \Delta F \quad (2.19)$$

and for the limiting case $\Delta a \to 0$ we may write,

$$dU_p = dU_a - dF \quad (2.20)$$

Equation (2.20) shows that dU_p will always be negative since dF provides both dU_a and dU_γ. Integrating equation (2.20) leads to,

$$\int dU_p = \int dU_a - \int dF \tag{2.21}$$

or

$$U_p = U_a - F + C \tag{2.22}$$

The integration constant is equal to U_{01}. This means,

$$U_p = U_a - F + U_{01} \tag{2.23}$$

This is equivalent to the definition of U_p in equation (2.11). In equation (2.23) $U_a + U_{01}$ is the total strain energy contained in the body. This total strain energy and F can be represented by equations (2.24) and (2.25) respectively.

$$U_a + U_{01} = \iint_A W dxdy \tag{2.24}$$

$$F = \int_\Gamma \overline{T} ds \bullet \overline{u} \tag{2.25}$$

Substituting equation (2.24) and (2.25) into equation (2.23) gives,

$$U_p = \iint_A W dxdy - \int_\Gamma \overline{T} ds \bullet \overline{u} \tag{2.26}$$

If the traction applied to the body is kept constant we may write,

$$\frac{dU_p}{da} = \iint_A \frac{\partial W}{\partial a} dxdy - \int_\Gamma \overline{T} \bullet \frac{\partial \overline{u}}{\partial a} ds \tag{2.27}$$

Note: It is known that $\partial W / \partial a$ has a $1/r^2$ singularity at the crack tip (where r is the distance from the tip) in LEFM because $W \sim 1/r$, as $r \to 0$. Hence, the differentiation with respect to the crack length a cannot be directly performed within the area integral and the divergence theorem cannot be used directly.

Equation (2.27) is an expression for the change in potential energy per unit crack extension, which can be modified as follows. As shown in Figure 2.2, the coordinate system can be taken such that the origin is at the crack tip a. If the perimeter Γ is fixed, $da = -dx$ and thus $d/da = -d/dx$. Then,

$$\frac{dU_p}{da} = -\iint_A \frac{\partial W}{\partial x} dxdy + \int_\Gamma \overline{T} \bullet \frac{\partial \overline{u}}{\partial x} ds \tag{2.28}$$

Using Green's theorem on equation (2.28), we can eliminate A and express dU_p / da as a line integral along the perimeter Γ. Therefore, equation (2.28) becomes equation (2.29) and J is now given by equation (2.30), which is the definition of the J-integral.

Note: It is known that $\partial W / \partial x$ has a $1/r^2$ singularity at the crack tip (where r is the distance from the tip) in LEFM because $W \sim 1/r$, as $r \to 0$. Hence, Green's theorem cannot be used directly.

$$\frac{dU_p}{da} = -\int_\Gamma W dy + \int_\Gamma \overline{T} \bullet \frac{\partial \overline{u}}{\partial x} ds \tag{2.29}$$

$$J = \int_\Gamma W dy - \int_\Gamma T_i \frac{\partial u_i}{\partial x} ds \tag{2.30}$$

2.1.2 M. F. Kanninen and C. H. Popelar (derivation of J-integral)

Kanninen and Popelar [41] considered a two-dimensional cracked body bounded by the curve Γ_0 (Figure 2.3). Let A_0 denote the area of the body. The segments Γ_t and Γ_u are the portions of the contour on which tractions and displacements are defined. The tractions are assumed to be independent of the crack length a and the crack surfaces are taken to be traction free. Under quasistatic conditions and in the absence of body forces, potential energy of the cracked body per unit thickness is given by equation (2.31). By considering the change in potential energy resulting from a virtual extension of the crack length a, strain energy release rate per unit thickness G given by equation (2.32).

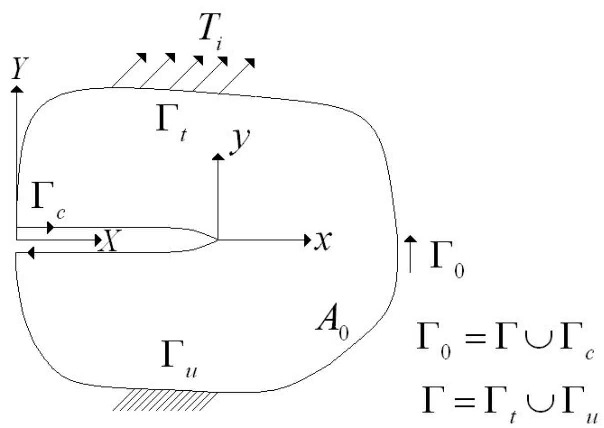

Figure 2.3: Kanninen and Popelar's two-dimensional cracked body bounded by Γ_0

$$\Pi = \Pi(a) = \iint_{A_0} W dA - \int_{\Gamma_t} T_i u_i d\Gamma \tag{2.31}$$

$$G = -\frac{d\Pi}{da} = -\iint_{A_0} \frac{dW}{da} dA + \int_{\Gamma_t} T_i \frac{du_i}{da} d\Gamma \tag{2.32}$$

Note: It is known that $\partial W / \partial a$ has a $1/r^2$ singularity at the crack tip (where r is the distance from the tip) in LEFM because $W \sim 1/r$, as $r \to 0$. Hence, the differentiation with respect to the crack length a cannot be directly performed within the area integral. However, this is done by Kanninen and Popelar, even though they acknowledge the singularity at the crack tip.

When the crack grows, the coordinate axis moves. Therefore, in performing the differentiation, a coordinate system attached at the crack tip is introduced in equation (2.33). Since $\partial x / \partial a = -1$, equation (2.34) can be written.

$$x = X - a \qquad y = Y \tag{2.33}$$

$$\frac{d}{da} = \frac{\partial}{\partial a} + \frac{\partial x}{\partial a}\frac{\partial}{\partial x} = \frac{\partial}{\partial a} - \frac{\partial}{\partial x} \qquad dx = dX\,, \qquad dy = dY \tag{2.34}$$

The line integration in (2.32) can be performed over the entire contour Γ_0 in the counterclockwise direction from the lower crack face to the upper one because $du_i / da = 0$ over Γ_u, the region where displacements are specified, and $T_i = 0$ on the crack faces Γ_c. Applying equation (2.34) to (2.32) gives equation (2.35).

$$G = -\iint_{A_0} \left(\frac{\partial W}{\partial a} - \frac{\partial W}{\partial x} \right) dA + \int_{\Gamma_0} T_i \left(\frac{\partial u_i}{\partial a} - \frac{\partial u_i}{\partial x} \right) d\Gamma \tag{2.35}$$

By invoking the definition of strain energy density given by equation (2.2), equation (2.36) is achieved. Note that this expression applies only when W exhibits the properties of an elastic potential. Since $\sigma_{ij} = \sigma_{ji}$, use of strain-displacement relationship for small strains (constitutive relation $\varepsilon_{ij} = \partial u_i / \partial x_j$) in equation (2.36) gives (2.37).

$$\frac{\partial W}{\partial x} = \frac{\partial W}{\partial \varepsilon_{ij}}\frac{\partial \varepsilon_{ij}}{\partial x} = \sigma_{ij}\frac{\partial \varepsilon_{ij}}{\partial x} \tag{2.36}$$

$$\frac{\partial W}{\partial x} = \sigma_{ij} \frac{\partial}{\partial x}\left[\frac{1}{2}\left(\frac{\partial u_i}{\partial x_j} + \frac{\partial u_j}{\partial x_i}\right)\right] = \sigma_{ij} \frac{\partial}{\partial x_j}\left(\frac{\partial u_i}{\partial x}\right) \tag{2.37}$$

When applying the same assumptions shown in equation (2.36) and (2.37), the expression shown in equation (2.38) is obtained.

$$\frac{\partial W}{\partial a} = \frac{\partial W}{\partial \varepsilon_{ij}} \frac{\partial \varepsilon_{ij}}{\partial a} = \sigma_{ij} \frac{\partial}{\partial x_j}\left(\frac{\partial u_i}{\partial a}\right) \tag{2.38}$$

Using (2.3) and the divergence theorem in two dimensions, equation (2.39) is written. Due to equilibrium conditions ($\partial \sigma_{ij} / \partial x_j = 0$), equation (2.39) becomes equation (2.40). Recalling equation (2.38), the expression presented in equation (2.41) is obtained.

$$\int_{\Gamma_0} T_i \frac{\partial u_i}{\partial a} d\Gamma = \int_{\Gamma_0} \sigma_{ij} n_j \frac{\partial u_i}{\partial a} d\Gamma = \int_{\Gamma_0} \sigma_{ij} \frac{\partial u_i}{\partial a} n_j d\Gamma = \iint_{A_0} \frac{\partial}{\partial x_j}\left(\sigma_{ij} \frac{\partial u_i}{\partial a}\right) dA \tag{2.39}$$

$$\int_{\Gamma_0} T_i \frac{\partial u_i}{\partial a} d\Gamma = \iint_{A_0} \sigma_{ij} \frac{\partial}{\partial x_j}\left(\frac{\partial u_i}{\partial a}\right) dA \tag{2.40}$$

$$\int_{\Gamma_0} T_i \frac{\partial u_i}{\partial a} d\Gamma = \iint_{A_0} \frac{\partial W}{\partial a} dA \tag{2.41}$$

Substituting equation (2.41) into equation (2.35) gives equation (2.42).

$$G = \iint_{A_0} \frac{\partial W}{\partial x} dA - \int_{\Gamma_0} T_i \frac{\partial u_i}{\partial x} d\Gamma \tag{2.42}$$

Applying the divergence theorem and multiplying both sides by -1 leads to equation (2.43). Noting that $n_x d\Gamma = dy$ and $\Gamma_0 = \Gamma \cup \Gamma_c$ leads to equation (2.44). $T_i = dy = 0$ on the crack faces Γ_c. Thus equation (2.44) becomes equation (2.45).

Note: It is known that $\partial W / \partial x$ has a $1/r^2$ singularity at the crack tip (where r is the distance from the tip) in LEFM because $W \sim 1/r$, as $r \to 0$. Hence, the divergence theorem cannot be used directly. However, this is done by Kanninen and Popelar, even though they acknowledge the singularity at the crack tip.

$$G = \int_{\Gamma_0} \left(W n_x - T_i \frac{\partial u_i}{\partial x} \right) d\Gamma \tag{2.43}$$

$$G = \int_{\Gamma + \Gamma_c} \left(W dy - T_i \frac{\partial u_i}{\partial x} d\Gamma \right) \tag{2.44}$$

$$G = \int_{\Gamma} \left(W dy - T_i \frac{\partial u_i}{\partial x} d\Gamma \right) = J \tag{2.45}$$

2.1.3 Z. H. Jin and C. T. Sun (derivation of J-integral)

In this derivation, the effect of the crack tip stress singularity is considered and the divergence theorem is properly applied [42]. The derivation of the J-integral done by Rice in 1968 [38] was based on the fact that J is equal to the strain energy release rate per unit thickness G given by equation (2.46).

$$G = -\frac{d\Pi}{da} \tag{2.46}$$

With this approach the derivation of the J-integral done by Z. H. Jin and C. T Sun is simply to show that the G of the above definition leads to the well known expression of J-integral. Consider a two-dimensional cracked body shown in Figure 2.4 with an area A_0 subjected to prescribed tractions T_i on the boundary segment Γ_t and the prescribed displacements on the boundary segment Γ_u. The whole boundary Γ_0 of the cracked body consists of Γ_t, Γ_u and the crack faces Γ_c.

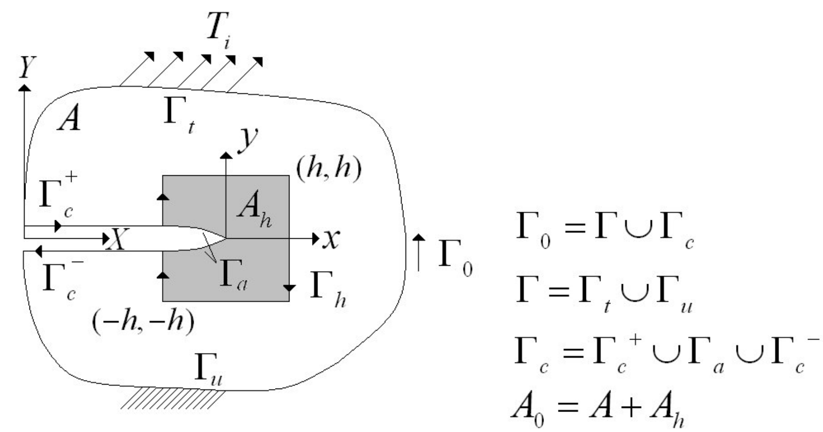

Figure 2.4: Jin and Sun's two-dimensional cracked body bounded by Γ_0

The positive contour direction of Γ_0 is when one travels along it, the domain of interest always lies to the left of the traveler. The potential energy of the cracked body per unit thickness is given by equation (2.47), where (X, Y) is a stationary Cartesian coordinate system. The energy release rate associated with the quasi-static crack extension is defined by equation (2.48).

$$\Pi = \Pi(a) = \iint_{A_0} W dX dY - \int_{\Gamma_t} T_i u_i d\Gamma \tag{2.47}$$

$$G = -\frac{d\Pi}{da} = -\frac{d}{da}\iint_{A_0} W dX dY + \frac{d}{da}\int_{\Gamma_t} T_i u_i d\Gamma \tag{2.48}$$

Consider a small square A_h with the center at the crack tip as shown in Figure 2.4. The side length of the square is $2h$ and the boundary is denoted by Γ_h. The region of the cracked body excluding A_h is denoted by A. Therefore,

$$G = -\frac{d}{da}\left[\iint_A W dX dY + \iint_{A_h} W dX dY\right] + \int_{\Gamma_t} T_i \frac{du_i}{da} d\Gamma \tag{2.49}$$

Because no stress singularity exists in A and along Γ_t, equation (2.49) can be written as equation (2.50), where the integration along Γ_t is extended to the whole boundary Γ_0 because $T_i = 0$ on the crack faces Γ_c and $du_i / da = 0$ on Γ_u.

$$G = -\iint_A \frac{dW}{da} dX dY + \int_{\Gamma_0} T_i \frac{du_i}{da} d\Gamma - \frac{d}{da}\iint_{A_h} W dX dY \tag{2.50}$$

A local coordinate system (x, y) attached at the crack tip was introduced in equation (2.33) leading to equation (2.34) when the filed variables are described in the local coordinate system (x, y). Use of equation (2.34) in equation (2.50) leads to the expression presented in equation (2.51).

$$\begin{aligned} G = &-\iint_A \frac{\partial W}{\partial a} dx dy + \iint_A \frac{\partial W}{\partial x} dx dy \\ &+ \int_{\Gamma_0} T_i \frac{\partial u_i}{\partial a} d\Gamma - \int_{\Gamma_0} T_i \frac{\partial u_i}{\partial x} d\Gamma - \frac{d}{da}\iint_{A_h} W dX dY \end{aligned} \tag{2.51}$$

The third term on the right hand side of equation (2.51) can be written as equation (2.41). Here the singularity in $\partial W / \partial a$ ($1/r$ near the crack tip) is a weak singularity because $dA = r dr d\theta$, making the divergence theorem applicable. The use of equation (2.41) in (2.51), and the notion that $A_0 - A = A_h$ leads to equation (2.52). Here, the integration along the whole boundary Γ_0 is reduced to Γ because $T_i = 0$ on Γ_c.

$$G = \iint_A \frac{\partial W}{\partial x} dxdy - \int_\Gamma T_i \frac{\partial u_i}{\partial x} d\Gamma + \iint_{A_h} \frac{\partial W}{\partial a} dxdy - \frac{d}{da} \iint_{A_h} W dX dY \qquad (2.52)$$

Applying the divergence theorem to the first term on the right hand side of equation (2.52) yields equation (2.53), whose substitution into equation (2.52) leads to equation (2.54).

$$\iint_A \frac{\partial W}{\partial x} dxdy = \int_\Gamma W dy + \int_{\Gamma_h} W dy \qquad (2.53)$$

$$G = \int_\Gamma W dy + \int_{\Gamma_h} W dy - \int_\Gamma T_i \frac{\partial u_i}{\partial x} d\Gamma + \iint_{A_h} \frac{\partial W}{\partial a} dxdy - \frac{d}{da} \iint_{A_h} W dX dY \qquad (2.54)$$

In the region near the moving crack tip, the strain energy density function has the universal separable form presented in equation (2.55), Where $B(a)$ may depend on loading and other factors but not on the local coordinates, and $\tilde{W}(x, y)$ is a function of local coordinates only. Now assume that A_h is so small that equation (2.55) holds in a region containing A_h.

$$W = B(a)\tilde{W}(X - a, Y) = B(a)\tilde{W}(x, y) \qquad (2.55)$$

With equation (2.55), the contour integral over Γ_h (second integral) in equation (2.54) can thus be evaluated as equation (2.56), and the area integral over A_h (fourth integral) in equation (2.54) becomes equation (2.57).

$$\int_{\Gamma_h} W dy = \int_{-h}^{h} B(a)\tilde{W}(-h, y)\,dy + \int_{h}^{-h} B(a)\tilde{W}(h, y)\,dy \tag{2.56}$$

$$\iint_{A_h} \frac{\partial W}{\partial a}\,dxdy = \iint_{A_h} B'(a)\tilde{W}(x, y)\,dxdy \tag{2.57}$$

Now evaluate the last term in equation (2.54). Noting that noting that $x = X - a$, it follows from the definition of a derivative and the expression presented in equation (2.55) that equation (2.58) is obtained.

$$\frac{d}{da}\iint_{A_h} W dXdY = \lim_{\Delta a \to 0} \frac{1}{\Delta a}\left[\iint_{A_h}\left(B(a+\Delta a)\tilde{W}(x-\Delta a, y) - B(a)\tilde{W}(x, y)\right)dxdy\right] \tag{2.58}$$

Letting $x^* = x - \Delta a$ makes the expression presented in equation (2.59) valid. If the integration over x^* is divided into three integrals, equation (2.60) is achieved. Noting that x^* is a dummy variable, equation (2.61) can be obtained.

$$\iint_{A_h} \tilde{W}(x-\Delta a, y)\,dxdy = \int_{-h}^{h}\left[\int_{-h-\Delta a}^{h-\Delta a} \tilde{W}(x^*, y)\,dx^*\right]dy \tag{2.59}$$

$$\iint_{A_h} \tilde{W}(x-\Delta a, y)\,dxdy = \int_{-h}^{h}\left[\begin{array}{l}\displaystyle\int_{-h-\Delta a}^{-h} \tilde{W}(x^*, y)\,dx^* + \int_{-h}^{h} \tilde{W}(x^*, y)\,dx^* \\ \displaystyle + \int_{h}^{h-\Delta a} \tilde{W}(x^*, y)\,dx^*\end{array}\right]dy \tag{2.60}$$

$$\begin{aligned}\iint_{A_h} \tilde{W}(x-\Delta a, y)\,dxdy &= \iint_{A_h} \tilde{W}(x, y)\,dxdy + \\ &\int_{-h}^{h}\left[\int_{-h-\Delta a}^{-h} \tilde{W}(x, y)\,dx - \int_{h-\Delta a}^{h} \tilde{W}(x, y)\,dx\right]dy\end{aligned} \tag{2.61}$$

When Δa becomes infinitesimally small, equation (2.61) becomes (2.62). Applying the definition of a derivative, equation (2.63) can be written.

$$\iint_{A_h} \tilde{W}(x-\Delta a, y)\,dxdy = \iint_{A_h} \tilde{W}(x, y)\,dxdy + \int_{-h}^{h} \left[\tilde{W}(-h, y)\Delta a - \tilde{W}(h, y)\Delta a\right] dy \qquad \Delta a \to 0 \qquad (2.62)$$

$$B(a+\Delta a) = B(a) + B'(a)\Delta a \qquad \Delta a \to 0 \qquad (2.63)$$

Substitution of equations (2.62) and (2.63) into (2.58) yields equation (2.64).

$$\frac{d}{da}\iint_{A_h} WdXdY = B'(a)\iint_{A_h} \tilde{W}(x, y)\,dxdy + B(a)\int_{-h}^{h}\left[\tilde{W}(-h, y) - \tilde{W}(h, y)\right]dy \qquad (2.64)$$

Substituting equations (2.56), (2.57) and (2.64) into equation (2.54), we obtain,

$$G = \int_{\Gamma} Wdy - \int_{\Gamma} T_i \frac{\partial u_i}{\partial x} ds = J \qquad (2.65)$$

2.2 J-integral Along a Closed Path

Rice [31, 38] considered a closed curve Γ^* enclosing an area A^* in a two dimensional deformation field free of body forces under elastic (linear or non linear) assumptions. The J-integral along Γ^* is,

$$J = \int_{\Gamma^*} Wdy - \int_{\Gamma^*} T_i \frac{\partial u_i}{\partial x} ds \qquad (2.66)$$

Using Green's theorem,

$$\int_{\Gamma^*} W dy = \int_{A^*} \frac{\partial W}{\partial x} dx dy \tag{2.67}$$

Note: The integrand on the right hand side is again $\partial W / \partial x$. However, this step is valid. The reason for this validity is that the integration is done over an area A^* which does not need to be the entire area of the body. It only has to be the area (free of singularities) enclosed by a closed path Γ^*. Therefore, this area A^* could be the area enclosed by the closed path shown in Figure 2.5 (page26), which clearly exclude the crack tip singularity that is present if the crack shown in Figure 2.5 was a sharp crack and LEFM was considered.

Differentiating the strain energy density, and using small displacement theory,

$$\frac{\partial W}{\partial x} = \frac{\partial W}{\partial \varepsilon_{ij}} \frac{\partial \varepsilon_{ij}}{\partial x} = \sigma_{ij} \frac{\partial \varepsilon_{ij}}{\partial x} = \sigma_{ij} \frac{\partial}{\partial x}\left(\frac{1}{2}\left(\frac{\partial u_i}{\partial x_j} + \frac{\partial u_j}{\partial x_i} \right)\right) = \sigma_{ij} \frac{\partial}{\partial x_j}\left(\frac{\partial u_i}{\partial x} \right) \tag{2.68}$$

and since $\partial \sigma_{ij} / \partial x_j = 0$,

$$\frac{\partial W}{\partial x} = \frac{\partial}{\partial x_j}\left(\sigma_{ij} \frac{\partial u_i}{\partial x} \right) \tag{2.69}$$

which can be used in equation (2.67) giving,

$$\int_{\Gamma^*} W dy = \int_{A^*} \frac{\partial}{\partial x_j}\left(\sigma_{ij} \frac{\partial u_i}{\partial x} \right) dx dy \tag{2.70}$$

Noting that $T_i = \sigma_{ij} n_j$ we can rewrite,

$$\int_{\Gamma^*} T_i \frac{\partial u_i}{\partial x} ds = \int_{\Gamma^*} \sigma_{ij} n_j \frac{\partial u_i}{\partial x} ds = \int_{\Gamma^*} \sigma_{ij} \frac{\partial u_i}{\partial x} n_j ds \tag{2.71}$$

and expanding the terms in Einstein notation gives,

$$\int_{\Gamma^*} T_i \frac{\partial u_i}{\partial x} ds = \int_{\Gamma^*} \left(\sigma_{11} \frac{\partial u_1}{\partial x} + \sigma_{21} \frac{\partial u_2}{\partial x} \right) n_1 ds + \int_{\Gamma^*} \left(\sigma_{12} \frac{\partial u_1}{\partial x} + \sigma_{22} \frac{\partial u_2}{\partial x} \right) n_2 ds \tag{2.72}$$

which, since $dy = n_1 ds$ and $dx = -n_2 ds$, can be written as,

$$\int_{\Gamma^*} T_i \frac{\partial u_i}{\partial x} ds = \int_{\Gamma^*} \left(\sigma_{11} \frac{\partial u_1}{\partial x} + \sigma_{21} \frac{\partial u_2}{\partial x} \right) dy - \int_{\Gamma^*} \left(\sigma_{12} \frac{\partial u_1}{\partial x} + \sigma_{22} \frac{\partial u_2}{\partial x} \right) dx \tag{2.73}$$

Using Green's theorem,

$$\int_{\Gamma^*} T_i \frac{\partial u_i}{\partial x} ds = \int_{A^*} \left[\frac{\partial}{\partial x} \left(\sigma_{11} \frac{\partial u_1}{\partial x} + \sigma_{21} \frac{\partial u_2}{\partial x} \right) + \frac{\partial}{\partial y} \left(\sigma_{12} \frac{\partial u_1}{\partial x} + \sigma_{22} \frac{\partial u_2}{\partial x} \right) \right] dxdy \tag{2.74}$$

which can be rewritten as,

$$\int_{\Gamma^*} T_i \frac{\partial u_i}{\partial x} ds = \int_{A^*} \frac{\partial}{\partial x_j} \left(\sigma_{ij} \frac{\partial u_i}{\partial x} \right) dxdy \tag{2.75}$$

Therefore, substituting equations (2.70) and (2.75) into equation (2.66) gives,

$$J = \int_{A^*} \frac{\partial}{\partial x_j} \left(\sigma_{ij} \frac{\partial u_i}{\partial x} \right) dxdy - \int_{A^*} \frac{\partial}{\partial x_j} \left(\sigma_{ij} \frac{\partial u_i}{\partial x} \right) dxdy = 0 \tag{2.76}$$

This shows that J-integral along a closed path is zero.

2.3 Path Independence of the J-integral

Consider any two paths Γ_1 and Γ_2 surrounding the notch tip as shown as in Figure 2.5. Traverse Γ_1 in the counterclockwise sense, continue along the upper flat notch surface to where Γ_2 intersects the notch, traverse Γ_2 in the clockwise sense, and then continue along the lower flat notch surface to the starting point where Γ_1 intersects the notch. This describes a closed contour so that j-integral vanishes. But $\overline{T} = 0$ and $dy = 0$ on the portions of path along the flat notch surfaces. Thus the integral along Γ_1 counterclockwise and the integral along Γ_2 clockwise sum to zero. J has the same value when computed by integrating along either Γ_1 or Γ_2, and path independence is proven. The utility of the method rest in the fact that alternate choices of integration paths often permit a direct evaluation of J .

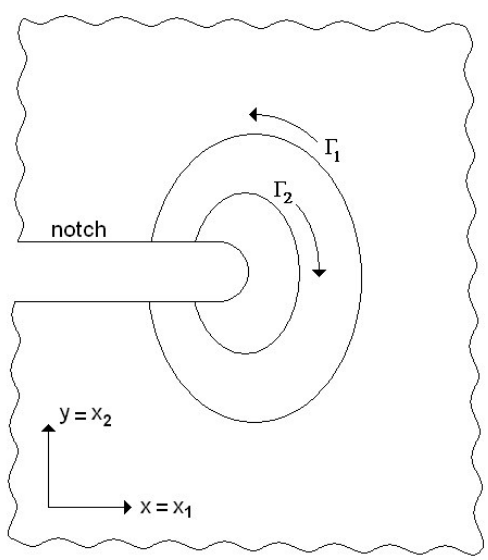

Figure 2.5: Flat surfaced notch in two-dimensional deformation field

2.4 Current Computational Procedures Used for Stress Intensity Factor Calculations

2.4.1 Methods of Determining the Stress Intensity Factor

Many methods of obtaining K-solutions have been developed. These methods are divided in three categories or stages depending on their degree of sophistication and the time required to obtain a solution. This is shown in Figure 2.6. For simple geometrical configurations, or where a complex structure can be simply modeled, it may be possible to use reference books. When a solution cannot be obtained directly from a reference book, then one of the relatively simple methods in stage 2 may be adequate since they will seldom require more than a couple of man-hours to obtain K-values [3].

STAGE 1	STAGE 2	STAGE 3
HANDBOOKS	SUPERPOSITION	COLLOCATION METHOD
	STRESS CONCENTRATION	INTEGRAL TRANSFORM
	STRESS DISTRIBUTION	BODY FORCE METHOD
	GREEN'S FUNCTION	EDGE FUNCTION METHOD
	APPROX. WEIGHT FUNCTION	METHOD OF LINES
	COMPOUNDING METHOD	BOUNDARY ELEMENT METHOD
		FINITE DIFFERENCE METHOD
		FINITE ELEMENT METHOD

Figure 2.6: Methods of determining the stress intensity factor

Although stage 2 methods cannot produce very accurate solutions, for most practical crack problems in real engineering structures they can be helpful in obtaining rough, approximate K-solutions relatively quickly. The use of more than one model and/or more than one method may enable upper and lower bounds for K-solutions to the real problem.

When a particular stress intensity factor is required repeatedly, say for a standard test-piece, and high accuracy is important, then numerical methods in stage 3 become necessary. These methods are also essential for complex structural configurations. The practical application will influence the choice of method. Today the finite element method is the most widely method for obtaining solutions in fracture mechanics, and techniques for extracting stress intensity factors fall into one of two categories: (i) direct approaches, which correlate the stress intensity factors with finite element results directly, (ii) and energy approaches, which first compute energy release rates. In general, the energy approaches are more accurate and preferable. However, the direct approaches have utility and are especially useful as a check on energy approaches because their expressions are simple enough and hence are amenable for hand calculations. A large number of different techniques for extracting stress intensity factors using finite element processes have been presented in the literature. The main 4 techniques are: displacement correlation (direct approach), virtual crack extension (energy approach), crack tip opening displacement (CTOD) (direct approach), and the J-integral (energy approach). An in-depth view of these other techniques using finite element processes, and methods listed above can be seen in ref. [2, 3, and 5].

Amongst all the techniques mentioned above, the J-integral approach is the most accurate and hence preferred. The implementation of the method is quite involved. The displacement correlation technique is the least accurate but is simple enough for hand calculations. Since it does not require additional terms for cases with crack-face tractions or body forces, it provides a simple "sanity" check for more accurate techniques to ensure that they are formulated correctly and are being used properly.

2.4.2 Special Crack Tip Elements

Early attempts of finite element application on the evaluation of the stress intensity factors were unsatisfactory, even though a very large number of elements with uniform mesh refinement was used. In 1970, Chan and co-workers [6] used classical triangular elements with first order displacement functions. Chan's study included the use of the displacement method and the line J-integral. Determination of stress intensity factors by employing conventional types of elements was not satisfactory, which was believed to be due to an inability of the polynomial basis functions to represent the singular crack-tip stress and strain fields predicted by the theory. Chan did an extensive finite element study of crack problems using constant stress triangular elements. An extrapolation of the solution away from the tip was used to estimate K_I since the near tip solutions were not reasonable. They reported K_I of an edge-cracked plate under eccentric loads (gained from extrapolating a solution involving 2000 degrees of freedom) within 5 percent of the results obtained from a collocation solution.

As a consequence, a new type of finite element was introduced by Tracey in 1971 [20], which introduced the $\sqrt{r}$ displacement into the shape function representation and hence a $1/\sqrt{r}$ singularity into the strain variation. Singularity triangular elements were obtained considering each triangle as a four node quadrilateral with two nodes coincident at the crack tip and with the displacement function of $u(\xi,\eta) = b_1 + b_2\sqrt{\xi} + b_3\sqrt{\xi\eta} + b_4\eta$ along with the auxiliary constraint $u_A = u_B$ at the crack tip, where ξ and η are the elements' natural coordinates. Singularity triangular elements were used in the first ring of elements centered about the crack tip. Outside this, rings of trapezoidal isoparametric elements were employed. The far field consisted of rectangular isoparametric elements. No incompatibilities of displacement were introduced along inter-element boundaries. In all isoparametric elements, the displacement within the element was assumed to be linear. The near tip solutions yield K_I values within 5 percent of accepted values when using the displacement method and 250 degrees of freedom. In these approaches the approximate representation of the geometry remains the same as in conventional elements.

Henshell and Shaw [21] and Barsoum [18] independently observed that by moving 2 of the center nodes of an eight nodded quadrilateral element to a quarter point position (bring the center nodes closer to the crack tip), a singularity into the mapping between the element's parametric coordinate space and Cartesian space is introduced and the desired $1/\sqrt{r}$ variation in the strains can be achieved and the singularity occurs exactly at the corner of an element. These new type of elements are known as "quarter-point elements". It was noticed the stresses and displacements in the elements adjacent to the crack tip were very poor. Therefore, displacements on the elements adjacent to the crack tip had to be ignored when calculating K_I using the displacement method.

Barsoum [18] however, showed that the $1/\sqrt{r}$ variation for strains in quadrilateral quarter-point elements is not achieved along rays, within the element, that emanate from the node at the crack tip. He enforced this condition by collapsing a regular 8-node quadrilateral element into a "triangular quarter-point element" by coalescing nodes along one side and moving 2 of the center nodes to a quarter point position [19]. Barsoum [19] showed that triangular quarter-point elements give better results than 8- node quadrilateral quarter-point elements. In 1977, Hibbitt [22] published a note showing that the strain energy (and hence the stiffness) of such quadrilateral elements is unbounded (stiffness is singular if integrated exactly) and in triangular form, the elements offer bounded strain energy. With these new triangular quarter-point elements standard and widely available, finite element programs can be used to model crack tip fields with only minimal preprocessing required. These include: one, two and three-dimensional quarter-point elements, which are all isoparametric, and can be of any order and also hierarchical [6]. If the quarter-point geometry mapping is used for hierarchical elements, then as terms are added to the polynomial order of the element, additional terms of the LEFM crack-tip fields are modeled. Since then, quadrilateral quarter-point elements have been used less frequently in practice than the triangular versions. Hibbitt assertion published in 1977 (stiffness of quadrilateral quarter-point elements being singular) has been claimed not to be true (Ying in 1982 [27], Banks-Sill in

1984 [28]). Banks-Sills and Bortman demonstrated that quadrilateral quarter-point elements have a square root singularity along all rays emanating from the crack tip, but only in a small neighborhood near the tip, and only if the element has a rectangular shape. In 1987, Banks-Sills and Einav [29] showed that the region of singular stresses is slightly larger for 9-noded quadrilateral elements providing the central node is suitably positioned (at a location on the diagonal between the crack-tip and the far corner, 11/32nds of the distance from the crack-tip). A reason of why quadrilateral quarter-point elements are less accurate might be that fewer of these elements can be placed conveniently around a crack tip. With fewer elements, the circumferential variation of the stress and displacement fields about a crack tip may be less accurately represented than in the triangular case where more elements can be used.

Benzley [25] introduced the elements known as "enriched elements". These involve adding the analytic expression of the crack-tip field to the conventional finite element polynomial approximation for the displacement resulting also in strain singularity. These elements will produce an incompatibility of displacements with adjoining element nodes. Therefore, the analytic expression is multiplied by a smoothing function that is unity on boundaries adjacent to enriched elements and equal to zero on boundaries adjacent to conventional elements. Tong, Pian and Lasry [26] introduced the elements known as "hybrid elements", which are similar to enriched elements, in the sense that both approaches are based on assumed displacement near the crack tip. The major difference is in the method of enforcing the inter-element compatibility of the displacement variables. Further details on hybrid elements for the solution of crack problems can be found in ref [26].

2.4.3 Finite Element Techniques for Calculating J-integral

Berkovic [7] starts with the definition of the J-integral given in (2.1). Taking into account the symmetry of σ_{ij} he writes (2.2) as (2.77), where $u_{ij} = \partial u_i / \partial x_j$. In the plane problem, normal vector coordinates are given by (2.78) and for isotropic homogeneous plane stress linear elasticity, the stress tensor is given by (2.79). Substituting (2.77) through (2.79) into (2.1), a new expression for J-integral is presented in (2.80).

$$W = \frac{1}{2}\sigma_{ij}u_{ij} \tag{2.77}$$

$$n_1 = \frac{dx_2}{ds}, \qquad n_2 = -\frac{dx_1}{ds} \tag{2.78}$$

$$\sigma_{ij} = \frac{2\mu}{1-\nu}\left[\nu\delta_{ij}\delta_{kl} + (1-\nu)\delta_{ik}\delta_{jl}\right]u_{kl} \tag{2.79}$$

$$J = \frac{1}{2}\frac{\mu}{1-\nu}\left\{\begin{array}{l} \int_\Gamma \left[\begin{array}{l}(1-\nu)(u_{1,2}+u_{2,1})(u_{1,2}-u_{2,1}) \\ +2(u_{2,2}+u_{1,1})(u_{2,2}-u_{1,1})\end{array}\right] dx_2 + \\ \\ \int_\Gamma 2\left[\begin{array}{l}(1-\nu)u_{1,1}u_{1,2} \\ +(1+\nu)u_{1,1}u_{2,1} + 2u_{2,1}u_{2,2}\end{array}\right] dx_1 \end{array}\right\} \tag{2.80}$$

On parts of the integration path that are parallel to the x_1 axis, dx_2 equals 0, and vice-versa, which reduces the amount of calculations required. This is the case of rectangular paths. For the assumed linear displacement field, the derivative of the displacement in the tangential and normal direction can be calculated using equation (2.81), where the normal derivative is an average value.

$$\frac{\partial u}{\partial t} = \frac{u_K - u_J}{t_K - t_J}, \qquad \frac{\partial u}{\partial n} = \frac{1}{2}\left(\frac{u_K - u_M}{n_K - n_M} + \frac{u_J - u_L}{n_J - n_L}\right) \tag{2.81}$$

In these expressions, t_K and n_K are coordinates of point "K" in the Cartesian coordinate system. Also dx_1 is replaced by $x_{1K} - x_{1J}$ and dx_2 is replaced by $x_{2K} - x_{2J}$.

Finally the integral is replaced with a sum of segments of the observed contour and noting that a factor of 2 must be introduced because only the upper half of the plate will be taken into account due to symmetry. Equation (2.80) becomes (2.82).

$$J = \frac{\mu}{1-\nu} \sum_{J,K=1,2}^{J<K=N-1,N} \left\{ \begin{array}{l} \begin{bmatrix} (1-\nu)(u_{1,2}+u_{2,1})(u_{1,2}-u_{2,1}) \\ +2(u_{2,2}+u_{1,1})(u_{2,2}-u_{1,1}) \end{bmatrix} (x_{2K}-x_{2J}) \\ \\ +2\begin{bmatrix} (1-\nu)u_{1,1}u_{1,2} \\ +(1+\nu)u_{1,1}u_{2,1}+2u_{2,1}u_{2,2} \end{bmatrix} (x_{1K}-x_{1J}) \end{array} \right\} \tag{2.82}$$

He carries out a dimensionless analysis with a 6 by 6 square plate with a central symmetrical crack. The applied tensile load is p=1 and the total crack length is 2. Only one quarter of the plate was modeled using symmetry conditions. A rectangular mesh of 58 elements was used with a total of 8 different rectangular integration paths. The K_I solutions obtained had 1.65%, 1.49%, 0.83 %, 2.81%, 2.48%, 1.98%, 1.65%, 1.65% deviation from numerical results obtained by Hellen [9], where the first solution corresponds to the farthest path away from the crack tip, which is the boundary of plate.

Conway [13] evaluated the integral along the specimen boundary Γ^*. Integration of this path was performed numerically using the finite element method. Nodal density was used, since the path follows a line of low strain and stress gradient. The integration is expressed in lumped form where the energy density W_i is given in terms of the stress and strain at element i along Γ^*.

$$\begin{aligned} J &= 2\sum_i [W_i(b-a, y_i) - W_i(-a, y_i)]\Delta y_i \\ &\quad + 2\sum_j [\sigma_{j\infty}(x_j, h/2)\Delta u_j(x_j, h/2)] \end{aligned} \tag{2.83}$$

$$W_i = \frac{1}{2}\sigma_i \varepsilon_i \tag{2.84}$$

A 4.75in by 10 in plate with 2 collinear edge crack was considered. The plate is subjected to a uniform tensile stress of 100 psi under isotropic homogeneous plane stress linear elastic assumptions. Only one quarter of the plate was modeled using symmetry conditions. Triangular and quadratic linear-strain elements were implemented. Four different crack lengths were used (2.235 in, 2.111 in, 1.900 in and 1.583 in), which gave 9.7 %, 1.7%, 2.4% and 3.5 % deviation in the K_I results from an analytical solution developed by Paris and Sih [11].

Sedmak [14] employed isoparametric triangular elements. Constitutive relations for a isotropic homogeneous linear isotropic body, as well as strain-displacement relationship for small displacement gradients were used. For the plane problem the final relation for J-integral is a function of displacement gradients only given by equation (2.85), where k_1 and k_2 are constants characterizing the type of the problem. This is the very same approach taken by Berkovic [7] and equation (2.85) is exactly equation (2.80).

$$J = \frac{\mu}{2} \int_{\Gamma} \left\{ F_y dy + F_x dx \right\} \tag{2.85}$$

where

$$F_x = k_1 \left(\frac{\partial v}{\partial y} - \frac{\partial u}{\partial x} \right) \left(\frac{\partial v}{\partial y} + \frac{\partial u}{\partial x} \right) + \left(\frac{\partial u}{\partial y} + \frac{\partial v}{\partial x} \right) \left(\frac{\partial u}{\partial y} - \frac{\partial v}{\partial x} \right)$$

$$F_y = 2 \left[\left(\frac{\partial u}{\partial x} \frac{\partial u}{\partial y} \right) + k_2 \left(\frac{\partial u}{\partial x} \frac{\partial v}{\partial x} \right) + k_1 \left(\frac{\partial v}{\partial x} \frac{\partial v}{\partial y} \right) \right]$$

$$k_1 = \frac{2(1-\nu)}{1-2\nu} \qquad k_2 = \frac{1}{1-2\nu} \quad ; \quad \text{for plane strain}$$

$$k_1 = \frac{2}{1-\nu} \qquad k_2 = \frac{1+\nu}{1-\nu} \quad ; \quad \text{for plane stress}$$

The displacement gradients were calculated directly from the known displacement field. Under the assumption of a linear variation of displacements in the elements, the integral in equation (2.85) was transformed into a sum suitable for calculation. This is given in equation (2.86), where FY and FX are the expressions multiplying dy and dx in equation (2.85), respectively, which are constants inside an element since linear variation of displacements was assumed. The terms y_{KJ} and x_{KJ} are the differences of the coordinates of points K and J along the integration path, and N is the number of elements along the integration path.

$$J = \frac{\mu}{2} \sum_{J,K=1,2}^{N-1,N} \left(FY.y_{KJ} + FX.x_{KJ} \right) \qquad (2.86)$$

A dimensionless analysis was carried out using a double edge cracked tension 2 by 2 plate under isotropic homogeneous plane strain linear elastic conditions. The applied load is 1, the crack length is 0.5, the young modulus being 1, poisons ratio of 0.3 and a unit thickness. Only one quarter of the plate was modeled using symmetry conditions. Five meshes were tested. All of them obtained by adding one new layer of elements in the lower half of the domain (rapid mesh refinement). Only one integration path was used. Meshes with 32, 44, 60, 84 and 108 elements were created obtaining K_I values of -13.12%, -7.13%, -4.73%, -3.54%, -2.94% deviation from a result reported by Hellen in 1973 obtained using crack extension method [15].

Li Shih and A. Needleman [16] (using the principles of virtual crack extension) showed how the contour J-integral can be transformed to an equivalent area integral, and has been shown by Banks-Sills and Sherman in 1992 [17] to be objective with respect to the domain of integration. The area form of the integral is,

$$J = \int_A \left[\sigma_{ij} \frac{\partial u_i}{\partial x_1} - W \delta_{1j} \right] \frac{\partial q_1}{\partial x_j} dA \qquad (2.87)$$

where δ_{1j} is the Kronecker delta and q_1 is sufficiently smooth function (a weighting function) defined over the domain of integration. Physically, q_1 can be thought of as the displacement field due to a virtual crack extension. The domain of integration can be defined in two ways. Either an annular region that surrounds the crack tip (Figure 2.7a), or the inner contour can be contracted all the way to the crack tip (Figure 2.7b). The later case where only crack tip elements are used in the integration is particularly convenient to implement in a finite element program. These cases are conceptually similar to the virtual crack extension, but no actual physical displacements are imposed. The q_1 function is defined by prescribing nodal values that are interpolated over elements in the domain using the standard shape functions as shown in equation (2.88). Other quantities in equation (2.87) are easily computed in a finite element context using equation (2.89).

$$q_1 = \sum N_i q_{1i} \qquad \text{and} \qquad \frac{\partial q_1}{\partial x_j} = \sum \frac{\partial N_i}{\partial x_j} q_{1i} \tag{2.88}$$

$$W = \frac{1}{2}\sigma_{ij}\varepsilon_{ij} \tag{2.89}$$

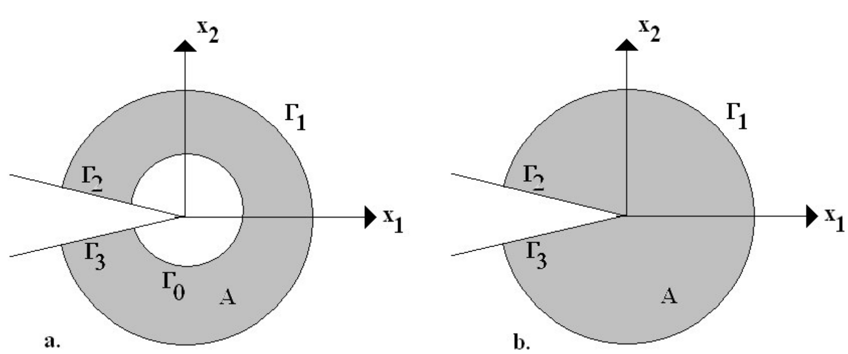

Figure 2.7: Domain of integration for an equivalent domain evaluation of J-integral

The q_1 function should have a value of one on the inner contour of the domain,

(Figure 2.7a), or the crack tip, (Figure 2.7b), and have a value of zero on the outer contour of the domain. A linear spatial variation is usually assumed between the two contours. For an eight nodded, isoparametric element, Banks-Sills and Sherman [17] used equation (2.87), where ξ and η are the coordinates of the parent element and q_{1i} are the values of q_1 at the element nodal points. In their investigation, 2 eight-node quarter-point elements at the crack tip were used and the rest of the mesh was composed by eight-node isoparametric elements. Virtual crack extension is shown in Figure 2.8.

$$q_1 = \sum_{i=1}^{8} N_i(\xi,\eta) q_{1i} \qquad (2.90)$$

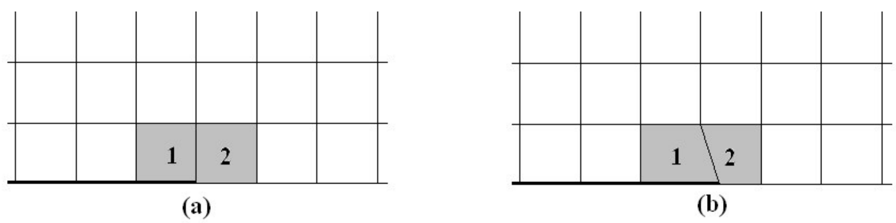

Figure 2.8: Mesh (a) before and (b) after virtual crack extension

For the specific case with 2 eight-node quarter-point elements, if the domain of integration is these 2 crack tip elements only, and 8-nodded quarter-point elements are used, the nodal values for q_1 should be 1 at the crack-tip node, 0.75 at the quarter-point nodes, and 0 at all other element nodes as shown in Figure 2.9. This maps the nodal points of the quarter-point elements during the virtual crack extension to positions such that the distorted element remains quarter-point. Other choices of q_1 lead to less accurate results [17].

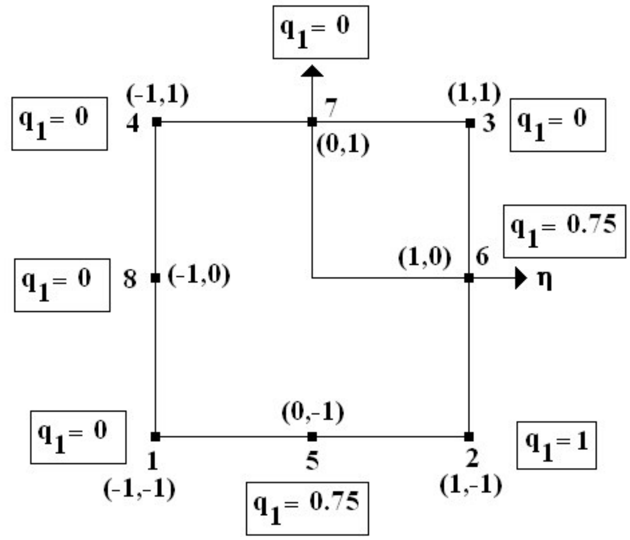

Figure 2.9: q_1 values for crack-tip parent element of element 1 shown in Figure 2.8

It is possible to implement the area J-integral over a region larger than the two elements adjacent to the crack tip. If this is the case, then the deformed elements due to the virtual crack extension will be the ones along the integration path. Elements inside, but not along, the integration path are translated but not deformed. For this case, a proper definition of q_{1i} is required. Banks-Sills and Sherman showed that nearly the same results are obtained whether integration is performed over two elements or many.

L. Banks-Sills and D. Sherman [17] considered a central crack and a single edge crack plate where a/b is 0.5 and h/b being 1. Here a is half the crack length for the central crack, and the total crack length for the single edge crack, b is half the width of the plate for the central crack, and the total width for the single edge crack, and finally h is the total height of both plates. For the central crack problem, only a quarter of the plate was considered and for the single edge crack case, half the plate was considered due to symmetry. In both cases, the same mesh was used, which included 100 rectangular elements, two of them being quarter-point elements. Six different integration paths were chosen, the smallest one being through the quarter-point elements. For the central crack case, the deviation between K_I calculated based on the line form of the J-integral and an exact solution [35] is 0.30%, 0.37%, 0.37%, 0.75%, 1.27% and 24.81%, the first one being along elements at the boundary of the plate and the last one along the two quarter-point elements. Based on the area form of the J-integral, the deviation is 0.30%, 0.30%, 0.30%, 0.30%, 0.30%, 0.22%. For the edge crack case, the deviation between K_I calculated based on the line form of the J-integral and a numerical solution [36] is 0.18%, 0.25%, 0.32%, 0.75%, 1.26% and 32.42%. Based on the area form of J, the deviation is 0.21%, 0.21%, 0.21%, 0.21%, 0.21% and 0.14%.

Prasad Pondugala [34] starts with the definition of J-integral given by equation (2.1). The path was selected such that it always coincides with $\xi = \xi_p = \text{constant}$, as shown in Figure 2.10. A unit normal n to the contour Γ (contour along which the J-integral is evaluated) is defined. In order to do this, two vectors A and B were defined along $\xi = \text{constant}$ and $\eta = \text{constant}$. The cross product of the vectors A and B gives the unit vector that is normal to these two vectors which is perpendicular to the plane of the element. This vector is given by equation (2.92). Now, the vector normal to the contour Γ which is along the curve defined by $\xi = \text{constant}$ is obtained by the cross product between vectors C and A. This is vector D and given by equation (2.93), and the unit vector is given by equation (2.94). The elemental arc length ds along the curve $\xi = \text{constant}$ is given by (2.96).

$$A^T = \left[\frac{\partial x}{\partial \eta}, \frac{\partial y}{\partial \eta}, 0 \right] \quad ; \quad B^T = \left[\frac{\partial x}{\partial \xi}, \frac{\partial y}{\partial \xi}, 0 \right] \tag{2.91}$$

$$C^T = \left[0, 0, \left(\frac{\partial x}{\partial \eta}\frac{\partial y}{\partial \xi} - \frac{\partial y}{\partial \eta}\frac{\partial x}{\partial \xi} \right) \right] \tag{2.92}$$

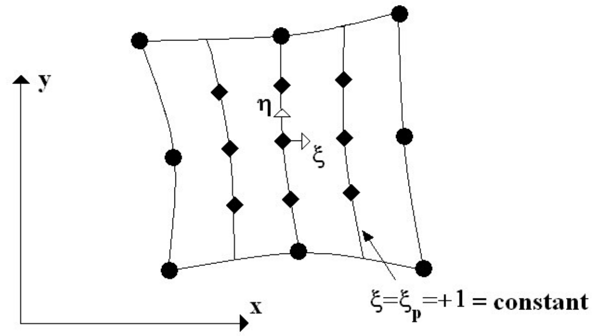

Figure 2.10: Gauss point numbering sequence

$$D = \begin{Bmatrix} \dfrac{\partial y}{\partial \eta}\left(\dfrac{\partial y}{\partial \eta}\dfrac{\partial x}{\partial \xi} - \dfrac{\partial x}{\partial \eta}\dfrac{\partial y}{\partial \xi} \right) \\ \dfrac{\partial x}{\partial \eta}\left(\dfrac{\partial x}{\partial \eta}\dfrac{\partial y}{\partial \xi} - \dfrac{\partial y}{\partial \eta}\dfrac{\partial x}{\partial \xi} \right) \\ 0 \end{Bmatrix} \tag{2.93}$$

$$n^T = [n_1, n_2, 0] = \left[\frac{D_1}{\sqrt{D_1^{\,2} + D_2^{\,2}}} \quad , \quad \frac{D_2}{\sqrt{D_1^{\,2} + D_2^{\,2}}} \quad , \quad 0 \right] \tag{2.94}$$

$$dy = \frac{\partial y}{\partial \eta} d\eta \,; \quad dx = \frac{\partial x}{\partial \eta} d\eta \tag{2.95}$$

$$ds = \sqrt{dx^2 + dy^2} = \left\{ \sqrt{\left(\frac{\partial x}{\partial \eta} \right)^2 + \left(\frac{\partial y}{\partial \eta} \right)^2} \right\} d\eta \tag{2.96}$$

The study is restricted to isotropic homogeneous plane stress linear elasticity, and substituting equations (2.94) and (2.96) into the definition of J-integral, equation (2.97) is obtained and the numerically integration is achieved by equation (2.98), in which $NGAUS$ represents the order of Gaussian numerical integration and I is evaluated at the Gaussian sampling points ξ_p and η_q. The term W_q is the weighting factor corresponding to η_q. The J-integral is obtained by accumulating the contributions from all sampling points by equation (2.98) from the path $\xi_p = \text{constant}$ through all the neighboring elements around the crack tip.

$$J^{(e)} = \int_{-1}^{1} \left\{ \begin{array}{l} \left[\sigma_{xx} \dfrac{\partial u}{\partial x} + \sigma_{xy} \left(\dfrac{\partial u}{\partial y} + \dfrac{\partial v}{\partial x} \right) + \sigma_{yy} \dfrac{\partial v}{\partial y} \right] \dfrac{\partial y}{\partial \eta} \\ -\left[\left(\sigma_{xx} n_1 + \sigma_{xy} n_2 \right) \dfrac{\partial u}{\partial x} + \right. \\ \left. \left(\sigma_{xy} n_1 + \sigma_{yy} n_2 \right) \dfrac{\partial v}{\partial x} \right] \sqrt{\left(\dfrac{\partial x}{\partial \eta} \right)^2 + \left(\dfrac{\partial y}{\partial \eta} \right)^2} \end{array} \right\} d\eta = \int_{-1}^{1} I d\eta \qquad (2.97)$$

$$J^{(e)} = \sum_{q=1}^{NGAUS} I\left(\xi_p, \eta_q \right) W_q \qquad (2.98)$$

A plate of unit thickness with a central crack subjected to uniform tensile loading was considered. Height, width and crack length are $2h = 50$, $2b = 20$ and $2a = 8$ respectively. A Young's modulus of $E = 10,000$ and Poisson's ratio of $\nu = 0.3$ were used. Due to symmetry, only a quarter of the plate was modeled. A total of 20 eight-node isoparametric elements were employed. Three different element paths (Element path 3 being closer to the crack tip) were considered, and through each of these element paths, three J-contours were obtained, corresponding to $\xi = -1$, $\xi = 0$ and $\xi = +1$ ($\xi = -1$ being closer to the crack tip). The solutions obtained were: for element path 1; 2.12, 1.02 and 1.84 % deviation, for element path 2; 2.38, 0.85 and 2.05 % deviation, and for element path 3; 5.73, -1.06 and 3.48 % deviation from previously reported numerical results [37].

2.5 Remarks on Chapter 2

1. It is important to clarify a very important misconception. The J-integral is thought of as a nonlinear elastic equivalent of the strain energy release rate , G , per unit thickness. This statement has been encountered in the published literature [1, 3, 42] and has lead to the belief that G is only valid for linear elastic behavior. In all three derivations presented in this work, it is shown that J-integral is equal to G by definition. Furthermore, G arrived from Griffith's energy balance approach, which is valid as long as the behavior remains elastic. It does not have to be linear [1, 3, 42]. Griffith showed that for the case presented in Figure 2.1,

$$G = \frac{\pi\sigma^2 a}{E} \quad \text{; isotropic homogeneous plane stress linear elasticity (infinite medium)} \tag{2.99}$$

$$G = \left(1-\nu^2\right)\frac{\pi\sigma^2 a}{E} \quad \text{; isotropic homogeneous plane strain linear elasticity (infinite medium)} \tag{2.100}$$

It is also important to mention a major contribution made my Irwin. He modified Griffith's theory by introducing the stress intensity factor K and presenting the "Irwin relationship",

$$G = \frac{{K_I}^2}{E} \quad \text{; isotropic homogeneous plane stress linear elasticity (infinite medium)} \tag{2.101}$$

$$G = \left(1-\nu^2\right)\frac{{K_I}^2}{E} \quad \text{; isotropic homogeneous plane strain linear elasticity (infinite medium)} \tag{2.102}$$

Now, equations (2.99) through (2.102) are valid only for isotropic homogeneous linear elastic behavior, but the concept of G is always valid as long as the behavior remains elastic. Furthermore, we note that since J equals G, we may write $J = G = K_I^2 / E$ for isotropic homogeneous plane stress linear elasticity, and $J = G = \left(1-\nu^2\right) K_I^2 / E$ for isotropic homogeneous plane strain linear elastic behavior.

2. A second issue to be discussed is Kanninen and Popelar's flawed derivation of the J-integral pointed out by Jin and Sun's work. The differentiation with respect to the crack length a has been performed within the integral signs and the divergence theorem has been used to evaluate the area integral. This is shown in equation (2.32). However, it is known that $\partial W / \partial a$ has a $1/r^2$ singularity at the crack tip (where r is the distance from the tip) in LEFM because $W \sim 1/r$, as $r \to 0$. Hence, the differentiation with respect to the crack length a cannot be directly performed within the area integral and the divergence theorem cannot be used directly. This is the reason why in equation (2.49), the area of integration A_0 is divided into A and A_h, where A_h is the area containing the singularity. Following the same reasoning, the very last step of Ewarlds and Wanhill's derivation is also flawed, more specifically equation (2.29). In this case, it is Green's theorem that is not applied properly.

3. Equation (2.67) also shows the use of Green's theorem, and the integrand on the right hand side is again $\partial W / \partial x$. However, this step is valid. The reason for this validity is that the integration is done over an area A^* which does not need to be the entire area of the body A_0. It only has to be the area (free of singularities) enclosed by a closed path Γ^*. Therefore, this area A^* could be the area enclosed by the closed path shown in Figure 2.5, which clearly exclude the crack tip singularity that is present if the crack shown in Figure 2.5 was a sharp crack and

LEFM was considered. Of course, if a smooth crack tip was considered, then the area of integration A^* could very well be the entire area of the body A_0.

4. As stated before, J-integral along a closed path is zero. A direct consequence of this is the proof of J-integral path independence. A key step in this proof is that $\bar{T} = 0$ and $dy = 0$ on the portions of path along the flat notch surfaces. If the notch considered was not a flat one, $\bar{T} = 0$ would still hold along the notch surfaces, but dy would not be zero. This means that the J-integral is only path independent if the section of the notch where J-integral values are computed is flat. Furthermore, the validity of this proof is only granted if two-dimensional deformation fields of materials exhibiting linear or nonlinear elastic behavior (reversible process) are considered.

5. Clearly the integration path Γ might be shrunk to the tip of a smooth-ended crack Γ_t, and since $\bar{T} = 0$, the J-integral would be the averaged measure of the strain on the crack tip $J = \int_{\Gamma_t} W dy$. This is not meaningful for a sharp crack. However, the treatment of blunt cracks is beyond the scope of this work.

6. The J-integral is the strain energy release rate per unit thickness, or the rate of change of the total potential energy for a crack extension in elastic materials under quasistatic conditions. Its path independency allows calculation along a contour remote from the crack tip. This is what makes the J-integral concept so attractive. The primary interest in discussing nonlinear materials lies with elastic-plastic behavior, particularly in relation to elastic-plastic fracture mechanics (EPFM). Contours can be chosen to contain only elastic loads and displacements, and the J-integral concept can be used in EPFM. Thus an elastic-plastic energy release rate can be obtained from an elastic calculation along a

contour for which loads and displacements are known. However, the extension of non-linear elastic to elasto-plastic behavior is beyond the scope of this work.

7. Many methods of obtaining K-solutions have been developed. Amongst all the techniques mentioned above, the J-integral approach is the most accurate and hence preferred. The implementation of the method is quite involved. The displacement correlation technique is the least accurate but is simple enough for hand calculations. Obtaining solutions for the J-integral in actual specimens turns out to be difficult. Some closed form expressions have been developed for very few standard specimens, however it is generally necessary to use computational methods such as finite element techniques. Using finite element processes, the J-integral concept can be used in LEFM to calculate stress intensity factors in structures that do not posses a closed form solution for K, and compare them with critical stress intensity factors K_C.

8. Special treatments and complicated modifications to Rice's original J-integral expression are being employed in the currently used computations to circumvent or alleviate the errors introduced in the J-integral computations. In addition, since theoretical solutions of singular BVP are not analytic at the crack tip due to the fact that solution gradients approach infinity at such points, quarter point elements, special basis functions and other special crack tip elements that incorporate the strength of the singularity are also utilized in the currently used computations.

Chapter 3
EQUATION CHAPTER 3 SECTION 1
Mathematical Models, Finite Element Formulations and J-integral Computations in *h,p,k* Framework

3.1 Mathematical Models

In the development of mathematical models we assume linear elasticity (i.e. small deformation, small strain) and hookean constitutive equations with isotropic and homogeneous material. We further assume the matter to be incompressible, i.e. volume-preserving, and hence the density remains constant during deformation. Due to linear elasticity assumptions, the deformed coordinates $\{\bar{x}\} = [\bar{x}, \bar{y}, \bar{z}]^t$ and undeformed coordinates $\{x\} = [x, y, z]^t$ of a material particle remain the same. Hence the Jacobian is,

$$[J] = \left[\frac{\bar{x}, \bar{y}, \bar{z}}{x, y, z}\right] = [I] \tag{3.1}$$

Therefore,

$$|J| = 1 \tag{3.2}$$

Thus, for this type of of deformation, Lagrangian and Eulerian descriptions are identical.

Continuity Equation:

Conservation of mass during deformation yields,

$$\rho dV = \bar{\rho} d\bar{V} \tag{3.3}$$

Since $dV = |J| d\bar{V} = d\bar{V}$ due to (3.2), equation (3.3) reduces to,

$$\rho = \bar{\rho} \tag{3.4}$$

Momentum Equations:

Let $\{u_i\} = \vec{u} = \mathbf{u} = [u, v, w]^t$ be the displacement of a material particle $P(x, y, z)$, $\{v_i\} = \vec{v} = \mathbf{v} = \left[v_x, v_y, v_z\right]^t$ be its velocities given by equation (3.5), and $\vec{F}^b = \left[F_x^b, F_y^b, F_z^b\right]^t$ be the body forces per unit mass in x, y, z directions. The application of Newton's second law to a control volume dV (or $d\bar{V}$) gives the momentum equations (3.6).

$$v_i = \frac{\partial u_i}{\partial t} \tag{3.5}$$

$$\rho \frac{\partial \mathbf{v}}{\partial t} - \nabla . \boldsymbol{\sigma} - \vec{F}^b \rho = 0 \tag{3.6}$$

Substitution of equation (3.5) into equation (3.6) gives,

$$\rho \frac{\partial^2 \mathbf{u}}{\partial t^2} - \nabla . \boldsymbol{\sigma} - \vec{F}^b \rho = 0 \tag{3.7}$$

which in Einstein notation can be expressed as equation (3.8).

$$\rho \frac{\partial^2 u_i}{\partial t^2} - \frac{\partial \sigma_{ij}}{\partial x_j} - F_i^b \rho = 0; \qquad i, j = 1,2,3 \tag{3.8}$$

In equation (3.8), σ_{ij} are Cauchy stresses. If we consider a stationary process (invariant of time), and two dimensional elasticity, i.e. $i = 1,2$ and $j = 1,2$, then equation (3.8) reduces to equation (3.9).

$$\frac{\partial \sigma_{ij}}{\partial x_j} + F_i^b \rho = 0; \qquad i, j = 1,2 \tag{3.9}$$

Constitutive Equations:

The constitutive equations are a relationship between Cauchy stresses σ_{ij} and Cauchy strains ε_{ij}. For hookean solids we can write,

$$\sigma_{ij} = c_{ijkl}\varepsilon_{kl} \tag{3.10}$$

in which c_{ijkl} is a fourth order tensor containing material behavior. For isotropic, homogeneous linear elastic solids (i.e. hookean), equation (3.10) reduces to (3.11) or (3.12), in which $[C] = [D]^{-1}$.

$$\{\sigma\} = [D]\{\varepsilon\} \tag{3.11}$$

$$\{\varepsilon\} = [C]\{\sigma\} \tag{3.12}$$

The stress and strain vectors are given by,

$$\{\sigma\} = \left[\sigma_{xx}, \sigma_{yy}, \sigma_{zz}, \tau_{yz}, \tau_{zx}, \tau_{xy}\right]^t \tag{3.13}$$

$$\{\varepsilon\} = \left[\varepsilon_{xx}, \varepsilon_{yy}, \varepsilon_{zz}, \gamma_{yz}, \gamma_{zx}, \gamma_{xy}\right]^t \tag{3.14}$$

where

$$\gamma_{ij} = 2\varepsilon_{ij} \tag{3.15}$$

For a 2-D case (x,y plane), equations (3.13) through (3.15) are reduced to:

$$\{\sigma\} = \left[\sigma_{xx}, \sigma_{yy}, \tau_{xy}\right]^t \tag{3.16}$$

$$\{\varepsilon\} = \left[\varepsilon_{xx}, \varepsilon_{yy}, \gamma_{xy}\right]^t \tag{3.17}$$

where

$$\gamma_{xy} = 2\varepsilon_{xy} \tag{3.18}$$

For two dimensional linear elasticity the strains are given by,

$$\varepsilon_{xx} = \frac{\partial u}{\partial x}, \qquad \varepsilon_{yy} = \frac{\partial u}{\partial y}, \qquad \gamma_{xy} = \frac{\partial u}{\partial y} + \frac{\partial v}{\partial x} \tag{3.19}$$

The material matrix $[C]$ for 2D plane strain linear elasticity can be written as,

$$[C]=\begin{bmatrix} C_{11} & C_{12} & C_{13} \\ C_{21} & C_{22} & C_{23} \\ C_{31} & C_{32} & C_{33} \end{bmatrix} = \frac{(1+\nu)}{E}\begin{bmatrix} 1-\nu & -\nu & 0 \\ -\nu & 1-\nu & 0 \\ 0 & 0 & 2 \end{bmatrix} \tag{3.20}$$

in which, E is modulus of elasticity and ν is Poisson's ratio. The material matrix $[D]$ is obtained by taking the inverse of $[C]$ and is given by equation (3.21).

$$[D]=\begin{bmatrix} D_{11} & D_{12} & D_{13} \\ D_{21} & D_{22} & D_{23} \\ D_{31} & D_{32} & D_{33} \end{bmatrix} = \frac{E}{(1+\nu)(1-2\nu)}\begin{bmatrix} 1-\nu & \nu & 0 \\ \nu & 1-\nu & 0 \\ 0 & 0 & \frac{1-2\nu}{2} \end{bmatrix} \tag{3.21}$$

In Einstein's notation, we can consolidate these equations in a compact form,

$$\frac{\partial \sigma_{ij}}{\partial x_j} + F_i^b \rho = 0; \qquad i,j = 1,2 \tag{3.22}$$

$$\sigma_{ij} = c_{ijkl}\varepsilon_{kl} \tag{3.23}$$

$$\varepsilon_{kl} = \frac{1}{2}\left(\frac{\partial u_k}{\partial x_l} + \frac{\partial u_l}{\partial x_k}\right); \qquad k,l = 1,2 \tag{3.24}$$

It can be shown that the relation presented in equation (3.23) is reduced $\sigma_i = \underset{\sim}{D}_{ik}\varepsilon_k$ where the indices $1,2,3$ in the stresses and strains represent xx, yy, xy respectively. $\underset{\sim}{D}_{ik}$ is the same as D_{ik} except $\underset{\sim}{D}_{33} = 2D_{33}$ due to ε_{xy}. Equations (3.22) through (3.24) provide complete mathematical description of the mathematical model for 2D plane strain linear elasticity.

3.2 Differential Forms of Mathematical Model Suitable for Finite Element Formulations

The specific form of partial differential equations (PDEs) in the mathematical models is important in constructing the finite element computational processes. We describe two such forms in the following that are used in the present work.

3.2.1 Strong Form of Governing Differential Equations

If we substitute ε_{kl} from (3.24) into (3.23), we obtain,

$$\sigma_{ij} = \frac{1}{2} c_{ijkl} \left(\frac{\partial u_k}{\partial x_l} + \frac{\partial u_l}{\partial x_k} \right) \tag{3.25}$$

Now, we can substitute σ_{ij} from (3.25) into (3.22). Then we obtain,

$$\frac{\partial}{\partial x_j} \left(\frac{1}{2} c_{ijkl} \left(\frac{\partial u_k}{\partial x_l} + \frac{\partial u_l}{\partial x_k} \right) \right) + F_i^b \rho = 0 \tag{3.26}$$

Equation (3.26) is a system of second order PDEs in displacements u and v. The expanded form of (3.26) is given by,

$$\begin{aligned} &\frac{\partial}{\partial x} \left(D_{11} \frac{\partial u}{\partial x} + D_{12} \frac{\partial v}{\partial y} \right) + \frac{\partial}{\partial y} \left(D_{33} \left(\frac{\partial u}{\partial y} + \frac{\partial v}{\partial x} \right) \right) + F_x^b \rho = 0 \\ &\frac{\partial}{\partial x} \left(D_{33} \left(\frac{\partial u}{\partial y} + \frac{\partial v}{\partial x} \right) \right) + \frac{\partial}{\partial y} \left(D_{12} \frac{\partial u}{\partial x} + D_{22} \frac{\partial v}{\partial y} \right) + F_y^b \rho = 0 \end{aligned} \tag{3.27}$$

Since D_{ik} are constant,

$$D_{11}\frac{\partial^2 u}{\partial x^2}+D_{33}\frac{\partial^2 u}{\partial y^2}+\left(D_{12}+D_{33}\right)\frac{\partial^2 v}{\partial y\partial x}+F_x^b\rho=0$$

$$D_{33}\frac{\partial^2 v}{\partial x^2}+D_{22}\frac{\partial^2 v}{\partial y^2}+\left(D_{12}+D_{33}\right)\frac{\partial^2 u}{\partial y\partial x}+F_y^b\rho=0 \qquad (3.28)$$

Both, equations (3.27) and (3.28) are a system of second order PDEs in displacements u and v. These will be referred to as strong form of GDEs. Symbolically we can write either one of them as,

$$\mathbf{A\Phi}-\mathbf{F}=0 \qquad (3.29)$$

3.2.2 Weak Form of Governing Differential Equations

The weak form of GDEs is a system of first order PDEs in the dependent variables. The incentive for constructing these is to be able to utilize C^{00} local approximations in the finite element processes (see chapter 4). We note that the equations derived in section (3.1) are a system of first order equations. Thus in this case we can use equations (3.22) and (3.25),

$$\frac{\partial\sigma_{ij}}{\partial x_j}+F_i^b\rho=0$$

$$\sigma_{ij}=\frac{1}{2}c_{ijkl}\left(\frac{\partial u_k}{\partial x_l}+\frac{\partial u_l}{\partial x_k}\right) \qquad (3.30)$$

Equations (3.30) is a system of first order PDEs in displacements u and v and stresses σ_{xx}, σ_{yy} and τ_{xy}. The expanded form of these equations are given by,

$$\frac{\partial \sigma_{xx}}{\partial x} + \frac{\partial \tau_{xy}}{\partial y} + F_x^b \rho = 0 \tag{3.31}$$

$$\frac{\partial \tau_{xy}}{\partial x} + \frac{\partial \sigma_{yy}}{\partial y} + F_y^b \rho = 0 \tag{3.32}$$

$$\sigma_{xx} = D_{11} \frac{\partial u}{\partial x} + D_{12} \frac{\partial v}{\partial y} \tag{3.33}$$

$$\sigma_{yy} = D_{12} \frac{\partial u}{\partial x} + D_{22} \frac{\partial v}{\partial y} \tag{3.34}$$

$$\tau_{xy} = D_{33} \left(\frac{\partial u}{\partial y} + \frac{\partial v}{\partial x} \right) \tag{3.35}$$

Symbolically we can write,

$$\underset{\sim}{\mathbf{A}} \underset{\sim}{\mathbf{\Phi}} - \underset{\sim}{\mathbf{F}} = 0 \tag{3.36}$$

3.3 Description of the Boundary Value Problem Associated with the Mathematical Model in Section 3.1

From section 3.2, the mathematical models can be written in two alternate forms,

$$\mathbf{A\Phi} - \mathbf{F} = 0 \quad \text{in } \Omega \tag{3.37}$$

$$\underset{\sim}{\mathbf{A}} \underset{\sim}{\mathbf{\Phi}} - \underset{\sim}{\mathbf{F}} = 0 \quad \text{in } \Omega \tag{3.38}$$

where Ω is the domain, and $\bar{\Omega} = \Omega \cup \Gamma$; Γ being the closed boundary of Ω.

For both forms of GDEs, we consider the following boundary conditions (two-dimensional case).

$$\begin{aligned} u &= u_0 \\ v &= v_0 \end{aligned} \qquad \text{on } \Gamma_1 \tag{3.39}$$

$$\begin{aligned} \sigma_{xx} n_x + \tau_{xy} n_y &= t_x \\ \tau_{xy} n_x + \sigma_{yy} n_y &= t_y \end{aligned} \qquad \text{on } \Gamma_2 \tag{3.40}$$

where $\Gamma = \Gamma_1 \cup \Gamma_2$, and $\{\vec{n}\} = \left[n_x, n_y \right]^t$ is a unit exterior normal to Γ_2, and t_x and t_y are tractions in x and y directions. The details are well known and are omitted for the sake of brevity [53].

In equation (3.40) we can also substitute second equation of (3.30) to obtain these in terms of gradients of u and v. This form of (3.40) is in fact needed if the strong form of GDEs (3.37) are used. Thus, we have two alternate descriptions of the two-dimensional BVP describing two-dimensional plane strain linear elasticity.

3.4 Finite Element Formulations of BVP Described in Section 3.3

Based on references [48, 49, 50], it can be shown that the differential operator $\mathbf{A}$ in the strong form of GDEs (3.37) is self-adjoint. Hence, (i) the integral form resulting from Galerkin method with weak form is variationally consistent (VC) when the functional $B(.,.)$ is symmetric. (ii) the integral form resulting from least squares process is also variationally consistent (VC). (iii) The integral forms resulting from all other methods of approximation are variationally inconsistent (VIC).

The differential operator $\underset{\sim}{\mathbf{A}}$ in the weak form of GDEs (3.38) is non-self-adjoint, hence the integral forms resulting from all methods of approximation except least squares process are variationally inconsistent [48, 49, 50]. The variationally consistent integral forms yield algebraic systems in which the coefficient matrices are symmetric and positive definite with real basis and have eigenvalues greater than zero. Such algebraic systems ensure a unique solution. VIC integral forms on the other hand yield algebraic systems in which the coefficient matrices are non-symmetric which may have partial or completely complex basis and the same holds for eigenvalues. A unique solution from such algebraic systems is not always ensured [48, 49, 50].

Based on the above discussion, we only consider (i) Galerkin method with weak form for the strong form of GDEs (3.37) with boundary conditions (3.39) and (3.40) (ii) Least square method for strong form of GDEs (3.37) as well as weak form of GDEs (3.38) with boundary conditions (3.39) and (3.40). In both cases we have VC integral forms.

3.4.1 Discretizations and Approximations

Let $\bar{\Omega}^T = \bigcup_e \bar{\Omega}^e$ be a discretization of $\bar{\Omega}$ in which $\bar{\Omega}^e = \Omega^e \cup \Gamma^e$ is an element e and Γ^e is the boundary of the element. Let Φ_h be the global approximation of Φ over $\bar{\Omega}^T$ and Φ_h^e be the local approximation of Φ over $\bar{\Omega}^e$. Then, $\Phi_h = \bigcup_e \Phi_h^e$. Furthermore, let $\Phi_h^e \in V_h$ be an approximation of Φ over $\bar{\Omega}^e$ in which V_h is subspace of an appropriate scalar product space. Φ is a vector of dependent variables which are u and v in case of the strong form of GDEs (3.37) and u, v, σ_{xx}, σ_{yy} and σ_{xy} in case of the weak form of GDEs (3.38).

In the following we present details of constructing integral forms using the Galerkin method with weak form for strong form of GDEs (3.37) and the least square method using strong form of GDEs (3.37) and weak form of GDEs (3.38).

3.4.2 Galerkin Method with Weak Form Using Strong Form of GDEs (3.37)

We consider the strong form of GDEs (3.27),

$$\frac{\partial}{\partial x}\left(D_{11}\frac{\partial u}{\partial x} + D_{12}\frac{\partial v}{\partial y}\right) + \frac{\partial}{\partial y}\left(D_{33}\left(\frac{\partial u}{\partial y} + \frac{\partial v}{\partial x}\right)\right) + F_x^b \rho = 0 \tag{3.41}$$

$$\frac{\partial}{\partial x}\left(D_{33}\left(\frac{\partial u}{\partial y} + \frac{\partial v}{\partial x}\right)\right) + \frac{\partial}{\partial y}\left(D_{12}\frac{\partial u}{\partial x} + D_{22}\frac{\partial v}{\partial y}\right) + F_y^b \rho = 0 \tag{3.42}$$

which can be written as,

$$A_1\Phi + F_x^b \rho = 0, \qquad A_2\Phi + F_y^b \rho = 0 \qquad \text{with} \quad \Phi = [u, v]^t \tag{3.43}$$

with boundary conditions,

$$\begin{aligned} u &= u_0 \\ v &= v_0 \end{aligned} \qquad \text{on } \Gamma_1 \tag{3.44}$$

$$\begin{aligned} &\left(D_{11}\frac{\partial u}{\partial x} + D_{12}\frac{\partial v}{\partial y}\right) n_x + D_{33}\left(\frac{\partial u}{\partial y} + \frac{\partial v}{\partial x}\right) n_y = t_x \\ &D_{33}\left(\frac{\partial u}{\partial y} + \frac{\partial v}{\partial x}\right) n_x + \left(D_{12}\frac{\partial u}{\partial x} + D_{22}\frac{\partial v}{\partial y}\right) n_y = t_y \end{aligned} \qquad \text{on } \Gamma_2 \tag{3.45}$$

Let $\Phi_h = [u_h, v_h]^t$ over $\bar{\Omega}^T$ and $\Phi_h^e = [u_h^e, v_h^e]^t$ over $\bar{\Omega}^e$ be approximations of $\Phi = [u, v]^t$.

In the Galerkin method with weak form over $\bar{\Omega}^T$, we begin with (based on fundamental lemma [51, 52, 53]),

$$\left(A_1\Phi_h + F_x^b\rho \ , \ w_1\right)_{\bar{\Omega}^T} = 0 \tag{3.46}$$

$$\left(A_2\Phi_h + F_y^b\rho \ , \ w_2\right)_{\bar{\Omega}^T} = 0 \tag{3.47}$$

where w_1 and w_2 are test functions such that $w_1 = \delta u_h$ and $w_2 = \delta v_h$. Performing integration by parts once, we obtain,

$$B_1\left(u_h, v_h; w_1\right) = l_1\left(w_1\right) \tag{3.48}$$

$$B_2\left(u_h, v_h; w_2\right) = l_2\left(w_2\right) \tag{3.49}$$

where

$$B_1\left(u_h, v_h; w_1\right) = \int_{\bar{\Omega}^T} \left(\frac{\partial w_1}{\partial x}\left(D_{11}\frac{\partial u_h}{\partial x} + D_{12}\frac{\partial v_h}{\partial y} \right) + \frac{\partial w_1}{\partial y}\left(D_{33}\left(\frac{\partial u_h}{\partial y} + \frac{\partial v_h}{\partial x} \right)\right)\right) d\Omega \tag{3.50}$$

$$B_2\left(u_h, v_h; w_2\right) = \int_{\bar{\Omega}^T} \left(\frac{\partial w_2}{\partial x}\left(D_{33}\left(\frac{\partial u_h}{\partial y} + \frac{\partial v_h}{\partial x} \right)\right) + \frac{\partial w_2}{\partial y}\left(D_{12}\frac{\partial u_h}{\partial x} + D_{22}\frac{\partial v_h}{\partial y} \right)\right) d\Omega \tag{3.51}$$

$$l_1\left(w_1\right) = \oint_{\Gamma} w_1 q_x^n d\Gamma + \int_{\bar{\Omega}^T} F_x^b \rho w_1 d\Omega \tag{3.52}$$

$$l_2(w_2) = \oint_{\Gamma} w_2 q_y^n d\Gamma + \int_{\bar{\Omega}^T} F_y^b \rho w_2 d\Omega \tag{3.53}$$

where the secondary variables q_x^n and q_y^n are,

$$q_x^n = \left(D_{11} \frac{\partial u_h}{\partial x} + D_{12} \frac{\partial v_h}{\partial y} \right) n_x + D_{33} \left(\frac{\partial u_h}{\partial y} + \frac{\partial v_h}{\partial x} \right) n_y \tag{3.54}$$

$$q_y^n = D_{33} \left(\frac{\partial u_h}{\partial y} + \frac{\partial v_h}{\partial x} \right) n_x + \left(D_{12} \frac{\partial u_h}{\partial x} + D_{22} \frac{\partial v_h}{\partial y} \right) n_y \tag{3.55}$$

The integral forms (3.48) and (3.49) are weak forms of (3.46) and (3.47). Equations (3.48) and (3.49) over $\bar{\Omega}^T$ containing M elements can be written as,

$$\sum_{e=1}^{M} B_1^e \left(u_h^e, v_h^e \ ; \ w_1^e \right) = \sum_{e=1}^{M} l_1^e \left(w_1^e \right) \tag{3.56}$$

$$\sum_{e=1}^{M} B_2^e \left(u_h^e, v_h^e \ ; \ w_2^e \right) = \sum_{e=1}^{M} l_2^e \left(w_2^e \right) \tag{3.57}$$

where $B_1^e(\ . \ ; \ . \ ) = l_1^e(\ . \ )$ and $B_2^e(\ . \ ; \ . \ ) = l_2^e(\ . \ )$ hold for an element e, and $w_1^e = \delta u_h^e$ and $w_2^e = \delta v_h^e$.

Approximation Spaces and Local Approximations

In this section we discuss approximation spaces and local approximation for u and v over $\bar{\Omega}^e$.

(1) First, we consider integrals in (3.46) and (3.47). Since the operators A_1 and A_2 contain derivatives of u and v up to second order, the continuity of integrand over $\bar{\Omega}^T$ requires $\Phi_h \in C^{JJ}(\bar{\Omega}^T)$; $J \geq 2$ in which $J = 2$ is minimally conforming. When $J \geq 2$ the integrals in (3.46) and (3.47) are Riemann. If we maintain $\Phi_h^e \in C^{JJ}(\bar{\Omega}^e)$; $J \geq 2$ in (3.56) and (3.57), then $\Phi_h \in C^{JJ}(\bar{\Omega}^T)$ obviously holds. In this case (3.46) and (3.47) can be recovered from (3.48) and (3.49) by reverse integration by parts. All integrals in the entire process are Riemann with this choice of Φ_h^e.

(2) If we just consider the integrals in the weak form (3.48) and (3.49) obtained after performing integration by parts once, then the continuity of the integrand requires $\Phi_h \in C^{JJ}(\bar{\Omega}^T)$; $J \geq 1$ in which $J = 1$ is minimally conforming i.e. lowest value of J for which the integrals are Riemann. With the choice of $J \geq 1$ the integrals in (3.48) and (3.49) are Riemann for all values of J. However, when $J = 1$, the integrals in (3.46) and (3.47) are Lebesgue. In this case (3.46) and (3.47) are not recoverable precisely form (3.48) and (3.49) by reverse integration by parts. That is we can only go from (3.46) and (3.47) to (3.48) and (3.49) assuming Lebesgue measures in (3.46) and (3.47). Naturally coming back from (3.48) and (3.49) to (3.46) and (3.47) also requires similar assumption.

(3) If we choose $\Phi_h^e \in C^{00}(\bar{\Omega}^e)$, then the integrals in the weak form (3.48) and (3.49) are Lebesgue and we cannot go back to (3.46) and (3.47) by reverse integration by parts.

(4) Thus, we see that there are numbers of different choices for Φ_h^e approximation. However, only once choice, $\Phi_h^e \in C^{JJ}(\bar{\Omega}^e)$; $J \geq 2$ maintains all integrals Riemann and provides mathematically consistent formulation in which all integral forms are equivalent and precise in the sense of calculus of continuous and differentiable functions.

(5) Since the operators A_1 and A_2 both contain derivatives of u and v up to second order, we can choose equal order equal degree approximation for both u and v i.e. the approximation spaces for u_h^e and v_h^e can be the same. Based on references [48, 49, 50], we can write,

$$\Phi_h^e \in V_h \in H^{k,p}(\bar{\Omega}^e) = \left\{ w = w\big|_{\bar{\Omega}^e} \in C^{k-1}(\bar{\Omega}^e); w = w\big|_{\bar{\Omega}^e} \in P^p(\bar{\Omega}^e); p \geq 2k-1, k \geq 3 \right\} \quad (3.58)$$

and we can write,

$$\left.\begin{aligned} u_h^e &= \sum_{i=1}^{n} N_i^{k-1,p}(\bar{\Omega}^e) u_i^e \\ v_h^e &= \sum_{i=1}^{n} N_i^{k-1,p}(\bar{\Omega}^e) v_i^e \end{aligned}\right\} \quad ; \qquad N_i^{k-1,p}(\bar{\Omega}^e) \in V_h \qquad (3.59)$$

with this choice,

$$w_1^e = w_2^e = N_i^{k-1,p}(\bar{\Omega}^e) \ ; \ j = 1, 2, \ldots, n \qquad (3.60)$$

Since local approximation functions $N_i^{k-1,p}(\bar{\Omega}^e) \in V_h$; $u_h^e \in V_h$ and $v_h^e \in V_h$ naturally holds.

From (3.59) and (3.60) we can substitute in the weak form and obtain element matrices and vectors. The details are standard and hence not presented here.

3.4.3 Least Squares Finite Element Processes

In this section we consider least squares finite element formulations using strong form of GDEs (3.28) as well as weak form of GDEs ((3.31) - (3.35)). The details of the least squares process are identical regardless of the type of GDEs, only the choice of local approximations is effected. In the following we present details of least squares method applicable to both forms of GDEs.

Let Φ_h be an approximation of Φ in $\bar{\Omega}^T$ and let Φ_h^e be an approximation of Φ over $\bar{\Omega}^e$. Then by substituting Φ_h^e in these GDEs we obtain element error or residual equations.

$$E_i^e(\Phi_h^e) \quad \forall \ x, y \in \bar{\Omega}^e \quad ; \quad i = 1, 2, ..., ne \tag{3.61}$$

ne is the number of equations.

(i) Existence of functional $I(\Phi_h)$

$$I(\Phi_h) = \sum_{e=1}^{M} I^e = \sum_{e=1}^{M} \sum_{i=1}^{ne} \left(E_i^e, E_i^e \right) \tag{3.62}$$

Thus, the existence of the least squares functional is by construction.

(ii) Necessary condition

If $I(\Phi_h)$ is differentiable in Φ_h, then,

$$\delta I(\Phi_h) = \sum_{e=1}^{M} \sum_{i=1}^{ne} \left(E_i^e, \delta E_i^e \right) = 0 \tag{3.63}$$

is a necessary condition for an extrema of (3.62).

(iii) Sufficient condition or extremum principle

If $I(\Phi_h)$ is differentiable twice in Φ_h, (noting that $\delta^2 E_i^e = 0$ since the operator is linear) then,

$$\delta^2 I(\Phi_h) = \sum_{e=1}^{M} \sum_{i=1}^{ne} \left(\delta E_i^e, \delta E_i^e \right) > 0 \tag{3.64}$$

is a unique extremum principle and Φ_h from (3.63) minimizes $I(\Phi_h)$ in (3.62). The minima of $I(\Phi_h)$ is zero. When $I(\Phi_h) \to 0$, $E_i^e \to 0 \ \forall \ x, y \in \bar{\Omega}^e$, i.e. GDEs are satisfied in the pointwise sense.

In the case of the strong form of GDEs, we have:

$$\Phi_h^e = \left[u_h^e, v_h^e \right]^t \tag{3.65}$$

and the element residual equations $\forall \ x, y \in \bar{\Omega}^e$ are:

$$E_1^e = D_{11} \frac{\partial^2 u_h^e}{\partial x^2} + D_{33} \frac{\partial^2 u_h^e}{\partial y^2} + \left(D_{12} + D_{33} \right) \frac{\partial^2 v_h^e}{\partial y \partial x} + F_x^b \rho = 0 \tag{3.66}$$

$$E_2^e = D_{33} \frac{\partial^2 v_h^e}{\partial x^2} + D_{22} \frac{\partial^2 v_h^e}{\partial y^2} + \left(D_{12} + D_{33} \right) \frac{\partial^2 u_h^e}{\partial y \partial x} + F_y^b \rho = 0 \tag{3.67}$$

In this case $ne = 2$.

In the case of the weak form of GDEs, we have,

$$\Phi_h^e = \left[u_h^e, v_h^e, (\sigma_{xx})_h^e, (\sigma_{yy})_h^e, (\sigma_{xy})_h^e \right]^t \tag{3.68}$$

Therefore $ne = 5$.

It has been shown that equal order equal degree local approximation does yield a convergent least squares process. Thus local approximations for displacements and stresses can be easily written (similar to (3.59)). The element residual equations $\forall \; x, y \in \bar{\Omega}^e$ are,

$$E_1^e = \frac{\partial (\sigma_{xx})_h^e}{\partial x} + \frac{\partial (\sigma_{xy})_h^e}{\partial y} + F_x^b \rho \tag{3.69}$$

$$E_2^e = \frac{\partial (\sigma_{xy})_h^e}{\partial x} + \frac{\partial (\sigma_{yy})_h^e}{\partial y} + F_y^b \rho = 0 \tag{3.70}$$

$$E_3^e = (\sigma_{xx})_h^e - D_{11} \frac{\partial u_h^e}{\partial x} - D_{12} \frac{\partial v_h^e}{\partial y} \tag{3.71}$$

$$E_4^e = (\sigma_{yy})_h^e - D_{12} \frac{\partial u_h^e}{\partial x} - D_{22} \frac{\partial v_h^e}{\partial y} \tag{3.72}$$

$$E_5^e = (\sigma_{xy})_h^e - D_{33} \left(\frac{\partial u_h^e}{\partial y} + \frac{\partial v_h^e}{\partial x} \right) \tag{3.73}$$

Approximation Spaces and Local Approximations

The main issue here is the choice of the class of local approximations that influences whether the integrals are Riemann or Lebesgue. We discuss this in the following.

(1) In the case of the strong form of GDEs, $\Phi_h \in C^{JJ}(\bar{\Omega}^T)$; $J \geq 2$ ensures the integrals to be Riemann in the LSP and $J = 2$ corresponds to the minimum order of continuity. When $J = 1$, i.e. Φ_h of class C^{11}, the integrals in the LSP are Lebesgue therefore $C^{00}(\bar{\Omega}^T)$ approximations are not admissible in the LSP utilizing strong form of GDEs.

(2) The weak form of GDEs are a system of first order PDEs in displacements and stresses. The problems associated with these types of PDEs have been discussed by Surana et al [54]. Nonetheless, we consider the LSP for the weak form of GDEs due to the fact that in this case we do have a convergent finite element process. When $\Phi_h \in C^{JJ}(\bar{\Omega}^T)$; $J \geq 1$, the integrals are Riemann and $J = 1$ corresponds to minimally conforming order of global differentiability. If we choose $\Phi_h \in C^{00}(\bar{\Omega}^T)$, then all integrals in the LSP are Lebesgue.

The choice of the order of global differentiability has been discussed by Surana et al [48, 49, 50]. The authors have shown that the order of global differentiability ensuring Riemann integrals is highly meritorious over those in which the integrals are in the Lebesgue sense.

3.5 J-integral Computations in *h,p,k* Mathematical and Computational Finite Element Framework

3.5.1 J-integral Proposed by Rice [31]

In this section, first we revisit J-integral derivation proposed by Rice [31] to better understand its validity in context with numerically computed approximate solutions of the BVPs. Let,

$$W = W(x, y) = \int_0^{\varepsilon} \sigma_{ij} d\varepsilon_{ij} \tag{3.74}$$

be the strain energy density function in which ε_{ij} are components of an infinitesimal strain tensor $[\varepsilon]$. Based on Rice [31], we consider the following integral,

$$J = \int_{\Gamma} \left(W dy - \mathbf{T} \frac{d\mathbf{u}}{dx} d\Gamma \right) \tag{3.75}$$

where Γ is a continuous and differentiable curve surrounding the crack tip. The integral is being evaluated in counterclockwise sense starting from the lower flat notch surface and continuing along the path Γ to the upper flat surface. $\mathbf{T}$ is a traction vector defined according to the outward normal along Γ, $T_i = \sigma_{ij} n_j$, $\mathbf{u}$ is the displacement vector and $d\Gamma$ is an infinitesimal arc length segment of Γ.

To prove path independence of J-integral, consider any close contour Γ^* enclosing an area A^* in a two dimensional deformation in the absence of body forces. An application of Green's theorem to (3.75) along Γ^* gives (after substituting for T_i),

$$J = \int_{\Gamma^*} \left(W dy - T_i \frac{du_i}{dx} d\Gamma \right) = \int_{A^*} \left(\frac{\partial W}{\partial x} - \frac{\partial}{\partial x_j} \left(\sigma_{ij} \frac{\partial u_i}{\partial x} \right) \right) dx dy \tag{3.76}$$

but

$$\frac{\partial W}{\partial x} = \frac{\partial W}{\partial \varepsilon_{ij}} \frac{\partial \varepsilon_{ij}}{\partial x} = \sigma_{ij} \frac{\partial \varepsilon_{ij}}{\partial x} \tag{3.77}$$

$$\varepsilon_{ij} = \frac{1}{2} \left(\frac{\partial u_i}{\partial x_j} + \frac{\partial u_j}{\partial x_i} \right) \tag{3.78}$$

$$\frac{\partial W}{\partial x}=\frac{1}{2}\sigma_{ij}\left(\frac{\partial}{\partial x}\left(\frac{\partial u_i}{\partial x_j}\right)+\frac{\partial}{\partial x}\left(\frac{\partial u_j}{\partial x_i}\right)\right) \tag{3.79}$$

$$\frac{\partial W}{\partial x}=\frac{1}{2}\sigma_{ij}\left(\frac{\partial}{\partial x_j}\left(\frac{\partial u_i}{\partial x}\right)+\frac{\partial}{\partial x_i}\left(\frac{\partial u_j}{\partial x}\right)\right) \tag{3.80}$$

$$\frac{\partial W}{\partial x}=\sigma_{ij}\frac{\partial}{\partial x_j}\left(\frac{\partial u_i}{\partial x}\right) \tag{3.81}$$

Adding and subtracting $\frac{\partial \sigma_{ij}}{\partial x_j}\frac{\partial u_i}{\partial x}$ in equation (3.81) gives,

$$\frac{\partial W}{\partial x}=\sigma_{ij}\frac{\partial}{\partial x_j}\left(\frac{\partial u_i}{\partial x}\right)+\frac{\partial \sigma_{ij}}{\partial x_j}\frac{\partial u_i}{\partial x}-\frac{\partial \sigma_{ij}}{\partial x_j}\frac{\partial u_i}{\partial x} \tag{3.82}$$

or

$$\frac{\partial W}{\partial x}=\frac{\partial}{\partial x_j}\left(\sigma_{ij}\frac{\partial u_i}{\partial x}\right)-\frac{\partial \sigma_{ij}}{\partial x_j}\frac{\partial u_i}{\partial x} \tag{3.83}$$

By substituting equation (3.83) into equation (3.76) we obtain,

$$J=\int_{\Gamma^*}\left(Wdy-T_i\frac{du_i}{dx}d\Gamma\right)=-\int_{A^*}\frac{\partial \sigma_{ij}}{\partial x_j}\frac{\partial u_i}{\partial x}dxdy \tag{3.84}$$

Thus this integral on the LHS is zero if and only if $A_J=\int_{A^*}\frac{\partial \sigma_{ik}}{\partial x_k}\frac{\partial u_i}{\partial x}dxdy=0$.

We note that $\frac{\partial \sigma_{ik}}{\partial x_k}=0$ are equations of equilibrium (in the absence of body forces) which are satisfied exactly if and only if σ_{ik} (numerically computed displacements or the displacement solutions from any other method of approximation) corresponds to the theoretical solution $\mathbf{u}$. Assuming $\frac{\partial \sigma_{ik}}{\partial x_k} = 0$ in (3.84) and that (3.84) holds for any close contour Γ^*, Rice [31] showed that J-integral in (3.75) is path independent. Thus the path independence of J-integral requires that $\int_{A^*} \frac{\partial \sigma_{ik}}{\partial x_k} \frac{\partial u_i}{\partial x} dxdy = 0$ or a more strict condition $\frac{\partial \sigma_{ik}}{\partial x_k} = 0 \quad \forall \ x, y \in A^*$ must hold.

3.5.2 J-integral Computations in *h,p,k* Finite Element Framework

If one constructs a finite element mesh for the crack problem and chooses Γ as a contour (Figure 3.1), where,

$$\Gamma = \bigcup_e \Gamma_j^e \tag{3.85}$$

in which Γ_j^e is j^{th} boundary of element e contributing to a segment of Γ. Referring to Figure 3.1, we can rewrite (3.75) as follows,

$$J = \int_\Gamma \left(\frac{1}{2} \{\sigma\}^T \{\varepsilon\} n_y - \sigma_{ij} n_j \frac{du_i}{dx} \right) d\Gamma \tag{3.86}$$

where $\{\sigma\} = \left[\sigma_{xx}, \sigma_{yy}, \sigma_{xy} \right]^t$ and $\{\varepsilon\} = \left[\varepsilon_{xx}, \varepsilon_{yy}, \gamma_{xy} \right]^t$.

3.6 Remarks on Chapter 3

(1) Based on Rice [31], J-integral in (3.86) is path independent if $\int_{A^*} \frac{\partial \sigma_{ij}}{\partial x_j} \frac{\partial u_i}{\partial x} dxdy = 0$ or $\frac{\partial \sigma_{ij}}{\partial x_j} = 0 \;\; \forall \;\; x, y \in A^*$ where A^* is the area bounded by Γ^* This amount to ensuring that equilibrium equations are satisfied by the approximation of $\mathbf{\Phi}$. This is very significant. In simple terms, if the finite element solution does not satisfy equations of equilibrium, then J-integral is not path independent. Thus, for each path Γ used for computing J-integral values we must show that $\int_{A^*} \frac{\partial \sigma_{ij}}{\partial x_j} \frac{\partial u_i}{\partial x} dxdy = 0$ holds for each element in the area enclosed by Γ in the pointwise sense. This feature of the J-integral computations is a significant aspect of the work presented here.

(2) In order for the integral in (3.86) to be meaningful, the path Γ must be continuous and differentiable, otherwise $d\Gamma$ is not defined. This aspect is mostly ignored in the computations of J-integral using finite element processes. Numerical studies are presented in chapter 4 to illustrate significance of this aspect in the J-integral computations.

(3) If one considers calculus of continuous and differentiable functions, then integrand in (3.86) must at least be continuous so that integral over Γ is Riemann. Furthermore, regardless of the finite element formulation strategy we must show that $\int_{A^*} \frac{\partial \sigma_{ij}}{\partial x_j} \frac{\partial u_i}{\partial x} dxdy = 0$ holds, otherwise J-integral is not path independent.

   (a) Computations of $\frac{\partial \sigma_{ij}}{\partial x_j}$ requires $u_h, v_h \in C^{JJ}(\bar{\Omega}^T)$; $J \geq 2$ when using strong form of GDEs in LSP. In this case J-integral is automatically Riemann.

(b) When using weak form of GDEs in LSP, we could choose $u_h, v_h \in C^{JJ}(\bar{\Omega}^T)$; $J \geq 1$ so that J-integral is Riemann. In this case σ_{ij} can be calculated using interpolation functions or derivatives of u and v. When the solutions are not sufficiently converged these two approaches may not give the same stresses. Studies show that the approach using derivatives of displacements is more accurate in terms of J-integral computations

(c) In finite element processes using Galerkin method with weak form we could choose $u_h, v_h \in C^{JJ}(\bar{\Omega}^T)$; $J \geq 1$. For this choice the J-integral is Riemann.

(4) When the integrand in (3.86) exhibits discontinuity across two element boundaries for Γ (in tangential as well as normal direction to Γ), the integral over Γ in (3.86) becomes Lebesgue. The discontinuity of integrand in the tangential direction only exists at the corner nodes.

(5) When integrals are Riemann in (3.86), the choice of mating element boundaries constituting Γ is irrelevant. But when the integral over Γ is in Lebesgue sense, different choices will yield different results unless the finite element computations are sufficiently converged. Numerical studies are presented in Chapter 4 to illustrate this.

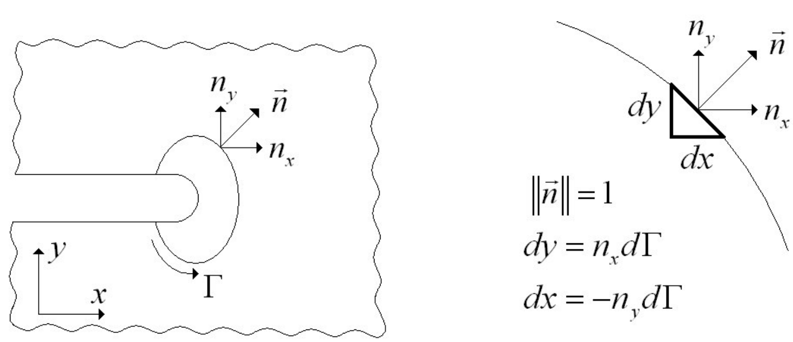

Figure 3.1: J-integral contour Γ

Chapter 4

EQUATION CHAPTER 4 SECTION 1

Numerical Studies: J-integral Computations in *h,p,k* Framework

4.1 Introduction

In this chapter various numerical studies are presented for J-integral computations in *h,p,k* framework. For this purpose we consider a model problem of a rectangular domain of width 2b and height 2h with sharp center crack of length $2a$ (Figure 4.1). Let the load σ consist of uniform tension in the y direction. We consider mode I fracture for linear elastic plane strain case and homogeneous isotropic material behavior. We have the following boundary conditions:

On AC : $v = 0$

$$\frac{\partial u}{\partial y} = 0 \quad \text{(due to symmetry)} \tag{4.1}$$

$$\tau_{xy} = 0 \quad \text{(due to symmetry)}$$

On AB : $\tau_{xy} = 0$ (free surface) (4.2)

$\sigma_{yy} = 0$ (no normal tractions)

On CF : $\tau_{xy} = 0$ (free surface) (4.3)

$\sigma_{xx} = 0$ (no normal tractions)

On DEF : $\sigma_{yy} = p$ (applied stress) (4.4)

$\tau_{xy} = 0$ (free surface)

On BD : $u = 0$

$$\frac{\partial v}{\partial x} = 0 \qquad \text{(due to symmetry)} \qquad (4.5)$$

$$\tau_{xy} = 0 \qquad \text{(due to symmetry)}$$

When $2b$ and $2h$ are large compared to $2a$, we can assume the crack of length 2a to be in an infinite domain i.e. in this case the size of the domain is sufficiently large so that boundaries do not influence the stress field created by the crack. In this case one could obtain the mode I stress intensity factor theoretically [1-3],

$$K_I = \sigma\sqrt{\pi a} \qquad (4.6)$$

where K_I is the mode I stress intensity factor and σ is the applied stress in the y direction far away from the crack. It can be shown that for mode I plane strain, the J-integral and K_I are related [1 - 3] by:

$$J = \frac{\left(1-\nu^2\right)}{E} K_I^{\,2} \qquad (4.7)$$

This means that for the case of $2b \to \infty$, $2h \to \infty$ (compared to $2a$), one could calculate J-integral numerically using any desired path (since it is path independent) and then use 4.2 to obtain K_I. If the numerical computations of J-integral do not have numerical errors, then K_I calculated using numerically computed J-integral must be identically same as given by (4.6) when $2b$, $2h$ are large compared to $2a$. This is an essential test to validate a numerical strategy of computing J-integrals to ensure that the stress intensity factor K_I using numerically calculated J-integral value and (4.7) indeed would not be in error.

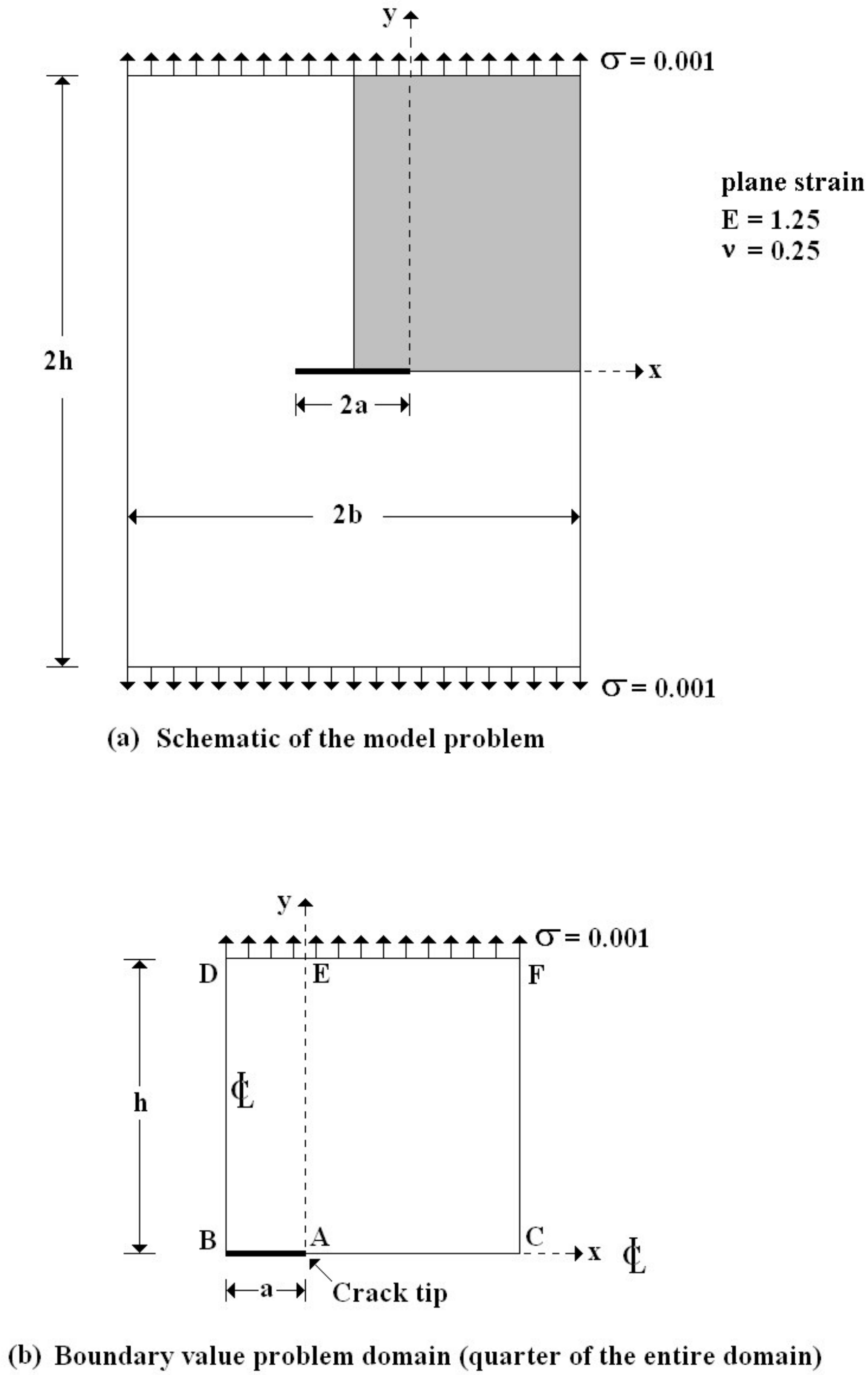

Figure 4.1: Schematic and domain of the model BVP (center crack panel)

In practical applications $2b$ and $2h$ may in fact be finite (henceforth referred to as finite medium) and small enough so that the stress field created by the crack may be influenced by the boundaries. In such cases (4.6) is not valid. To obtain accurate values of K_I in a finite medium we can proceed as follows.

(a) If a numerical computational strategy has been validated using (4.6) and (4.7) for an infinite medium then one could use this strategy to obtain J numerically and then use (4.7) to find K_I. By validation we mean that the choice of integral forms (in finite element context), *h* (mesh), *p* and *k* are appropriate enough to provide an exceptional correlation with (4.6) using (4.7) for an infinite medium. Then, one could use similar *h,p,k* and the same integral form for a finite medium with reasonable assurance of good accuracy of J-integral.

(b) In the second approach, based on σ and $2a$, one finds the value of K_I for an infinite medium. This obviously is not correct for the finite medium containing the crack at hand and hence must be corrected. Thus, if K_I is the theoretical value of the stress intensity factor for an infinite medium with crack size $2a$ (given by (4.6)) and if K_I^f is the stress intensity factor for the finite medium with same crack size then we could write:

$$K_I^f = K_I . C^f \tag{4.8}$$

where C^f is the correction factor that must be applied to K_I to account for the finite size of the medium. If has been shown that

$$C^f = C^f \left(b/a, h/a \right) \tag{4.9}$$

That is, the correction factor C^f depends upon the ratios b/a and h/a. For an infinite medium b/a and h/a approach infinity and hence C^f must approach unity in which case $K_I^f = K_I$. In the published work, expressions to calculate C^f values are reported which one could use to calculate K_I^f [44, 45]. However, these expressions are only available for the case of infinite strips (infinite height and finite width), where the analytical solution is expressed as a truncated infinite series. In such case, C^f is a function of b/a only. One of these available expressions [46] is Isida's equation (4.10). For the case of finite height and finite width, calculated values of C^f have been presented for specific values of b/a and h/a [44, 47] using numerical methods.

$$\begin{aligned} C^f = 1 &+ 0.5948\left(\frac{a}{b}\right)^2 + 0.4812\left(\frac{a}{b}\right)^4 + 0.3963\left(\frac{a}{b}\right)^6 \\ &+ 0.3367\left(\frac{a}{b}\right)^8 + 0.2972\left(\frac{a}{b}\right)^{10} + 0.2713\left(\frac{a}{b}\right)^{12} \\ &+ 0.2535\left(\frac{a}{b}\right)^{14} + 0.2404\left(\frac{a}{b}\right)^{16} + 0.2300\left(\frac{a}{b}\right)^{18} \end{aligned} \tag{4.10}$$

When analytical expressions for C^f are not available, the determination of C^f in the published work is based largely on numerical computations of K_I^f using J-integral and (4.7) which for a finite medium becomes,

$$J^f = \frac{\left(1-\nu^2\right)}{E}\left(K_I^f\right)^2 \tag{4.11}$$

The ratio of K_I^f / K_I is reported as correction factor C^f. In this approach the accuracy of C^f is highly dependent on the accuracy of J^f (J-integral for finite medium) which in tern is dependent on the computational methods employed in the numerical calculations. This procedure is dependent on many aspects and needs care to ensure that in fact J^f has the correct value so that C^f would have the right value for finite medium.

4.2 General Discussion Related to Present Numerical Studies

All numerical studies presented here are based on finite element computations in *h*,*p*,*k* framework i.e. we have control over discretization (*h*), degree of local approximation (*p*) and the global differentiability of local approximation (*k*-1). Since the numerical studies consider 2-D plane strain linear elastic behavior with homogeneous and isotropic medium, the differential operator (strong form of GDEs) in the description of the associated BVP is self-adjoint. Hence, the integral forms based on Galerkin method with weak form (Gal/WF) as well as last squares processes (LSP) are variationally consistent (VC). Thus, both approaches produce symmetric positive definite algebraic systems in the finite element computations. As shown in chapter 3, in LSP one could use weak form of GDEs (i.e. PDEs in displacements u and v, and stresses σ_{ij}) or strong form of GDEs (i.e. PDEs in displacements u and v). Both forms of GDEs and the associated finite element processes were presented in chapter 3. We make some important remarks.

Remarks:

(1) In Gal/WF the integrand in the integral form contains fist order derivatives of displacements as well as the test function. Hence approximations u_h and v_h of class $C^{11}(\bar{\Omega}^e)$ would yield Riemann integrals in the weak integral form but with these approximations the computation of residuals from the equilibrium equations would be in the Lebesgue sense.

(2) If we use u_h and v_h of class $C^{00}(\bar{\Omega}^e)$, then the integrals in weak form for Gal/WF would be in the Lebesgue sense and the computation of A_J is not possible.

(3) When using strong form of GDEs in LSP, u_h and v_h of class $C^{22}(\bar{\Omega}^e)$ would yield Riemann integrals in the integral form as well as in the computations of A_J. On the other hand, when u_h and v_h are of class $C^{00}(\bar{\Omega}^e)$, integrals in the LSP are in the Lebesgue sense and residual computations become Lebesgue.

(4) In case of weak form of GDEs in LSP, one could use u_h, v_h and $(\sigma_{ij})^h$ of class $C^{11}(\bar{\Omega}^e)$, in which case all integrals are Riemann, and when the local approximations for u_h and v_h, and $(\sigma_{ij})^h$ are of class $C^{00}(\bar{\Omega}^e)$, the integrals in the LSP and residual computations become Lebesgue.

(5) The choice of Riemann or Lebesgue measure is not arbitrary. Riemann integrals preserve physics in the computations for coarser discretizations and lower *p*-levels where as Lebesgue measures can give spurious results. Upon convergence i.e. solutions independent of *h* and *p*, the Lebesgue measures obviously approach Riemann.

(6) Another significant point to note is that for the J-integral to be path independent (see chapter 3), we must show that,

$$A_J = \int_{A^*} \frac{\partial \sigma_{ik}}{\partial x_k} \frac{\partial u_i}{\partial x} d\Omega = 0 \tag{4.12}$$

The continuity of the integrand in (4.12) ensures that (4.12) is in Riemann sense and requires σ_{ij} to be of class $C^{11}(\bar{\Omega}^e)$ which implies that u_h and v_h must be of class $C^{22}(\bar{\Omega}^e)$ in Gal/WF and LSP using strong form of GDEs. In case of LSP using weak form of GDEs, σ_{ij} can be of class $C^{11}(\bar{\Omega}^e)$. (this also has some consequences [48, 49,50, 54]).

(7) The computation of J-integral requires the path Γ to be continuous and differentiable (see chapter 3). Otherwise the J-integral is not defined.

(8) Based on (6) and (7) it is straight forward to conclude that if J-integral computations are to be done accurately then: (i) (4.12) must hold (ii) integrand in the J-integral must be continuous along the path Γ as well as normal to the path (iii) the path Γ must be continuous and differentiable (iv) we must show that the field used in computing J-integral is independent of *h,p* and *k*. When all of the above hold we have the right value of J^f for a finite medium and we could calculate K_I^f using (4.11).

The numerical studies presented in this thesis are designed to illustrate the various aspect described above. Accurate computation of J^f and hence K_I^f is possible when all of the above requirements are met in the computations.

4.3 Outline of Numerical Studies

The following is an outline of the numerical studies presented in this thesis.

Case (a) Integral form: Gal/WF

h-convergence studies

Solution classes: $C^{00}(\bar{\Omega}^e)$, $C^{11}(\bar{\Omega}^e)$

p-level: 5

$a = 0.4$, $b = 0.8$, $h = 0.7$

$E = 1.25$, $\nu = 0.25$, $\sigma = 0.001$

Meshes: 45, 180, 444 element graded discretizations

Case (b) Integral form: Gal/WF

Influence of h/a for large b/a (6) on J-integral computations

Solution classes: $C^{11}(\bar{\Omega}^e)$

p-level: 5

$a = 0.4$, $a = 1.2$

$E = 1.25$, $\nu = 0.25$, $\sigma = 0.001$

Meshes: 180 element graded discretizations at the zone of interest and coarser rectangular element mesh for the remainder of the domain

Case (c) Integral form: Gal/WF

Influence of b/a for large h/a (12) on J-integral computations

Solution classes: $C^{11}(\bar{\Omega}^e)$

p-level: 5

$a = 0.4$, $a = 1.2$

$E = 1.25$, $\nu = 0.25$, $\sigma = 0.001$

Meshes: 180 element graded discretizations at the zone of interest and coarser rectangular element mesh for the remainder of the domain

Case (d) Integral form: Gal/WF

Influence of solutions of higher order global differentiability on J-integral computations

$a = 0.4$, $b/a = 16$, $h/a = 35$ (close to infinite medium)

$E = 1.25$, $\nu = 0.25$, $\sigma = 0.001$

Meshes: 180 element graded discretizations at the zone of interest
and coarser mesh for the remainder of the domain

We study the following classes of solutions and *p*-levels,

$C^{00}(\bar{\Omega}^e)$; *p*-level: 3,5,7

$C^{11}(\bar{\Omega}^e)$; *p*-level: 3,5,7

$C^{22}(\bar{\Omega}^e)$; *p*-level: 5,7

$C^{33}(\bar{\Omega}^e)$; *p*-level: 7

Case (e) Integral form: Gal/WF

Influence of non differentiable integral paths on J-integral computations

Solution classes: $C^{11}(\bar{\Omega}^e)$

p-level: 5

$a = 0.4$, $b/a = 16$, $h/a = 35$ (close to infinite medium)

$E = 1.25$, $\nu = 0.25$, $\sigma = 0.001$

Meshes: 180 element graded discretizations at the zone of interest
and coarser mesh for the remainder of the domain

Case (f) Integral form: Gal/WF

Influence of differentiable but non circular paths on J-integral computations

Solution classes: $C^{11}(\bar{\Omega}^e)$

p-level: 5

$a = 0.1$, $b/a = 8$, $h/a = 7$ (half circular-half elliptical paths)

$a = 0.4$, $b/a = 8$, $h/a = 7$ (circular paths)

$E = 1.25$, $\nu = 0.25$, $\sigma = 0.001$

Meshes: 480, 1920 element graded discretizations

180 element graded discretizations at the zone of interest
and coarser mesh for the remainder of the domain

Case (g) Integral form: LSP using weak form of GDEs

Influence of solutions of higher order global differentiability on J-integral computations

$a = 0.4$, $b/a = 16$, $h/a = 35$ (close to infinite medium)

$E = 1.25$, $\nu = 0.25$, $\sigma = 0.001$

Meshes: 180 element graded discretizations at the zone of interest and coarser mesh for the remainder of the domain

We study the following classes of solutions and *p*-levels,

$C^{00}(\bar{\Omega}^e)$; *p*-level: 3,5,7

$C^{11}(\bar{\Omega}^e)$; *p*-level: 3,5,7

$C^{22}(\bar{\Omega}^e)$; *p*-level: 5,7

$C^{33}(\bar{\Omega}^e)$; *p*-level: 7

In all numerical studies we employ nine-nodes *p*-version elements of class $C^{JJ}(\bar{\Omega}^e)$ and choose J as indicated with each study listed above.

4.4 Case (a); Integral Form: Gal/WF; *h*-convergence Studies

In this section we present a series of *h*-convergence studies using local approximations of classes $C^{00}(\bar{\Omega}^e)$ and $C^{11}(\bar{\Omega}^e)$ with *p*-level of 5. Choices of a, b/a and h/a are not critical i.e. for a given choice we wish to demonstrate *h*-convergence for a given *p*-level for the two classes of local approximations. We choose $a = 0.4$, $b = 0.8$, $h = 0.7$, $E = 1.25$ and $\nu = 0.25$, $\sigma = 0.001$. A quarter of the domain is modeled using 45, 180 and 444 element graded discretizations. We discuss the details of the discretizations in the following.

(i) The first mesh consist of a 45 element graded discretization. The details of the entire mesh are shown in Figure 4.2 (a). The mesh details at the crack tip are shown in Figure 4.2 (b). The path closest to the crack tip (path 1) has a circular radius of 0.0005. A total of 6 paths are used for J-integral computations. All paths are circular rings with radia listed in Table 4.1.

(ii) The second mesh consists of 180 element graded discretization. The details of the entire mesh are shown in Figure 4.3 (a). The mesh details at the crack tip are shown in Figure 4.3 (b). The path closest to the crack tip (path 1) has a circular radius of 0.000375. A total of 13 paths are used for J-integral computations. All paths are circular rings with radia listed in Table 4.2.

(iii) The third mesh consists of 444 element graded discretization. The details of the entire mesh are shown in Figure 4.4 (a). The mesh details at the crack tip are shown in Figure 4.4 (b). The path closest to the crack tip (path 1) has a circular radius of 0.000375. A total of 35 paths are used for J-integral computations. All paths are circular rings with radia listed in Table 4.3.

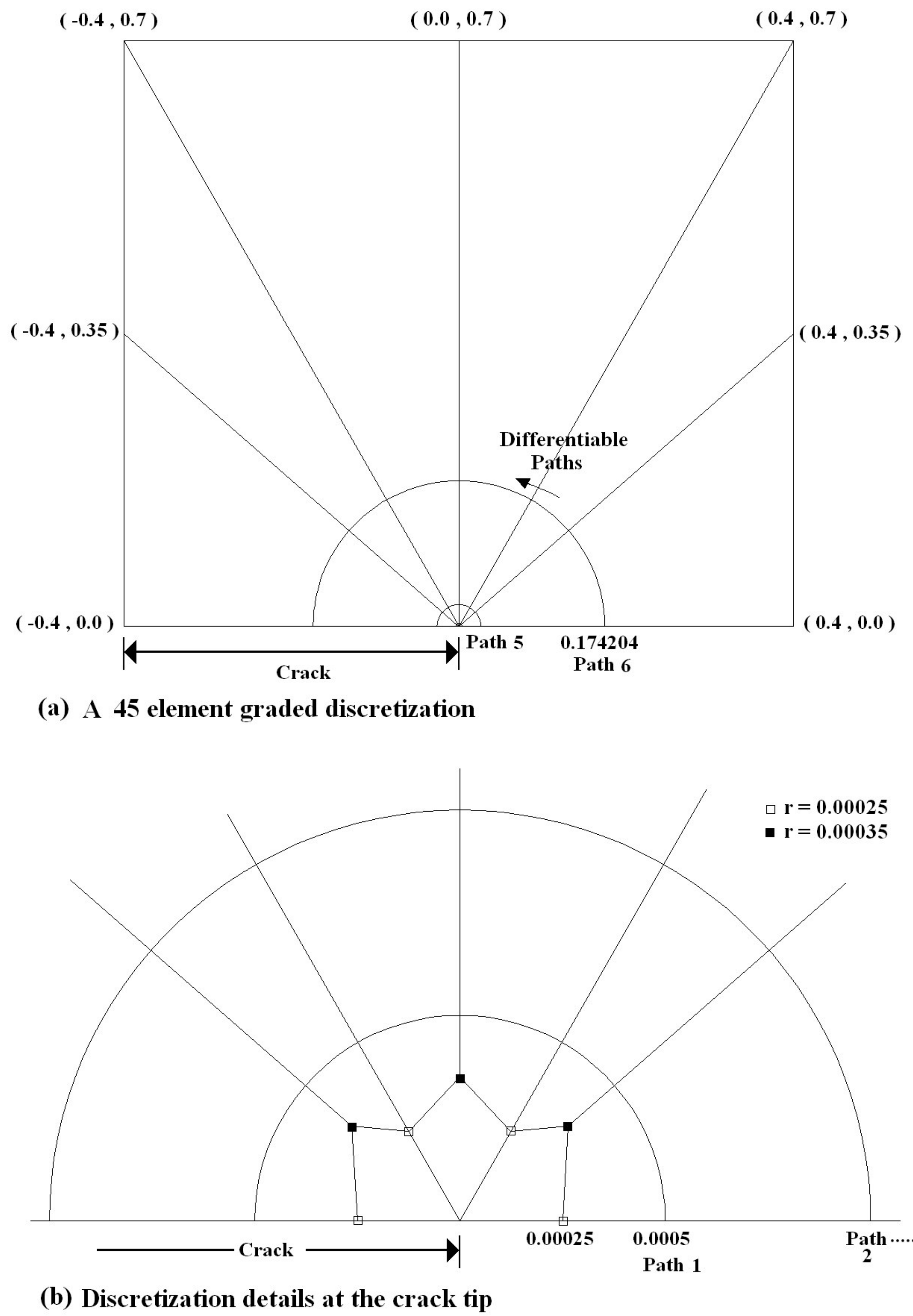

Figure 4.2: A 45 element graded finite element discretization of the quarter domain (a=0.4, b=0.8, h=0.7)

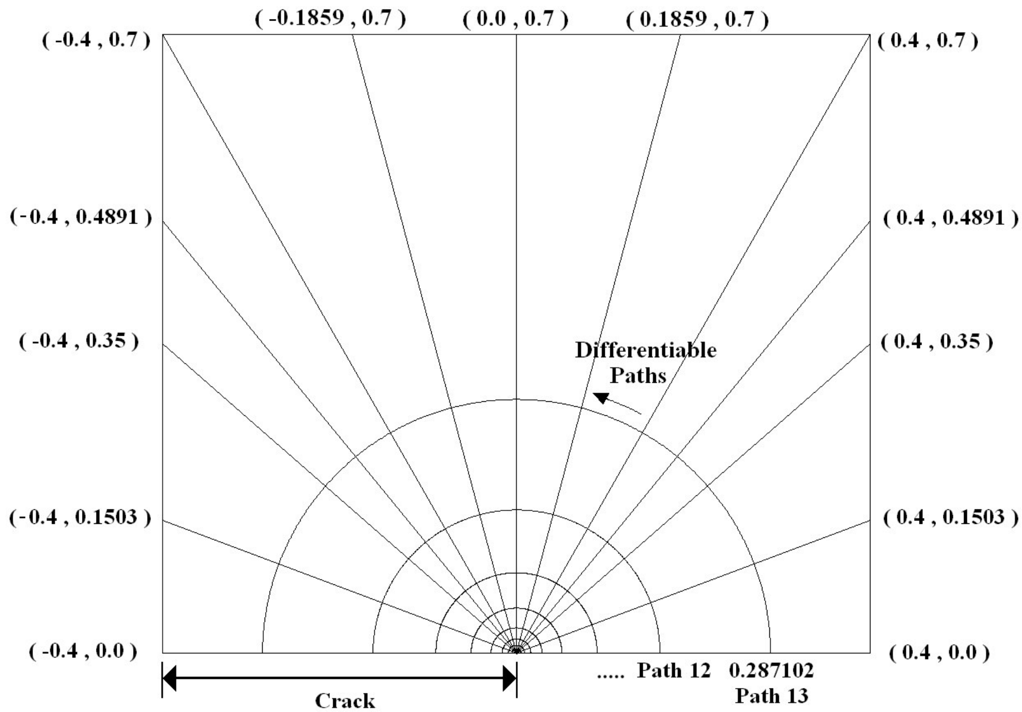

(a) A 180 element graded discretization

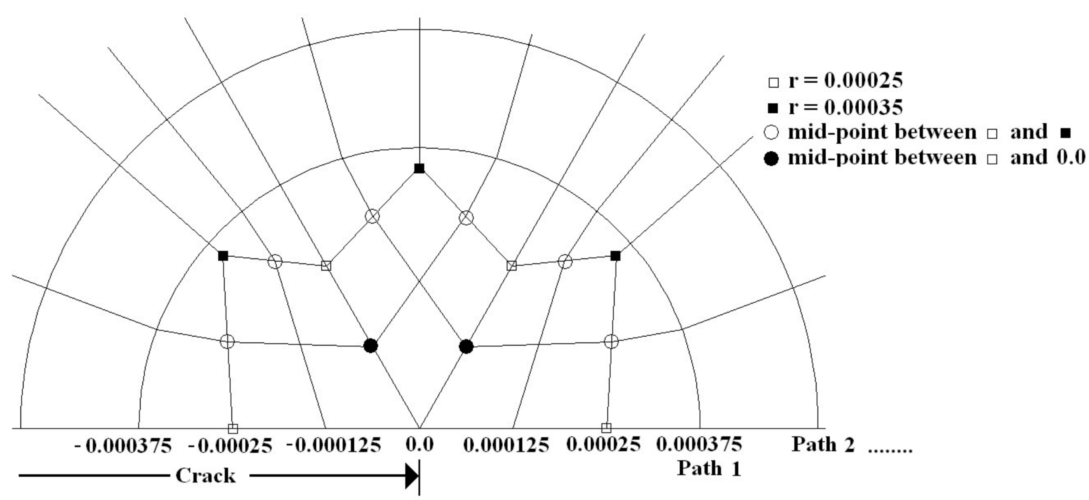

(b) Discretization details at the crack tip

Figure 4.3: A 180 element graded finite element discretization of the quarter domain (a=0.4, b=0.8, h=0.7)

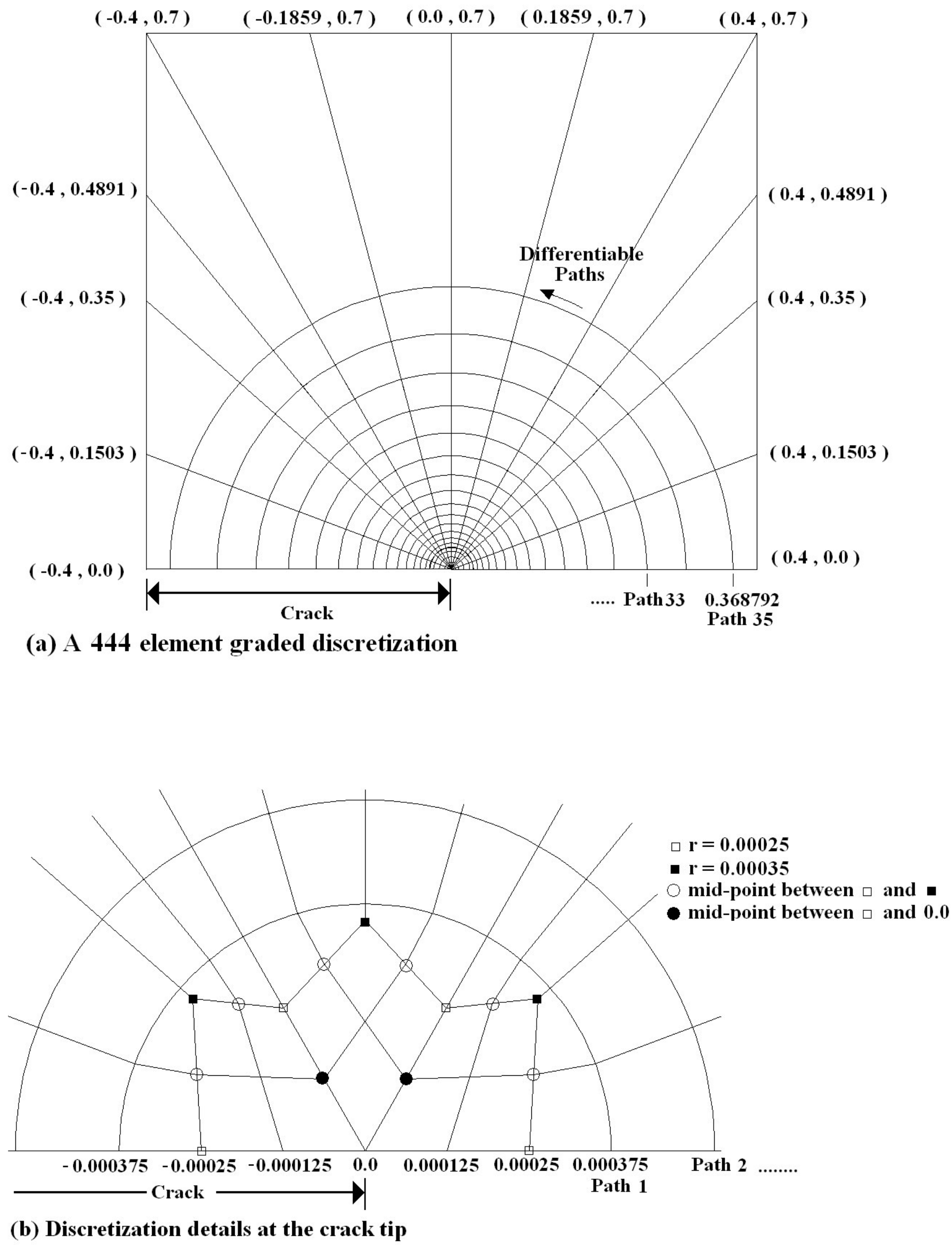

Figure 4.4: A 444 element graded finite element discretization of the quarter domain (a=0.4, b=0.8, h=0.7)

4.4.1 Solutions of class $C^{00}(\bar{\Omega}^e)$

For the three meshes shown in Figures 4.2 – 4.3, finite element solutions are computed at *p*-level of 5 using local approximations for u and v of class $C^{00}(\bar{\Omega}^e)$ and J-integral J^f is computed using these solutions. The paths used in J-integral computations are listed in Tables 4.1 to 4.3. Since in this case the local approximations are of class $C^{00}(\bar{\Omega}^e)$, the integrand in the J-integral computation is discontinuous at the inter-element boundaries along the paths as well as normal to the path. Therefore the J^f computations are in Lebesgue sense. Figure 4.5 shows that for a given path Γ there are two possible choices: Γ_1 or Γ_2. Due to the fact that integrand in the J-integral is not continuous normal to Γ, the choice of Γ_1 or Γ_2 may influence J^f if the solution of class $C^{00}(\bar{\Omega}^e)$ are not sufficiently converged. For this reason, J^f is computed using paths Γ_1 and Γ_2 for each path shown in Tables 4.1 – 4.3. The computed values of J^f using both Γ_1 and Γ_2 for the three discretizations are shown in Tables 4.1 – 4.3 for each path. To illustrate the influence of the choice of Γ_1 or Γ_2 for each path Γ, we define % difference in 2 ways:

$$\begin{array}{l} \%\ \ difference \\ using\ \ \Gamma_1\ \ reference \end{array} = \frac{\left(J^f\right)_{\Gamma_1} - \left(J^f\right)_{\Gamma_2}}{\left(J^f\right)_{\Gamma_1}}(100) \tag{4.13}$$

$$\begin{array}{l} \%\ \ difference \\ using\ \ \Gamma_2\ \ reference \end{array} = \frac{\left(J^f\right)_{\Gamma_2} - \left(J^f\right)_{\Gamma_1}}{\left(J^f\right)_{\Gamma_2}}(100) \tag{4.14}$$

These are also tabulated in tables 4.1 – 4.3 for each path for the three discretizations. We discuss the results in the following. In the case of the 45 element mesh, the influence of the choice of Γ_1 or Γ_2 can be clearly observed from the % differences due to the fact that for such coarse mesh the finite element solution is not sufficiently converged and hence the error caused due to Lebesgue measure depends on the choice of the path and is reflected in the % difference.

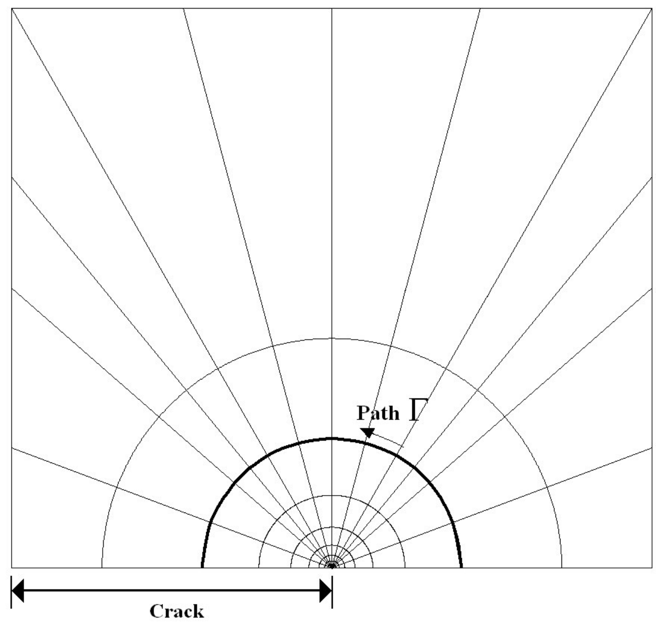

(a) Path Γ for J-integral computations

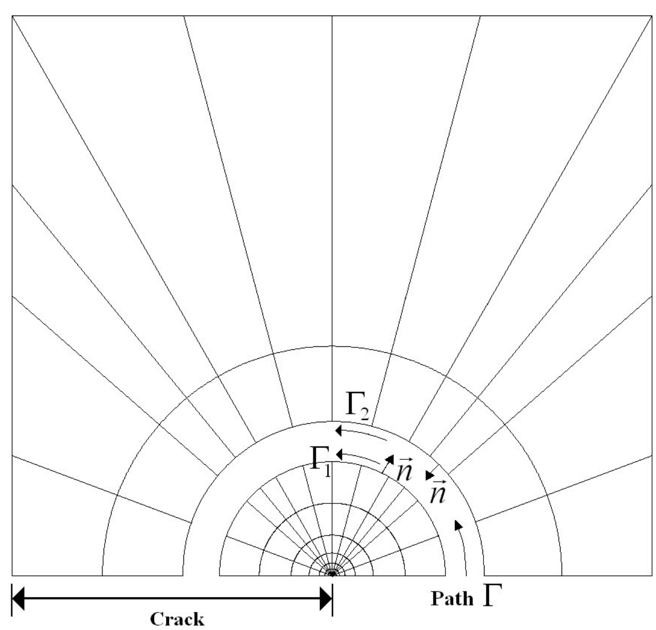

(b) Path Γ_1 or Γ_2 (two choices for Γ) for J-integral computations

Figure 4.5: Choice of paths for Γ: Γ_1 or Γ_2 for solutions of class C^{00}

Table 4.1: A 45 Element mesh (a=0.4, h=0.7, b=0.8) with Gal/WF: C^{00} solutions and p=5

Path	Radius	$J^f/2 : \Gamma_1$ path	$J^f/2 : \Gamma_2$ path	% Difference using Γ_1 as reference	% Difference using Γ_2 as reference	$C^f : \Gamma_1$ path	$C^f : \Gamma_1$ path
1	0.000500	8.19608E-07	9.53467E-07	-16.3321	14.0392	1.3188	1.4224
2	0.001000	9.55801E-07	9.55349E-07	0.0473	-0.0473	1.4242	1.4238
3	0.001500	9.55290E-07	9.54264E-07	0.1074	-0.1076	1.4238	1.4230
4	0.003833	9.55940E-07	9.54264E-07	0.1754	-0.1757	1.4243	1.4230
5	0.026056	9.66248E-07	9.25508E-07	4.2163	-4.4019	1.4319	1.4014
6	0.174204	9.64890E-07	9.24727E-07	4.1624	-4.3432	1.4309	1.4008

For 180 and 444 element meshes the % difference diminishes. Except for the last path, the % difference in tables 4.2 and 4.3 are in the same proximity confirming that 180 element mesh results are sufficiently converged. The computations of C^f are also tabulated for the three discretizations for both choices of paths in each mesh. C^f values also confirm the accuracy of 180 element mesh. From Tables 4.2 and 4.3, we observe that all paths yield almost the same values of C^f. We note that that path 1 has a radius of 0.000375 i.e. extremely close to the crack tip.

Table 4.2: A 180 Element mesh (a=0.4, h=0.7, b=0.8) with Gal/WF: C^{00} solutions and p=5

Path	Radius	$J^f/2 : \Gamma_1$ path	$J^f/2 : \Gamma_2$ path	% Difference using Γ_1 as reference	% Difference using Γ_2 as reference	$C^f : \Gamma_1$ path	$C^f : \Gamma_1$ path
1	0.000375	9.55441E-07	9.51453E-07	0.4174	-0.4192	1.4239	1.4209
2	0.000598	9.54816E-07	9.54729E-07	0.0091	-0.0091	1.4234	1.4234
3	0.000994	9.54783E-07	9.54720E-07	0.0066	-0.0066	1.4234	1.4234
4	0.001699	9.54785E-07	9.54709E-07	0.0080	-0.0080	1.4234	1.4234
5	0.002953	9.54788E-07	9.54702E-07	0.0090	-0.0090	1.4234	1.4234
6	0.005187	9.54791E-07	9.54697E-07	0.0098	-0.0098	1.4234	1.4234
7	0.009163	9.54792E-07	9.54694E-07	0.0103	-0.0103	1.4234	1.4233
8	0.016240	9.54793E-07	9.54690E-07	0.0108	-0.0108	1.4234	1.4233
9	0.028837	9.54794E-07	9.54687E-07	0.0112	-0.0112	1.4234	1.4233
10	0.051260	9.54794E-07	9.54687E-07	0.0111	-0.0111	1.4234	1.4233
11	0.091172	9.54791E-07	9.54719E-07	0.0076	-0.0076	1.4234	1.4234
12	0.162217	9.54774E-07	9.54910E-07	-0.0142	0.0142	1.4234	1.4235
13	0.287102	9.54682E-07	9.56782E-07	-0.2199	0.2194	1.4233	1.4249

Table 4.3: A 444 Element mesh (a=0.4, h=0.7, b=0.8) with Gal/WF: C^{00} solutions and *p*=5

Path	Radius	$J^f/2 : \Gamma_1$ path	$J^f/2 : \Gamma_2$ path	% Difference using Γ_1 as reference	% Difference using Γ_2 as reference	$C^f : \Gamma_1$ path	$C^f : \Gamma_1$ path
1	0.000375	9.41485E-07	9.51148E-07	-1.0263	1.0159	1.4135	1.4207
2	0.000525	9.54696E-07	9.54642E-07	0.0056	-0.0056	1.4234	1.4233
3	0.000705	9.54692E-07	9.54805E-07	-0.0118	0.0118	1.4233	1.4234
4	0.000921	9.54808E-07	9.54786E-07	0.0023	-0.0023	1.4234	1.4234
5	0.001180	9.54785E-07	9.54754E-07	0.0033	-0.0033	1.4234	1.4234
6	0.001491	9.54763E-07	9.54817E-07	-0.0056	0.0056	1.4234	1.4234
7	0.001864	9.54818E-07	9.54794E-07	0.0026	-0.0026	1.4234	1.4234
8	0.002312	9.54794E-07	9.54796E-07	-0.0002	0.0002	1.4234	1.4234
9	0.002850	9.54796E-07	9.54776E-07	0.0021	-0.0021	1.4234	1.4234
10	0.003495	9.54781E-07	9.54792E-07	-0.0011	0.0011	1.4234	1.4234
11	0.004269	9.54790E-07	9.54809E-07	-0.0019	0.0019	1.4234	1.4234
12	0.005198	9.54808E-07	9.54804E-07	0.0004	-0.0004	1.4234	1.4234
13	0.006312	9.54806E-07	9.54787E-07	0.0019	-0.0019	1.4234	1.4234
14	0.007649	9.54788E-07	9.54793E-07	-0.0004	0.0004	1.4234	1.4234
15	0.009254	9.54793E-07	9.54794E-07	-0.0001	0.0001	1.4234	1.4234
16	0.011180	9.54795E-07	9.54805E-07	-0.0011	0.0011	1.4234	1.4234
17	0.013491	9.54804E-07	9.54804E-07	0.0001	-0.0001	1.4234	1.4234
18	0.016265	9.54803E-07	9.54798E-07	0.0006	-0.0006	1.4234	1.4234
19	0.019593	9.54797E-07	9.54802E-07	-0.0006	0.0006	1.4234	1.4234
20	0.023586	9.54801E-07	9.54802E-07	-0.0001	0.0001	1.4234	1.4234
21	0.028378	9.54801E-07	9.54801E-07	0.0000	0.0000	1.4234	1.4234
22	0.034129	9.54801E-07	9.54801E-07	0.0000	0.0000	1.4234	1.4234
23	0.041030	9.54800E-07	9.54800E-07	0.0000	0.0000	1.4234	1.4234
24	0.049311	9.54800E-07	9.54802E-07	-0.0002	0.0002	1.4234	1.4234
25	0.059248	9.54800E-07	9.54802E-07	-0.0002	0.0002	1.4234	1.4234
26	0.071172	9.54801E-07	9.54802E-07	-0.0002	0.0002	1.4234	1.4234
27	0.085482	9.54801E-07	9.54805E-07	-0.0004	0.0004	1.4234	1.4234
28	0.102653	9.54804E-07	9.54810E-07	-0.0006	0.0006	1.4234	1.4234
29	0.123259	9.54810E-07	9.54817E-07	-0.0008	0.0008	1.4234	1.4234
30	0.147985	9.54818E-07	9.54830E-07	-0.0012	0.0012	1.4234	1.4235
31	0.177657	9.54834E-07	9.54851E-07	-0.0018	0.0018	1.4235	1.4235
32	0.213264	9.54861E-07	9.54887E-07	-0.0027	0.0027	1.4235	1.4235
33	0.255991	9.54909E-07	9.54948E-07	-0.0041	0.0041	1.4235	1.4235
34	0.307265	9.54996E-07	9.55003E-07	-0.0008	0.0008	1.4236	1.4236
35	0.368793	9.55160E-07	9.55983E-07	-0.0861	0.0860	1.4237	1.4243

This study demonstrates the *h*-convergence of the process for solutions of class $C^{00}(\bar{\Omega}^e)$ with fixed *p*-level of 5. For the solutions of class $C^{00}(\bar{\Omega}^e)$, computation of A_j is not possible, hence, it is not possible to determine how well the GDEs are satisfied by the computed solution. Overall, the 180 element mesh appears satisfactory and there seams no need to use 444 element mesh at least for *p*-level of 5.

4.4.2 Solutions of class $C^{11}(\bar{\Omega}^e)$

In this study we employ local approximations of class $C^{11}(\bar{\Omega}^e)$ at *p*-level of 5. All other details of 45, 180 and 444 element discretizations and the choices of paths for J-integral computations remain the same as in case of the solutions of class $C^{00}(\bar{\Omega}^e)$. Due to the fact that local approximations are of class $C^{11}(\bar{\Omega}^e)$, the integrand in the J-integral is continuous along the entire path Γ as well as normal to the path. In this case J-integral computations are in Riemann sense for all paths. Therefore, paths Γ_1 and Γ_2 would yield identical results and they do. Due to $C^{11}(\bar{\Omega}^e)$ nature of local approximation, it is possible to compute A_J (though in Lebesgue because σ_{ij} are of class $C^{00}(\bar{\Omega}^e)$) to determine its proximity to zero. Results are presented in Tables 4.4 – 4.6. Even from the 45 element discretization, C^f values are well within acceptable range for all paths. Virtually indistinguishable values of C^f in Table 4.5 and 4.6 that are independent of the paths confirm: (i) extremely good accuracy of 180 element mesh (ii) extremely good accuracy of J^f even when the path Γ is of radius 0.000375 (iii) improved accuracy for same *h* and *p* but higher *k* (2 compared to 1 for $C^{00}(\bar{\Omega}^e)$) shows the benefit of higher global differentiability and the importance of the J-integral in the Riemann sense. A_J of the $O(10^{-8})$ confirms that GDEs are satisfied well. Since 180 graded mesh yields good converged solutions at *p*-level of 5, in all further studies presented here, we maintain this mesh for lengths of 0.8 in the x-direction and 0.7 in the y-direction, and a coarser rectangular element mesh for the remainder of the domain.

Table 4.4: A 45 Element mesh (a=0.4, h=0.7, b=0.8) with Gal/WF: C^{11} solutions and p=5

Path	Radius	$J^f/2$: Γ_1 path	A_J	C^f
1	0.000500	9.57517E-07	1.437E-07	1.4255
2	0.001000	9.55660E-07	1.384E-07	1.4241
3	0.001500	9.54504E-07	1.441E-07	1.4232
4	0.003833	9.48735E-07	1.799E-07	1.4189
5	0.026056	9.56100E-07	3.631E-08	1.4244
6	0.174204	9.62568E-07	-4.044E-08	1.4292

Table 4.5: A 180 Element mesh (a=0.4, h=0.7, b=0.8) with Gal/WF: C^{11} solutions and p=5

Path	Radius	$J^f/2$: Γ_1 path	A_J	C^f
1	0.000375	9.55441E-07	1.631E-07	1.4239
2	0.000598	9.54816E-07	1.617E-07	1.4234
3	0.000994	9.54783E-07	1.612E-07	1.4234
4	0.001699	9.54785E-07	1.610E-07	1.4234
5	0.002953	9.54788E-07	1.608E-07	1.4234
6	0.005187	9.54791E-07	1.607E-07	1.4234
7	0.009163	9.54792E-07	1.605E-07	1.4234
8	0.016240	9.54793E-07	1.604E-07	1.4234
9	0.028837	9.54794E-07	1.603E-07	1.4234
10	0.051260	9.54794E-07	1.601E-07	1.4234
11	0.091172	9.54791E-07	1.600E-07	1.4234
12	0.162217	9.54774E-07	1.600E-07	1.4234
13	0.287102	9.54682E-07	1.606E-07	1.4233

Table 4.6: A 444 Element mesh (a=0.4, h=0.7, b=0.8) with Gal/WF: C^{11} solutions and p=5

Path	Radius	$J^f/2$: Γ_1 path	A_J	C^f
1	0.000375	9.55245E-07	1.641E-07	1.4238
2	0.000525	9.54782E-07	1.623E-07	1.4234
3	0.000705	9.54764E-07	1.619E-07	1.4234
4	0.000921	9.54760E-07	1.618E-07	1.4234
5	0.001180	9.54760E-07	1.618E-07	1.4234
6	0.001491	9.54759E-07	1.618E-07	1.4234
7	0.001864	9.54759E-07	1.619E-07	1.4234
8	0.002312	9.54759E-07	1.619E-07	1.4234
9	0.002850	9.54759E-07	1.619E-07	1.4234
10	0.003495	9.54759E-07	1.619E-07	1.4234
11	0.004269	9.54759E-07	1.619E-07	1.4234
12	0.005198	9.54759E-07	1.619E-07	1.4234
13	0.006312	9.54759E-07	1.619E-07	1.4234
14	0.007649	9.54759E-07	1.619E-07	1.4234
15	0.009254	9.54759E-07	1.619E-07	1.4234
16	0.011180	9.54759E-07	1.619E-07	1.4234
17	0.013491	9.54759E-07	1.619E-07	1.4234
18	0.016265	9.54759E-07	1.619E-07	1.4234
19	0.019593	9.54759E-07	1.619E-07	1.4234
20	0.023586	9.54759E-07	1.619E-07	1.4234
21	0.028378	9.54759E-07	1.619E-07	1.4234
22	0.034129	9.54759E-07	1.619E-07	1.4234
23	0.041030	9.54759E-07	1.620E-07	1.4234
24	0.049311	9.54759E-07	1.620E-07	1.4234
25	0.059248	9.54759E-07	1.620E-07	1.4234
26	0.071172	9.54759E-07	1.620E-07	1.4234
27	0.085482	9.54759E-07	1.620E-07	1.4234
28	0.102653	9.54759E-07	1.620E-07	1.4234
29	0.123259	9.54759E-07	1.620E-07	1.4234
30	0.147985	9.54759E-07	1.620E-07	1.4234
31	0.177657	9.54759E-07	1.620E-07	1.4234
32	0.213264	9.54759E-07	1.620E-07	1.4234
33	0.255991	9.54759E-07	1.620E-07	1.4234
34	0.307265	9.54759E-07	1.620E-07	1.4234
35	0.368793	9.54762E-07	1.620E-07	1.4234

4.5 Case (b); Integral Form: Gal/WF; Influence of *h/a* for Large *b/a* (6) on J-integral Computations

Since K_I is only valid for an infinite medium containing the crack, in this section we investigate the influence of h/a for a fixed b/a (6) (large enough so that the width has no effect on the results). We consider two crack lengths: $a = 0.4$ and $a = 1.2$. First, we consider the discretizations:

(i) Consider $a = 0.4$

The choice of $b/a = 6$ implies that $b = 2.4$ for $a = 0.4$. We consider h/a equal to 3, 4, 5, 6, 8, 10 and 12 which correspond to h values of 1.2, 1.6, 2.0, 2.4, 3.2 and 4.0. Since the 180 element discretization used in section 4.4 worked extremely well for $a = 0.4$, $b = 0.8$ and $h = 0.7$, we consider a zone at the crack tip of this same size containing the 180 element mesh shown in Figure 4.3. The remainder of the domain is discretized using a coarser mesh of rectangular elements. Details are shown in figure 4.6.

(ii) Consider $a = 1.2$

In this case $b/a = 6$ implies that $b = 7.2$ for $a = 1.2$. We consider h/a equal to 3, 4, 5, 6, 8, 10 and 12 which correspond to h values of 3.6, 4.8, 6.0, 7.2, 12 and 14.4. For the discretization, we adopt a strategy similar to that used for $a = 0.4$ except that 180 element mesh for length of 0.4, width of 0.8 and height of 0.7 is centered at the half crack tip as shown in Figure 4.7. The remainder of the domain is discretized coarsely using rectangular elements. Details are shown in Figure 4.7.

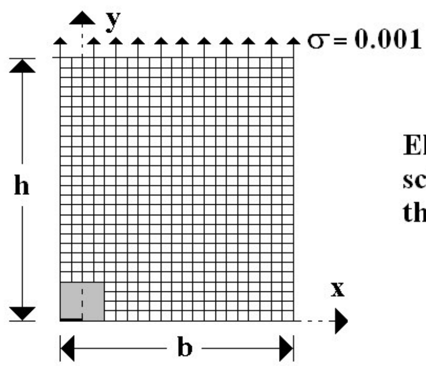

(a) Schematic of the mesh for (h/a) and (b/a) studies for a=0.4

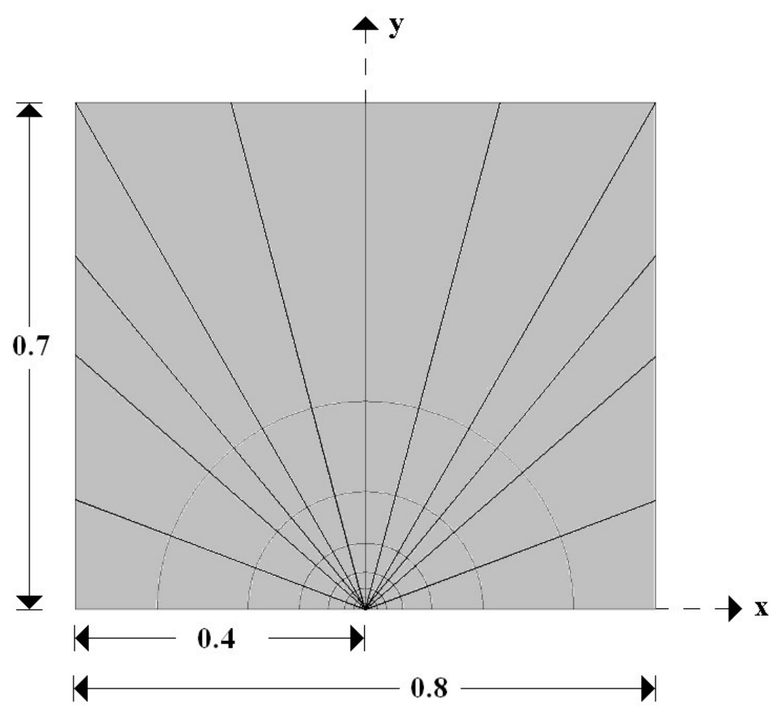

(b) A 180 element discretization shown in figure 4.3 used for the shaded region of figure 4.6 (a)

Figure 4.6: Discretization for (h/a) study for b/a=6 (b=2.4) with a=0.4

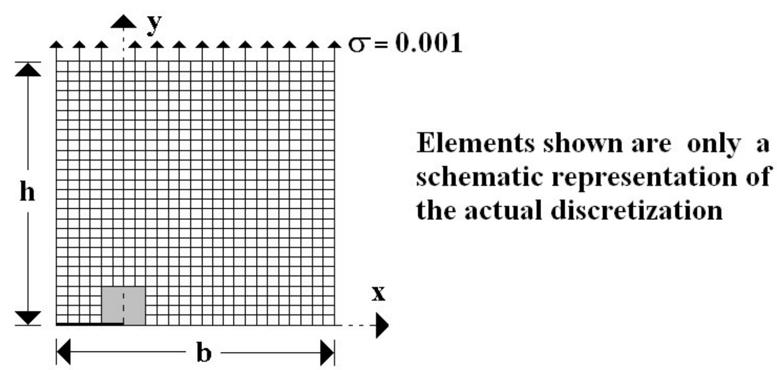

(a) Schematic of the mesh for (h/a) and (b/a) studies for a=1.2

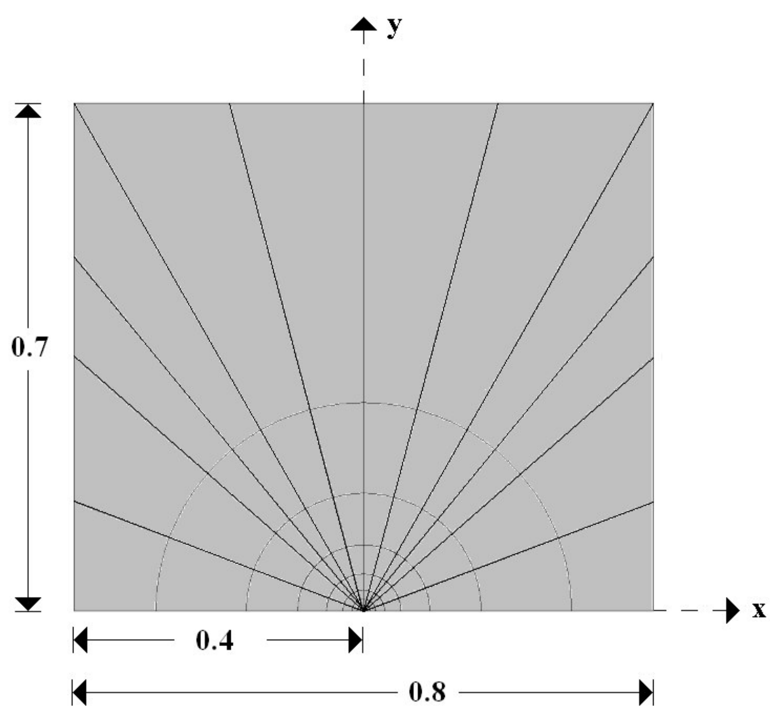

(b) A 180 element discretization shown in figure 4.3 used for the shaded region of figure 4.7 (a)

Figure 4.7: Discretization for (h/a) study for b/a=6 (b=7.2) with a=1.2

4.5.1 Numerical Studies for $a = 0.4$

Based on the studies in section 4.4, we choose local approximations of class $C^{11}(\bar{\Omega}^e)$ at p-level of 5. J^f, A_J and C^f for each h/a are tabulated in tables 4.7(a) – 4.7(b). We note that in all cases A_J of the $O(10^{-9})$ confirm that GDEs are satisfied well and that path independence of J-integral computations is valid in all cases. C^f value of 1.1193 for $h/a = 3$ indicates dependence of C^f on h/a. Progressively decreasing C^f with progressively increasing h/a confirms decreasing dependence of C^f on increasing h/a. When $h/a = 12$, $C^f = 1.0177$ indicates that the center crack is close to being in the infinite medium. Path independence of C^f for each h/a is another confirmation of high accuracy and assurance of the validity of computations of J^f that approaches J for progressively increasing h/a.

Table 4.7a: Influence of h/a (3,4,5) for large b/a (6) and a=0.4: A 180 element mesh in region of near the crack tip (Figure 4.6) using Gal/WF: C^{11} solutions and *p*=5

		h/a = 3			h/a = 4			h/a = 5		
Path	Radius	$J^f/2 : \Gamma_1$ path	A_J	C^f	$J^f/2 : \Gamma_1$ path	A_J	C^f	$J^f/2 : \Gamma_1$ path	A_J	C^f
1	0.000375	5.90786E-07	1.008E-07	1.1197	5.49573E-07	9.378E-08	1.0799	5.27509E-07	9.002E-08	1.0580
2	0.000598	5.90399E-07	9.996E-08	1.1193	5.49214E-07	9.300E-08	1.0796	5.27164E-07	8.928E-08	1.0577
3	0.000994	5.90379E-07	9.963E-08	1.1193	5.49195E-07	9.269E-08	1.0795	5.27146E-07	8.898E-08	1.0577
4	0.001699	5.90380E-07	9.951E-08	1.1193	5.49196E-07	9.258E-08	1.0796	5.27147E-07	8.887E-08	1.0577
5	0.002953	5.90382E-07	9.941E-08	1.1193	5.49198E-07	9.249E-08	1.0796	5.27148E-07	8.878E-08	1.0577
6	0.005187	5.90383E-07	9.932E-08	1.1193	5.49199E-07	9.240E-08	1.0796	5.27150E-07	8.870E-08	1.0577
7	0.009163	5.90384E-07	9.923E-08	1.1193	5.49200E-07	9.233E-08	1.0796	5.27150E-07	8.863E-08	1.0577
8	0.016240	5.90385E-07	9.915E-08	1.1193	5.49200E-07	9.225E-08	1.0796	5.27151E-07	8.855E-08	1.0577
9	0.028837	5.90385E-07	9.908E-08	1.1193	5.49200E-07	9.218E-08	1.0796	5.27151E-07	8.849E-08	1.0577
10	0.051260	5.90385E-07	9.900E-08	1.1193	5.49200E-07	9.211E-08	1.0796	5.27151E-07	8.842E-08	1.0577
11	0.091172	5.90385E-07	9.894E-08	1.1193	5.49200E-07	9.206E-08	1.0796	5.27150E-07	8.837E-08	1.0577
12	0.162217	5.90384E-07	9.890E-08	1.1193	5.49196E-07	9.204E-08	1.0796	5.27145E-07	8.836E-08	1.0577
13	0.287102	5.90365E-07	9.900E-08	1.1193	5.49164E-07	9.223E-08	1.0795	5.27109E-07	8.858E-08	1.0576

Table 4.7b: Influence of h/a (6,8,10) for large b/a (6) and a=0.4: A 180 element mesh in region near the crack tip (Figure 4.6) using Gal/WF: C^{11} solutions and p=5

		h/a = 6			h/a = 8			h/a = 10		
Path	Radius	$J^f/2 : \Gamma_1$ path	A_J	C^f	$J^f/2 : \Gamma_1$ path	A_J	C^f	$J^f/2 : \Gamma_1$ path	A_J	C^f
1	0.000375	5.07336E-07	8.658E-08	1.0376	4.94138E-07	8.432E-08	1.0240	4.89004E-07	8.380E-08	1.0187
2	0.000598	5.07004E-07	8.586E-08	1.0373	4.93815E-07	8.363E-08	1.0237	4.88562E-07	8.311E-08	1.0182
3	0.000994	5.06987E-07	8.558E-08	1.0372	4.93798E-07	8.335E-08	1.0237	4.88546E-07	8.283E-08	1.0182
4	0.001699	5.06987E-07	8.547E-08	1.0372	4.93799E-07	8.325E-08	1.0237	4.88546E-07	8.273E-08	1.0182
5	0.002953	5.06989E-07	8.539E-08	1.0372	4.93801E-07	8.316E-08	1.0237	4.88548E-07	8.265E-08	1.0182
6	0.005187	5.06990E-07	8.531E-08	1.0372	4.93802E-07	8.309E-08	1.0237	4.88549E-07	8.257E-08	1.0182
7	0.009163	5.06991E-07	8.524E-08	1.0372	4.93803E-07	8.302E-08	1.0237	4.88550E-07	8.250E-08	1.0182
8	0.016240	5.06991E-07	8.517E-08	1.0372	4.93803E-07	8.295E-08	1.0237	4.88550E-07	8.243E-08	1.0182
9	0.028837	5.06992E-07	8.510E-08	1.0372	4.93803E-07	8.289E-08	1.0237	4.88551E-07	8.237E-08	1.0182
10	0.051260	5.06991E-07	8.504E-08	1.0372	4.93803E-07	8.283E-08	1.0237	4.88550E-07	8.231E-08	1.0182
11	0.091172	5.06990E-07	8.500E-08	1.0372	4.93802E-07	8.278E-08	1.0237	4.88549E-07	8.227E-08	1.0182
12	0.162217	5.06985E-07	8.499E-08	1.0372	4.93797E-07	8.278E-08	1.0237	4.88544E-07	8.226E-08	1.0182
13	0.287102	5.06947E-07	8.522E-08	1.0372	4.93759E-07	8.301E-08	1.0236	4.88506E-07	8.250E-08	1.0182

Table 4.7c: Influence of h/a (12) for large b/a (6) and a=0.4: A 180 element mesh in region near the crack tip (Figure 4.6) using Gal/WF: C^{11} solutions and p=5

		h/a = 12		
Path	Radius	$J^f/2 : \Gamma_1$ path	A_J	C^f
1	0.000375	4.88029E-07	8.328E-08	1.0177
2	0.000598	4.87709E-07	8.259E-08	1.0173
3	0.000994	4.87693E-07	8.231E-08	1.0173
4	0.001699	4.87694E-07	8.221E-08	1.0173
5	0.002953	4.87695E-07	8.213E-08	1.0173
6	0.005187	4.87696E-07	8.205E-08	1.0173
7	0.009163	4.87697E-07	8.198E-08	1.0173
8	0.016240	4.87698E-07	8.192E-08	1.0173
9	0.028837	4.87698E-07	8.186E-08	1.0173
10	0.051260	4.87698E-07	8.180E-08	1.0173
11	0.091172	4.87696E-07	8.175E-08	1.0173
12	0.162217	4.87691E-07	8.175E-08	1.0173
13	0.287102	4.87653E-07	8.199E-08	1.0173

4.5.2 Numerical Studies for $a = 1.2$

Studies similar to those for $a = 0.4$ were also conducted for $a = 1.2$ at *p*-level of 5 and using local approximations of class $C^{11}(\bar{\Omega}^e)$. Results for J^f, A_J and C^f are summarized in tables 4.8(a) – 4.8(c). We note that values of A_J of the $O(10^{-8})$ assure path independence of J^f in the computational process. With progressively increasing h/a (from 3 to 12) we note a decrease of $C^f = 1.1192$ for $h/a = 3$ to $C_f = 1.01171$ for $h/a = 12$. Path independence of C^f is clearly observed for each h/a. For $h/a = 12$, $C^f = 1.01171$ (nearly equal to 1) indicating close to infinite size of the domain (compared to a). Since C^f is a function of b/a and h/a, and not the specific size of the crack, we expect C^f values in tables 4.7(a) – 4.7(c) for $a = 0.4$ to match with those in tables 4.8(a) – 4.8(c) for $a = 1.2$ for corresponding values of h/a (b/a being same in both cases) which in fact they do up to three or four decimal places. This study is exceptionally good confirmation of the accuracy of the entire J^f computational process.

Table 4.8a: Influence of h/a (3, 4, 5) for large b/a (6) and a=1.2: A 180 element mesh in region of near the crack tip (Figure 4.7) using Gal/WF: C^{11} solutions and *p*=5

		h/a = 3			h/a = 4			h/a = 5		
Path	Radius	$J^f/2 : \Gamma_1$ path	A_J	C^f	$J^f/2 : \Gamma_1$ path	A_J	C^f	$J^f/2 : \Gamma_1$ path	A_J	C^f
1	0.000375	1.77189E-06	3.007E-07	1.1195	1.64821E-06	2.797E-07	1.0798	1.58201E-06	2.685E-07	1.0578
2	0.000598	1.77072E-06	2.982E-07	1.1192	1.64713E-06	2.774E-07	1.0794	1.58097E-06	2.662E-07	1.0575
3	0.000994	1.77066E-06	2.972E-07	1.1191	1.64707E-06	2.764E-07	1.0794	1.58091E-06	2.653E-07	1.0575
4	0.001699	1.77067E-06	2.968E-07	1.1191	1.64707E-06	2.761E-07	1.0794	1.58091E-06	2.650E-07	1.0575
5	0.002953	1.77067E-06	2.965E-07	1.1191	1.64708E-06	2.758E-07	1.0794	1.58092E-06	2.648E-07	1.0575
6	0.005187	1.77068E-06	2.962E-07	1.1192	1.64708E-06	2.756E-07	1.0794	1.58092E-06	2.645E-07	1.0575
7	0.009163	1.77068E-06	2.960E-07	1.1192	1.64708E-06	2.753E-07	1.0794	1.58093E-06	2.643E-07	1.0575
8	0.016240	1.77068E-06	2.957E-07	1.1192	1.64708E-06	2.751E-07	1.0794	1.58093E-06	2.641E-07	1.0575
9	0.028837	1.77068E-06	2.955E-07	1.1192	1.64709E-06	2.749E-07	1.0794	1.58093E-06	2.639E-07	1.0575
10	0.051260	1.77069E-06	2.952E-07	1.1192	1.64709E-06	2.747E-07	1.0794	1.58093E-06	2.636E-07	1.0575
11	0.091172	1.77073E-06	2.965E-07	1.1192	1.64713E-06	2.742E-07	1.0794	1.58097E-06	2.632E-07	1.0575
12	0.162217	1.77092E-06	2.932E-07	1.1192	1.64731E-06	2.728E-07	1.0795	1.58114E-06	2.619E-07	1.0576
13	0.287102	1.77213E-06	2.832E-07	1.1196	1.64842E-06	2.635E-07	1.0798	1.58220E-06	2.530E-07	1.0579

Table 4.8b: Influence of h/a (6, 8, 10) for large b/a (6) and a=1.2: 180 element mesh in region of near the crack tip (Figure 4.7) using Gal/WF: C^{11} solutions and p=5

		h/a = 6			h/a = 8			h/a = 10		
Path	Radius	$J^f/2$: Γ_1 path	A_J	C^f	$J^f/2$: Γ_1 path	A_J	C^f	$J^f/2$: Γ_1 path	A_J	C^f
1	0.000375	1.52149E-06	2.582E-07	1.0374	1.48190E-06	2.515E-07	1.0238	1.46638E-06	2.488E-07	1.0185
2	0.000598	1.52049E-06	2.561E-07	1.0371	1.48093E-06	2.494E-07	1.0235	1.46541E-06	2.468E-07	1.0181
3	0.000994	1.52043E-06	2.552E-07	1.0371	1.48087E-06	2.486E-07	1.0235	1.46536E-06	2.459E-07	1.0181
4	0.001699	1.52044E-06	2.549E-07	1.0371	1.48088E-06	2.483E-07	1.0235	1.46536E-06	2.456E-07	1.0181
5	0.002953	1.52044E-06	2.546E-07	1.0371	1.48088E-06	2.480E-07	1.0235	1.46537E-06	2.454E-07	1.0181
6	0.005187	1.52045E-06	2.544E-07	1.0371	1.48088E-06	2.478E-07	1.0235	1.46537E-06	2.452E-07	1.0181
7	0.009163	1.52045E-06	2.542E-07	1.0371	1.48089E-06	2.476E-07	1.0235	1.46537E-06	2.450E-07	1.0181
8	0.016240	1.52045E-06	2.540E-07	1.0371	1.48089E-06	2.474E-07	1.0235	1.46537E-06	2.448E-07	1.0181
9	0.028837	1.52045E-06	2.538E-07	1.0371	1.48089E-06	2.472E-07	1.0235	1.46538E-06	2.446E-07	1.0181
10	0.051260	1.52046E-06	2.536E-07	1.0371	1.48090E-06	2.470E-07	1.0235	1.46538E-06	2.444E-07	1.0181
11	0.091172	1.52049E-06	2.532E-07	1.0371	1.48093E-06	2.466E-07	1.0235	1.46541E-06	2.440E-07	1.0181
12	0.162217	1.52066E-06	2.519E-07	1.0371	1.48109E-06	2.453E-07	1.0236	1.46557E-06	2.427E-07	1.0182
13	0.287102	1.52167E-06	2.433E-07	1.0375	1.48208E-06	2.370E-07	1.0239	1.46655E-06	2.345E-07	1.0185

Table 4.8c: Influence of h/a (12) for large b/a (6) and a=1.2: 180 element mesh in region of near the crack tip (Figure 4.7) using Gal/WF: C^{11} solutions and p=5

		h/a = 12		
Path	Radius	$J^f/2$: Γ_1 path	A_J	C^f
1	0.000375	1.46339E-06	2.483E-07	1.0174
2	0.000598	1.46243E-06	2.463E-07	1.0171
3	0.000994	1.46238E-06	2.454E-07	1.0171
4	0.001699	1.46238E-06	2.451E-07	1.0171
5	0.002953	1.46239E-06	2.449E-07	1.0171
6	0.005187	1.46239E-06	2.447E-07	1.0171
7	0.009163	1.46239E-06	2.445E-07	1.0171
8	0.016240	1.46239E-06	2.443E-07	1.0171
9	0.028837	1.46240E-06	2.441E-07	1.0171
10	0.051260	1.46240E-06	2.439E-07	1.0171
11	0.091172	1.46243E-06	2.435E-07	1.0171
12	0.162217	1.46259E-06	2.422E-07	1.0171
13	0.287102	1.46357E-06	2.340E-07	1.0175

4.6 Case (c); Integral Form: Gal/WF; Influence of *b/a* for Large *h/a* (12) on J-integral Computations

This study is similar to the one presented in case (b) except that here we study the influence of b/a on J^f for a fixed h/a (12). In this case also we consider $a = 0.4$ and $a = 1.2$. The mesh design strategy is exactly same as that described for case (b).

For both values of a (0.4 and 1.2) we computed solutions of class $C^{11}(\bar{\Omega}^e)$ at *p*-level of 5 and then J^f, A_J and C^f for each value of b/a and for each path. Path number, path radius, J^f, A_J and C^f for $a = 0.4$ for different values of b/a are tabulated in tables 4.9(a) – 4.9(c). Similar quantities for $a = 1.2$ are given in tables 4.10(a) – 4.10(c). For both values of a we note the following,

1. Path independence of C^f for each b/a
2. As b/a is increased, C^f approaches unity
3. C^f values for each b/a in tables 4.9 and 4.10 for the two values of a match very – very closely confirming that C^f is independent of a and that it is only a function of b/a and h/a which are same for the corresponding tables 4.9 and 4.10.
4. For both values of a computed values of C^f are in extremely close agreement with those reported by Isida [46].

(1) – (4) confirm accuracy and validity of the formulation and computational process used for J^f calculations.

Figure 4.8 (a) shows plots C^f versus b/a for $h/a=12$, and Figure 4.8 (b) shows C^f versus h/a for $b/a=6$, both for $a=0.4$ and $a=1.2$. We see virtually indistinguishable difference for two values of a. That is, $C^f = C^f(b/a, h/a)$ and C^f is not a function of a. It is shown that for large h/a ratio, as the b/a ratio increases, C^f converges to 1. Convergence to unity can also be obtained by decreasing a (increase of the b/a ratio).

Table 4.9a: Influence of b/a (2, 3) for large h/a (12) and a=0.4: A 180 element mesh in region of near the crack tip (Figure 4.6) using Gal/WF: C^{11} solutions and p=5

		b/a = 2 C^f Isida [46] = 1.1867			b/a = 3 C^f Isida [46] = 1.0726		
Path	Radius	$J^f/2$: Γ_1 path	A_J	C^f	$J^f/2$: Γ_1 path	A_J	C^f
1	0.000375	6.64490E-07	1.135E-07	1.1875	5.42739E-07	9.263E-08	1.0732
2	0.000598	6.64055E-07	1.126E-07	1.1871	5.42384E-07	9.186E-08	1.0728
3	0.000994	6.64033E-07	1.122E-07	1.1871	5.42365E-07	9.155E-08	1.0728
4	0.001699	6.64034E-07	1.120E-07	1.1871	5.42366E-07	9.144E-08	1.0728
5	0.002953	6.64036E-07	1.119E-07	1.1871	5.42368E-07	9.135E-08	1.0728
6	0.005187	6.64038E-07	1.118E-07	1.1871	5.42369E-07	9.127E-08	1.0728
7	0.009163	6.64039E-07	1.117E-07	1.1871	5.42370E-07	9.119E-08	1.0728
8	0.016240	6.64039E-07	1.116E-07	1.1871	5.42370E-07	9.112E-08	1.0728
9	0.028837	6.64039E-07	1.115E-07	1.1871	5.42371E-07	9.105E-08	1.0728
10	0.051260	6.64039E-07	1.115E-07	1.1871	5.42370E-07	9.099E-08	1.0728
11	0.091172	6.64036E-07	1.114E-07	1.1871	5.42369E-07	9.094E-08	1.0728
12	0.162217	6.64018E-07	1.115E-07	1.1871	5.42360E-07	9.095E-08	1.0728
13	0.287102	6.63912E-07	1.121E-07	1.1870	5.42308E-07	9.128E-08	1.0728

Table 4.9b: Influence of b/a (4, 5) for large h/a (12) and a=0.4: A 180 element mesh in region of near the crack tip (Figure 4.6) using Gal/WF: C^{11} solutions and p=5

		b/a = 4 C^f Isida [46] = 1.0391			b/a = 5 C^f Isida [46] = 1.0246		
Path	Radius	$J^f/2$: Γ_1 path	A_J	C^f	$J^f/2$: Γ_1 path	A_J	C^f
1	0.000375	5.09384E-07	8.692E-08	1.0397	4.95219E-07	8.450E-08	1.0251
2	0.000598	5.09051E-07	8.621E-08	1.0393	4.94895E-07	8.381E-08	1.0248
3	0.000994	5.09034E-07	8.592E-08	1.0393	4.94878E-07	8.353E-08	1.0248
4	0.001699	5.09034E-07	8.581E-08	1.0393	4.94879E-07	8.342E-08	1.0248
5	0.002953	5.09036E-07	8.573E-08	1.0393	4.94881E-07	8.334E-08	1.0248
6	0.005187	5.09037E-07	8.565E-08	1.0393	4.94882E-07	8.326E-08	1.0248
7	0.009163	5.09038E-07	8.558E-08	1.0393	4.94883E-07	8.319E-08	1.0248
8	0.016240	5.09039E-07	8.551E-08	1.0393	4.94883E-07	8.313E-08	1.0248
9	0.028837	5.09039E-07	8.544E-08	1.0393	4.94883E-07	8.306E-08	1.0248
10	0.051260	5.09039E-07	8.538E-08	1.0393	4.94883E-07	8.301E-08	1.0248
11	0.091172	5.09037E-07	8.534E-08	1.0393	4.94882E-07	8.296E-08	1.0248
12	0.162217	5.09031E-07	8.534E-08	1.0393	4.94876E-07	8.296E-08	1.0248
13	0.287102	5.08987E-07	8.561E-08	1.0393	4.94836E-07	8.321E-08	1.0247

Table 4.9c: Influence of b/a (6) for large h/a (12) and a=0.4: A 180 element mesh in region of near the crack tip (Figure 4.6) using Gal/WF: C^{11} solutions and p=5

		b/a = 6 C^f Isida[46] = 1.0169		
Path	Radius	$J^f/2$: Γ_1 path	A_J	C^f
1	0.000375	4.88029E-07	8.328E-08	1.0177
2	0.000598	4.87709E-07	8.259E-08	1.0173
3	0.000994	4.87693E-07	8.231E-08	1.0173
4	0.001699	4.87694E-07	8.221E-08	1.0173
5	0.002953	4.87695E-07	8.213E-08	1.0173
6	0.005187	4.87696E-07	8.205E-08	1.0173
7	0.009163	4.87697E-07	8.198E-08	1.0173
8	0.016240	4.87698E-07	8.192E-08	1.0173
9	0.028837	4.87698E-07	8.186E-08	1.0173
10	0.051260	4.87698E-07	8.180E-08	1.0173
11	0.091172	4.87696E-07	8.175E-08	1.0173
12	0.162217	4.87691E-07	8.175E-08	1.0173
13	0.287102	4.87653E-07	8.199E-08	1.0173

Table 4.10a: Influence of b/a (2, 3) for large h/a (12) and a=1.2: A 180 element mesh in region of near the crack tip (Figure 4.7) using Gal/WF: C^{11} solutions and p=5

		b/a = 2 C^f Isida [46] = 1.1867			b/a = 3 C^f Isida [46] = 1.0726		
Path	Radius	$J^f/2$: Γ_1 path	A_J	C^f	$J^f/2$: Γ_1 path	A_J	C^f
1	0.000375	1.99223E-06	3.382E-07	1.1871	1.62765E-06	2.762E-07	1.0730
2	0.000598	1.99092E-06	3.354E-07	1.1867	1.62658E-06	2.739E-07	1.0726
3	0.000994	1.99085E-06	3.343E-07	1.1867	1.62652E-06	2.730E-07	1.0726
4	0.001699	1.99085E-06	3.339E-07	1.1867	1.62652E-06	2.727E-07	1.0726
5	0.002953	1.99086E-06	3.335E-07	1.1867	1.62653E-06	2.724E-07	1.0726
6	0.005187	1.99087E-06	3.332E-07	1.1867	1.62653E-06	2.722E-07	1.0726
7	0.009163	1.99087E-06	3.330E-07	1.1867	1.62653E-06	2.719E-07	1.0726
8	0.016240	1.99087E-06	3.327E-07	1.1867	1.62653E-06	2.717E-07	1.0726
9	0.028837	1.99087E-06	3.324E-07	1.1867	1.62654E-06	2.715E-07	1.0726
10	0.051260	1.99088E-06	3.321E-07	1.1867	1.62654E-06	2.713E-07	1.0726
11	0.091172	1.99092E-06	3.316E-07	1.1867	1.62657E-06	2.708E-07	1.0726
12	0.162217	1.99113E-06	3.300E-07	1.1868	1.62675E-06	2.695E-07	1.0727
13	0.287102	1.99239E-06	3.193E-07	1.1872	1.62783E-06	2.604E-07	1.0731

Table 4.10b: Influence of b/a (4, 5) for large h/a (12) and a=1.2: A 180 element mesh in region of near the crack tip (Figure 4.7) using Gal/WF: C^{11} solutions and p=5

		b/a = 4 C^f Isida [46] = 1.0391			b/a = 5 C^f Isida [46] = 1.0246		
Path	Radius	$J^f/2 : \Gamma_1$ path	A_J	C^f	$J^f/2 : \Gamma_1$ path	A_J	C^f
1	0.000375	1.52762E-06	2.592E-07	1.0395	1.48597E-06	2.522E-07	1.0252
2	0.000598	1.52662E-06	2.571E-07	1.0392	1.48499E-06	2.501E-07	1.0249
3	0.000994	1.52656E-06	2.562E-07	1.0391	1.48494E-06	2.492E-07	1.0249
4	0.001699	1.52656E-06	2.559E-07	1.0391	1.48494E-06	2.489E-07	1.0249
5	0.002953	1.52657E-06	2.557E-07	1.0391	1.48495E-06	2.487E-07	1.0249
6	0.005187	1.52657E-06	2.554E-07	1.0391	1.48495E-06	2.485E-07	1.0249
7	0.009163	1.52658E-06	2.552E-07	1.0391	1.48496E-06	2.482E-07	1.0249
8	0.016240	1.52658E-06	2.550E-07	1.0391	1.48496E-06	2.480E-07	1.0249
9	0.028837	1.52658E-06	2.548E-07	1.0392	1.48496E-06	2.478E-07	1.0249
10	0.051260	1.52658E-06	2.546E-07	1.0392	1.48496E-06	2.476E-07	1.0249
11	0.091172	1.52661E-06	2.542E-07	1.0392	1.48499E-06	2.472E-07	1.0249
12	0.162217	1.52678E-06	2.529E-07	1.0392	1.48516E-06	2.460E-07	1.0250
13	0.287102	1.52780E-06	2.443E-07	1.0396	1.48615E-06	2.377E-07	1.0253

Table 4.10c: Influence of b/a (6) for large h/a (12) and a=1.2: A 180 element mesh in region of near the crack tip (Figure 4.7) using Gal/WF: C^{11} solutions and p=5

		b/a = 6 C^f Isida[46] = 1.0169		
Path	Radius	$J^f/2 : \Gamma_1$ path	A_J	C^f
1	0.000375	1.46339E-06	2.483E-07	1.0174
2	0.000598	1.46243E-06	2.463E-07	1.0171
3	0.000994	1.46238E-06	2.454E-07	1.0171
4	0.001699	1.46238E-06	2.451E-07	1.0171
5	0.002953	1.46239E-06	2.449E-07	1.0171
6	0.005187	1.46239E-06	2.447E-07	1.0171
7	0.009163	1.46239E-06	2.445E-07	1.0171
8	0.016240	1.46239E-06	2.443E-07	1.0171
9	0.028837	1.46240E-06	2.441E-07	1.0171
10	0.051260	1.46240E-06	2.439E-07	1.0171
11	0.091172	1.46243E-06	2.435E-07	1.0171
12	0.162217	1.46259E-06	2.422E-07	1.0171
13	0.287102	1.46357E-06	2.340E-07	1.0175

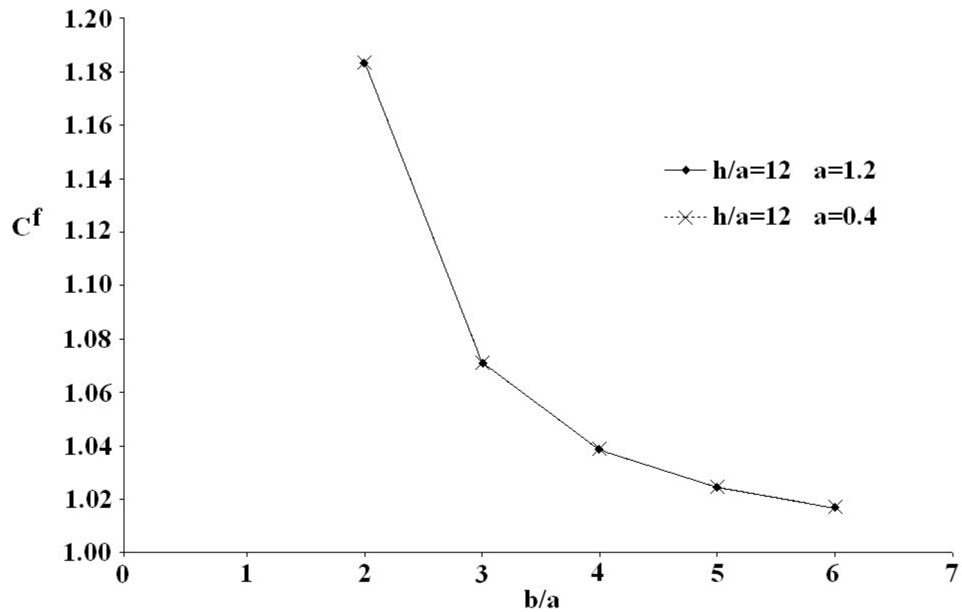

(a) C^f versus (b/a) for h/a=12 for a=0.4 and 1.2

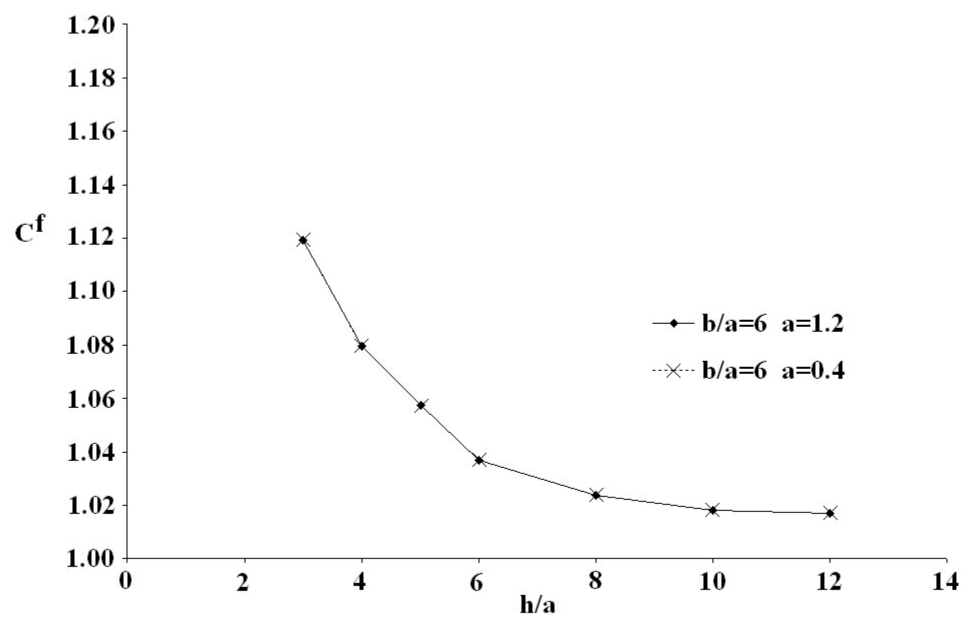

(b) C^f versus (h/a) for b/a=6 for a=0.4 and 1.2

Figure 4.8: C^f versus (b/a) and C^f versus (h/a) for h/a=12 and b/a=6 for a=0.4 and 1.2

4.7 Case (d); Integral Form: Gal/WF; Influence of solution of Higher Classes on J-integral Computations

In this study we investigate the influence of higher order global differentiability on J-integral computations. We consider $a = 0.4$, $b/a = 35$ ($h = 14.0$) and $b/a = 16$ ($b = 4.8$). The domain is close to infinite compared to the size of the crack. We consider a discretization strategy similar to that shown in Figure 4.6. The zone at the crack tip is modeled using a 180 element graded mesh shown in Figure 4.3 and the remainder of the domain is modeled using a coarse mesh. We investigate the following classes of solutions and *p*-levels:

$C^{00}(\bar{\Omega}^e)$; *p*-level of 3, 5, 7

$C^{11}(\bar{\Omega}^e)$; *p*-level of 3, 5, 7

$C^{22}(\bar{\Omega}^e)$; *p*-level of 5, 7

$C^{33}(\bar{\Omega}^e)$; *p*-level of 7

Integral paths, path radius, J^f, K_I^f, A_J and C^f are summarized in tables 4.11(a) – 4.11(d). We make the following observations and remarks.

(1) Since h/a and b/a are very large, we can consider the center crack to be in a infinite medium, and a 180 element mesh in the crack zone has proven to be excellent, we expect $C^f \cong 1$ in all studies.

(2) For all cases we note that $C^f = 1.00--$ indicating exceptional accuracy of all computed results for various orders of global differentiability listed above.

(3) Closer examination of C^f reveals improvement in the second and fourth decimal places for :

(a) increasing *p*-level for $C^{00}(\bar{\Omega}^e)$, $C^{11}(\bar{\Omega}^e)$ and $C^{22}(\bar{\Omega}^e)$ classes of solutions

(b) increasing order of global differentiability

(4) A_J well below $O(10^{-8})$ confirm path independence of J-integral in computations.

Table 4.11a: Influence of higher order global differentiability for b/a=16, h/a=35 and a=0.4: A 180 element mesh in region of near the crack tip (Figure 4.6) using Gal/WF: C^{00} solutions

Path	C^{00} p=3 $J^f/2:\Gamma_1$ path	A_J	K_I^f	% Error based on K_I	C^f	C^{00} p=5 $J^f/2:\Gamma_1$ path	A_J	K_I^f	% Error based on K_I	C^f	C^{00} p=7 $J^f/2:\Gamma_1$ path	A_J	K_I^f	% Error based on K_I	C^f
1	4.74207E-07		1.1245E-03	-0.3144	1.0031	4.73806E-07		1.1240E-03	-0.2720	1.0027	4.73750E-07		1.1240E-03	-0.2660	1.0027
2	4.74539E-07		1.1249E-03	-0.3496	1.0035	4.73694E-07		1.1239E-03	-0.2601	1.0026	4.73703E-07		1.1239E-03	-0.2611	1.0026
3	4.74780E-07		1.1252E-03	-0.3751	1.0038	4.73700E-07		1.1239E-03	-0.2608	1.0026	4.73703E-07		1.1239E-03	-0.2611	1.0026
4	4.74949E-07		1.1254E-03	-0.3928	1.0039	4.73705E-07		1.1239E-03	-0.2613	1.0026	4.73703E-07		1.1239E-03	-0.2611	1.0026
5	4.75060E-07		1.1255E-03	-0.4046	1.0040	4.73709E-07		1.1239E-03	-0.2617	1.0026	4.73703E-07		1.1239E-03	-0.2611	1.0026
6	4.75133E-07	not	1.1256E-03	-0.4123	1.0041	4.73711E-07	not	1.1239E-03	-0.2620	1.0026	4.73703E-07	not	1.1239E-03	-0.2611	1.0026
7	4.75180E-07	possible	1.1257E-03	-0.4173	1.0042	4.73713E-07	possible	1.1239E-03	-0.2621	1.0026	4.73703E-07	possible	1.1239E-03	-0.2611	1.0026
8	4.75210E-07		1.1257E-03	-0.4205	1.0042	4.73714E-07		1.1239E-03	-0.2622	1.0026	4.73703E-07		1.1239E-03	-0.2611	1.0026
9	4.75226E-07		1.1257E-03	-0.4222	1.0042	4.73714E-07		1.1239E-03	-0.2623	1.0026	4.73703E-07		1.1239E-03	-0.2611	1.0026
10	4.75224E-07		1.1257E-03	-0.4220	1.0042	4.73714E-07		1.1239E-03	-0.2623	1.0026	4.73703E-07		1.1239E-03	-0.2611	1.0026
11	4.75189E-07		1.1257E-03	-0.4182	1.0042	4.73714E-07		1.1239E-03	-0.2622	1.0026	4.73703E-07		1.1239E-03	-0.2611	1.0026
12	4.75085E-07		1.1256E-03	-0.4073	1.0041	4.73712E-07		1.1239E-03	-0.2620	1.0026	4.73703E-07		1.1239E-03	-0.2611	1.0026
13	4.74803E-07		1.1252E-03	-0.3774	1.0038	4.73706E-07		1.1239E-03	-0.2614	1.0026	4.73703E-07		1.1239E-03	-0.2611	1.0026

Table 4.11b: Influence of higher order global differentiability for b/a=16, h/a=35 and a=0.4: A 180 element mesh in region of near the crack tip (Figure 4.6) using Gal/WF: C^{11} solutions

Path	C^{11} p=3 $J^f/2:\Gamma_1$ path	A_J	K_I^f	% Error based on K_I	C^f	C^{11} p=5 $J^f/2:\Gamma_1$ path	A_J	K_I^f	% Error based on K_I	C^f	C^{11} p=7 $J^f/2:\Gamma_1$ path	A_J	K_I^f	% Error based on K_I	C^f
1	4.73856E-07	1.051E-07	1.1241E-03	-0.2772	1.0028	4.73920E-07	8.086E-08	1.1242E-03	-0.2840	1.0028	4.73838E-07	5.888E-08	1.1241E-03	-0.2754	1.0028
2	4.73817E-07	9.851E-08	1.1241E-03	-0.2732	1.0027	4.73610E-07	8.020E-08	1.1238E-03	-0.2512	1.0025	4.73656E-07	5.829E-08	1.1239E-03	-0.2561	1.0026
3	4.73636E-07	9.522E-08	1.1238E-03	-0.2540	1.0025	4.73594E-07	7.993E-08	1.1238E-03	-0.2495	1.0025	4.73650E-07	5.814E-08	1.1239E-03	-0.2555	1.0026
4	4.73577E-07	9.270E-08	1.1238E-03	-0.2477	1.0025	4.73594E-07	7.983E-08	1.1238E-03	-0.2496	1.0025	4.73649E-07	5.813E-08	1.1239E-03	-0.2554	1.0026
5	4.73543E-07	9.026E-08	1.1237E-03	-0.2442	1.0024	4.73596E-07	7.975E-08	1.1238E-03	-0.2498	1.0025	4.73649E-07	5.813E-08	1.1239E-03	-0.2554	1.0026
6	4.73518E-07	8.781E-08	1.1237E-03	-0.2415	1.0024	4.73597E-07	7.968E-08	1.1238E-03	-0.2499	1.0025	4.73649E-07	5.812E-08	1.1239E-03	-0.2554	1.0026
7	4.73496E-07	8.533E-08	1.1237E-03	-0.2392	1.0024	4.73598E-07	7.961E-08	1.1238E-03	-0.2500	1.0025	4.73649E-07	5.812E-08	1.1239E-03	-0.2554	1.0026
8	4.73522E-07	8.283E-08	1.1237E-03	-0.2420	1.0024	4.73598E-07	7.955E-08	1.1238E-03	-0.2500	1.0025	4.73649E-07	5.812E-08	1.1239E-03	-0.2554	1.0026
9	4.73594E-07	8.032E-08	1.1238E-03	-0.2495	1.0025	4.73598E-07	7.949E-08	1.1238E-03	-0.2500	1.0025	4.73649E-07	5.812E-08	1.1239E-03	-0.2554	1.0026
10	4.73511E-07	7.785E-08	1.1237E-03	-0.2408	1.0024	4.73598E-07	7.943E-08	1.1238E-03	-0.2500	1.0025	4.73649E-07	5.812E-08	1.1239E-03	-0.2554	1.0026
11	4.73561E-07	7.558E-08	1.1238E-03	-0.2461	1.0025	4.73597E-07	7.939E-08	1.1238E-03	-0.2499	1.0025	4.73650E-07	5.811E-08	1.1239E-03	-0.2555	1.0026
12	4.73514E-07	7.409E-08	1.1237E-03	-0.2411	1.0024	4.73592E-07	7.938E-08	1.1238E-03	-0.2494	1.0025	4.73656E-07	5.803E-08	1.1239E-03	-0.2562	1.0026
13	4.73644E-07	7.590E-08	1.1239E-03	-0.2549	1.0025	4.73556E-07	7.960E-08	1.1238E-03	-0.2456	1.0025	4.73701E-07	5.744E-08	1.1239E-03	-0.2609	1.0026

Table 4.11c: Influence of higher order global differentiability for b/a=16, h/a=35 and a=0.4: A 180 element mesh in region of near the crack tip (Figure 4.6) using Gal/WF: C^{22} solutions

	C^{22} p=5					C^{22} p=7				
Path	$J^f/2 : \Gamma_1$ path	A_J	K_I^f	% Error based on K_I	C^f	$J^f/2 : \Gamma_1$ path	A_J	K_I^f	% Error based on K_I	C^f
1	4.72119E-07	-1.102E-08	1.1220E-03	-0.0934	1.0009	4.73239E-07	-1.481E-08	1.1234E-03	-0.2120	1.0021
2	4.73668E-07	-1.191E-08	1.1239E-03	-0.2574	1.0026	4.73566E-07	-1.542E-08	1.1238E-03	-0.2466	1.0025
3	4.73393E-07	-1.100E-08	1.1236E-03	-0.2283	1.0023	4.73531E-07	-1.495E-08	1.1237E-03	-0.2429	1.0024
4	4.73429E-07	-1.127E-08	1.1236E-03	-0.2321	1.0023	4.73535E-07	-1.505E-08	1.1237E-03	-0.2433	1.0024
5	4.73427E-07	-1.129E-08	1.1236E-03	-0.2319	1.0023	4.73535E-07	-1.504E-08	1.1237E-03	-0.2433	1.0024
6	4.73428E-07	-1.135E-08	1.1236E-03	-0.2320	1.0023	4.73535E-07	-1.504E-08	1.1237E-03	-0.2433	1.0024
7	4.73428E-07	-1.140E-08	1.1236E-03	-0.2320	1.0023	4.73535E-07	-1.505E-08	1.1237E-03	-0.2433	1.0024
8	4.73428E-07	-1.144E-08	1.1236E-03	-0.2320	1.0023	4.73535E-07	-1.505E-08	1.1237E-03	-0.2433	1.0024
9	4.73428E-07	-1.149E-08	1.1236E-03	-0.2320	1.0023	4.73535E-07	-1.505E-08	1.1237E-03	-0.2433	1.0024
10	4.73428E-07	-1.151E-08	1.1236E-03	-0.2320	1.0023	4.73535E-07	-1.506E-08	1.1237E-03	-0.2433	1.0024
11	4.73428E-07	-1.161E-08	1.1236E-03	-0.2320	1.0023	4.73534E-07	-1.502E-08	1.1237E-03	-0.2432	1.0024
12	4.73425E-07	-1.139E-08	1.1236E-03	-0.2316	1.0023	4.73538E-07	-1.523E-08	1.1237E-03	-0.2437	1.0024
13	4.73394E-07	-1.188E-08	1.1236E-03	-0.2284	1.0023	4.73560E-07	-1.459E-08	1.1238E-03	-0.2460	1.0025

Table 4.11d: Influence of higher order global differentiability for b/a=16, h/a=35 and a=0.4: A 180 element mesh in region of near the crack tip (Figure 4.6) using Gal/WF: C^{33} solutions

	C^{33} p=7				
Path	$J^f/2 : \Gamma_1$ path	A_J	K_I^f	% Error based on K_I	C^f
1	4.73414E-07	-3.426E-09	1.1236E-03	-0.2305	1.0023
2	4.73407E-07	4.466E-10	1.1236E-03	-0.2298	1.0023
3	4.73420E-07	8.252E-10	1.1236E-03	-0.2312	1.0023
4	4.73414E-07	1.042E-09	1.1236E-03	-0.2305	1.0023
5	4.73412E-07	1.076E-09	1.1236E-03	-0.2303	1.0023
6	4.73411E-07	1.084E-09	1.1236E-03	-0.2302	1.0023
7	4.73411E-07	1.082E-09	1.1236E-03	-0.2302	1.0023
8	4.73410E-07	1.082E-09	1.1236E-03	-0.2301	1.0023
9	4.73410E-07	1.081E-09	1.1236E-03	-0.2301	1.0023
10	4.73411E-07	1.078E-09	1.1236E-03	-0.2302	1.0023
11	4.73412E-07	1.064E-09	1.1236E-03	-0.2303	1.0023
12	4.73419E-07	9.672E-10	1.1236E-03	-0.2310	1.0023
13	4.73417E-07	1.945E-10	1.1236E-03	-0.2308	1.0023

4.8 Case (e); Integral Form: Gal/WF; Influence of Non-differentiable Integral Paths on the J-integral Computations

In chapter 3 we have shown that for the J-integral to be valid the integral path Γ should be continuous and differentiable. Non differentiable paths are quite common in finite element fracture mechanics studies that insist on using linear local approximations for triangular or quadrilateral elements in which the element sides are straight lines. In the study presented here non-differentiable paths are artificially created by using zij-zag choices of boundaries to illustrate the damage done to the J^f computation by using such paths. The points where the path is non-differentiable will be referred to as sharp corners. We consider $h/a=35$, $b/a=16$ and $a=0.4$. The domain is close to infinite compared to the size of the crack. We consider a discretization strategy similar to that shown in Figure 4.6. The zone at the crack tip is modeled using 180 element graded mesh shown in Figure 4.3 and the remainder of the domain is modeled using a coarse mesh. Figure 4.9 shows various circular differentiable integration paths as well as the non-differentiable paths artificially created by using element boundaries. Each non-differentiable path contains four sharp corners. Figure 4.10 and Figure 4.11 also show non-differentiable paths for the same discretization. Each non-differentiable path in Figure 4.10 contains 10 sharp corners where as those in Figure 4.11 contain 22 sharp corners for each path. Computations are performed using local approximations of class $C^{11}(\bar{\Omega}^e)$ with *p*-level of 5. For the non-differentiable paths shown in Figure 4.9 through Figure 4.11, J^f, A_J and % error (compared to J using theoretical value of K_I for infinite medium) are computed and are tabulated in table 4.12. J^f, A_J and % error for the corresponding differentiable paths are also tabulated for comparison purposes. Progressive deterioration (i.e. increase in % error) of the computed results for increasing number of sharp corners is quite clear. Introducing 4 sharp corners along the integration paths increases the % error values up to -3.4654. When the number of sharp corners is increased to 10, the % error is increased to values up to -5.0433. When 22 sharp corners are considered, % error values up to -10.1928 are observed.

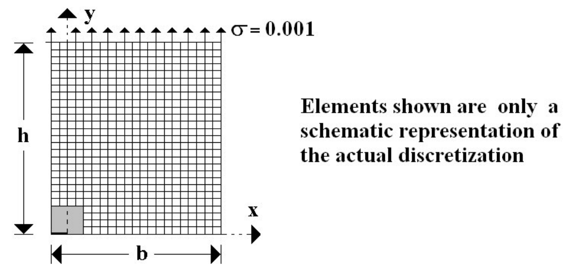

(a) Schematic of the mesh for (h/a) of 35 (b/a) of 16 and a=0.4

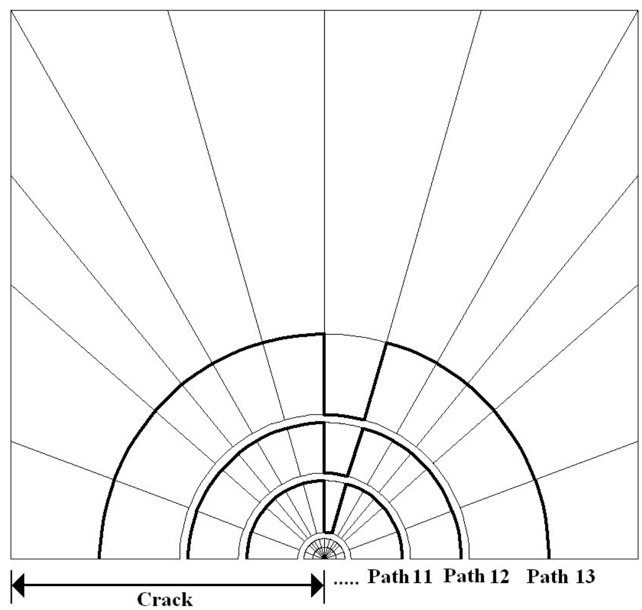

(b) A 180 element discretization shown in figure 4.3 for the shaded region of figure 4.9 (a)

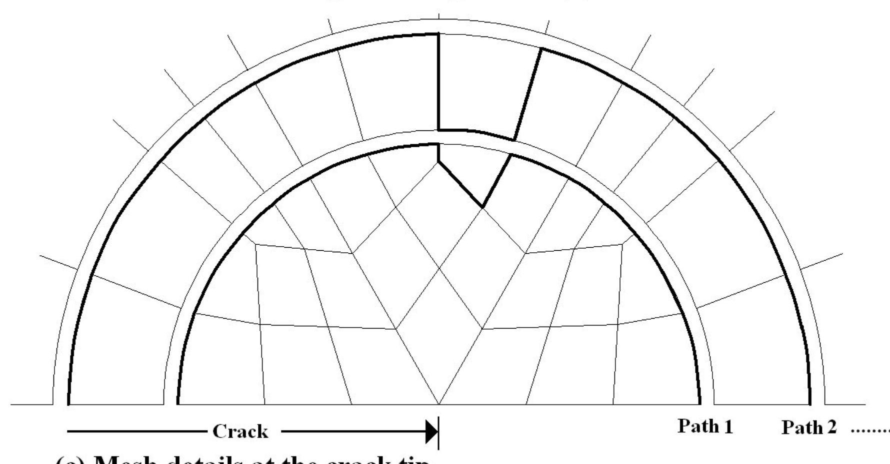

(c) Mesh details at the crack tip

Figure 4.9: Discretization for 4 sharp corners study for h/a=35, b/a=16 and a=0.4

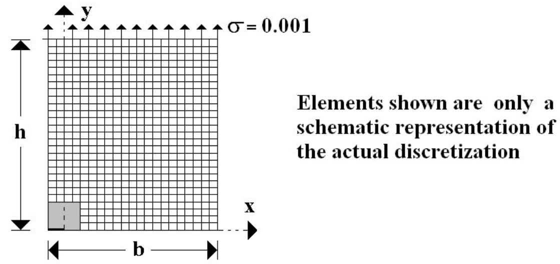

(a) Schematic of the mesh for (h/a) of 35 (b/a) of 16 and a=0.4

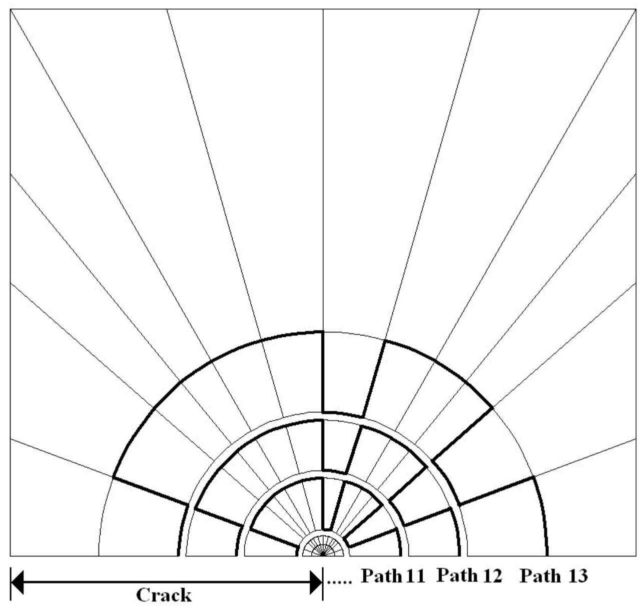

(b) A 180 element discretization shown in figure 4.3 for the shaded region of figure 4.10 (a)

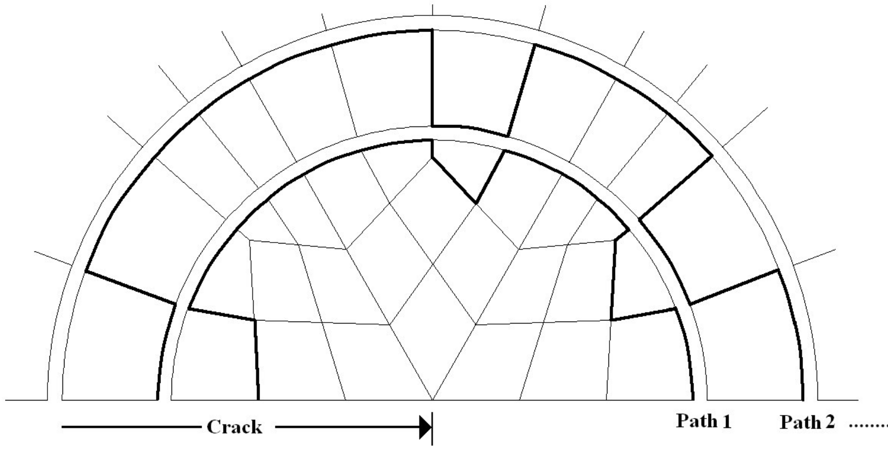

(c) Mesh details at the crack tip

Figure 4.10: Discretization for 10 sharp corners study for h/a=35, b/a=16 and a=0.4

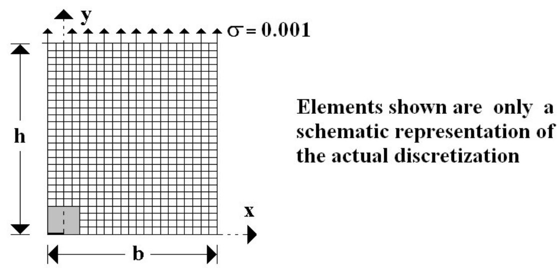

(a) Schematic of the mesh for (h/a) of 35 (b/a) of 16 and a=0.4

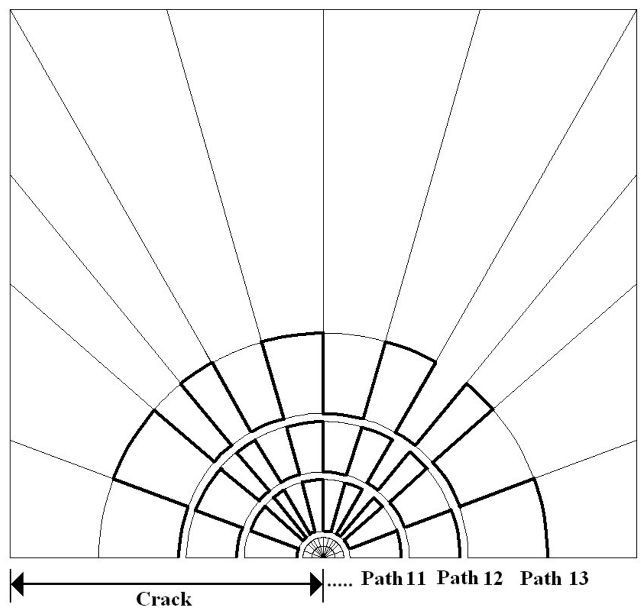

(b) A 180 element discretization shown in figure 4.3 for the shaded region of figure 4.11(a)

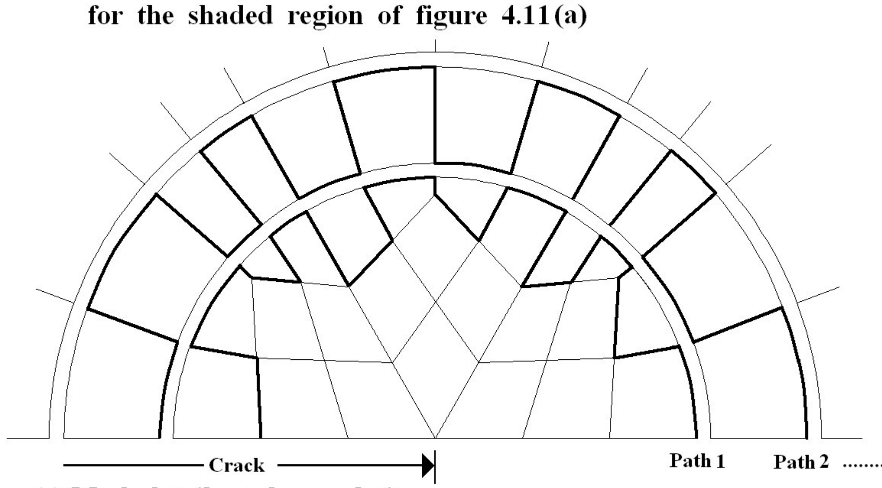

(c) Mesh details at the crack tip

Figure 4.11: Discretization for 22 sharp corners study for h/a=35, b/a=16 and a=0.4

Table 4.12a: Influence of non differentiable paths for b/a=16, h/a=35 and a=0.4: A 180 element mesh in the region near the crack tip (Figure 4.9) using Gal/WF: C^{11} solutions and p=5

		Differentiable paths					4 sharp corners				
Path	Radius	$J^f/2 : \Gamma_1$ path	A_J	K_I^f	% Error based on K_I	C^f	$J^f/2 : \Gamma_1$ path	A_J	K_I^f	% Error based on K_I	C^f
1	0.000375	4.73920E-07	8.086E-08	1.1242E-03	-0.2840	1.0028	4.64423E-07	8.09500E-08	1.1129E-03	0.7258	0.9927
2	0.000598	4.73610E-07	8.020E-08	1.1238E-03	-0.2512	1.0025	4.77656E-07	8.02040E-08	1.1286E-03	-0.6786	1.0068
3	0.000994	4.73594E-07	7.993E-08	1.1238E-03	-0.2495	1.0025	4.77194E-07	7.99329E-08	1.1281E-03	-0.6299	1.0063
4	0.001699	4.73594E-07	7.983E-08	1.1238E-03	-0.2496	1.0025	4.77059E-07	7.98376E-08	1.1279E-03	-0.6157	1.0062
5	0.002953	4.73596E-07	7.975E-08	1.1238E-03	-0.2498	1.0025	4.77294E-07	7.97581E-08	1.1282E-03	-0.6404	1.0064
6	0.005187	4.73597E-07	7.968E-08	1.1238E-03	-0.2499	1.0025	4.77871E-07	7.96859E-08	1.1289E-03	-0.7012	1.0070
7	0.009163	4.73598E-07	7.961E-08	1.1238E-03	-0.2500	1.0025	4.78755E-07	7.96187E-08	1.1299E-03	-0.7943	1.0079
8	0.016240	4.73598E-07	7.955E-08	1.1238E-03	-0.2500	1.0025	4.79925E-07	7.95550E-08	1.1313E-03	-0.9175	1.0092
9	0.028837	4.73598E-07	7.949E-08	1.1238E-03	-0.2500	1.0025	4.81407E-07	7.94944E-08	1.1330E-03	-1.0731	1.0107
10	0.051260	4.73598E-07	7.943E-08	1.1238E-03	-0.2500	1.0025	4.83362E-07	7.94387E-08	1.1353E-03	-1.2781	1.0128
11	0.091172	4.73597E-07	7.939E-08	1.1238E-03	-0.2499	1.0025	4.86374E-07	7.93946E-08	1.1389E-03	-1.5932	1.0159
12	0.162217	4.73592E-07	7.938E-08	1.1238E-03	-0.2494	1.0025	4.92146E-07	7.93880E-08	1.1456E-03	-2.1942	1.0219
13	0.287102	4.73556E-07	7.960E-08	1.1238E-03	-0.2456	1.0025	5.04465E-07	7.95995E-08	1.1598E-03	-3.4654	1.0347

Table 4.12b: Influence of non differentiable paths for b/a=16, h/a=35 and a=0.4: A 180 element mesh in region near the crack tip (Figure 4.10 and Figure 4.11) using Gal/WF: C^{11} solutions and p=5

		10 sharp corners					22 sharp corners				
Path	Radius	$J^f/2 : \Gamma_1$ path	A_J	K_I^f	% Error based on K_I	C^f	$J^f/2 : \Gamma_1$ path	A_J	K_I^f	% Error based on K_I	C^f
1	0.000375	4.48331E-07	8.070E-08	1.0934E-03	2.4609	0.9754	3.95708E-07	8.11949E-08	1.0272E-03	8.3639	0.9164
2	0.000598	4.78531E-07	8.036E-08	1.1296E-03	-0.7708	1.0077	4.87109E-07	8.04433E-08	1.1397E-03	-1.6700	1.0167
3	0.000994	4.78079E-07	7.998E-08	1.1291E-03	-0.7232	1.0072	4.85527E-07	7.99963E-08	1.1379E-03	-1.5046	1.0150
4	0.001699	4.78169E-07	7.984E-08	1.1292E-03	-0.7326	1.0073	4.85287E-07	7.98537E-08	1.1376E-03	-1.4796	1.0148
5	0.002953	4.78718E-07	7.976E-08	1.1299E-03	-0.7905	1.0079	4.86254E-07	7.97756E-08	1.1387E-03	-1.5807	1.0158
6	0.005187	4.79707E-07	7.969E-08	1.1310E-03	-0.8945	1.0089	4.88310E-07	7.97049E-08	1.1411E-03	-1.7952	1.0180
7	0.009163	4.81117E-07	7.962E-08	1.1327E-03	-1.0427	1.0104	4.91295E-07	7.96387E-08	1.1446E-03	-2.1059	1.0211
8	0.016240	4.82954E-07	7.956E-08	1.1348E-03	-1.2354	1.0124	4.95070E-07	7.95756E-08	1.1490E-03	-2.4973	1.0250
9	0.028837	4.85294E-07	7.950E-08	1.1376E-03	-1.4803	1.0148	4.99587E-07	7.95155E-08	1.1542E-03	-2.9639	1.0296
10	0.051260	4.88417E-07	7.944E-08	1.1412E-03	-1.8063	1.0181	5.05192E-07	7.94597E-08	1.1607E-03	-3.5399	1.0354
11	0.091172	4.93195E-07	7.940E-08	1.1468E-03	-2.3031	1.0230	5.13633E-07	7.94147E-08	1.1703E-03	-4.4013	1.0440
12	0.162217	5.02017E-07	7.939E-08	1.1570E-03	-3.2140	1.0321	5.30900E-07	7.94034E-08	1.1898E-03	-6.1417	1.0614
13	0.287102	5.19969E-07	7.960E-08	1.1775E-03	-5.0433	1.0504	5.72199E-07	7.96289E-08	1.2353E-03	-10.1928	1.1019

4.9 Case (f); Integral Form: Gal/WF; Accuracy of J-integral Computations for Differentiable but Non-circular Paths

We consider $a = 0.1$, $h/a = 7$, $b/a = 0.8$. Figure 4.12 shows a 480 element graded discretization. To the right of the crack tip, the paths are circular but to the left of the crack tip they are elliptic. All paths are continuous and differentiable. Figure 4.13 shows a 1920 element more refined and graded discretization with similar J-integral paths. In the zone near the crack tip, almost-circular paths (see table 4.13 and 4.14) are considered so that the J-integral values from these paths could be compared with those that are noncircular and are located outside the zone near the crack tip. We consider solutions of class $C^{11}(\bar{\Omega}^e)$ and *p*-level of 5. Tables 4.13 and 4.14 give the path description, J^f, A_J and C_f. The two discretizations yield identical results. Results from the circular paths are tabulated in Table 4.15. Each path in this case also yields almost same values of C^f which only differ from the C^f in Tables 4.13 and 4.14 at the third decimal place. Excessively distorted elements to the left of the crack tip in discretizations of Figure 4.12 and Figure 4.13 do not affect the accuracy of the computations.

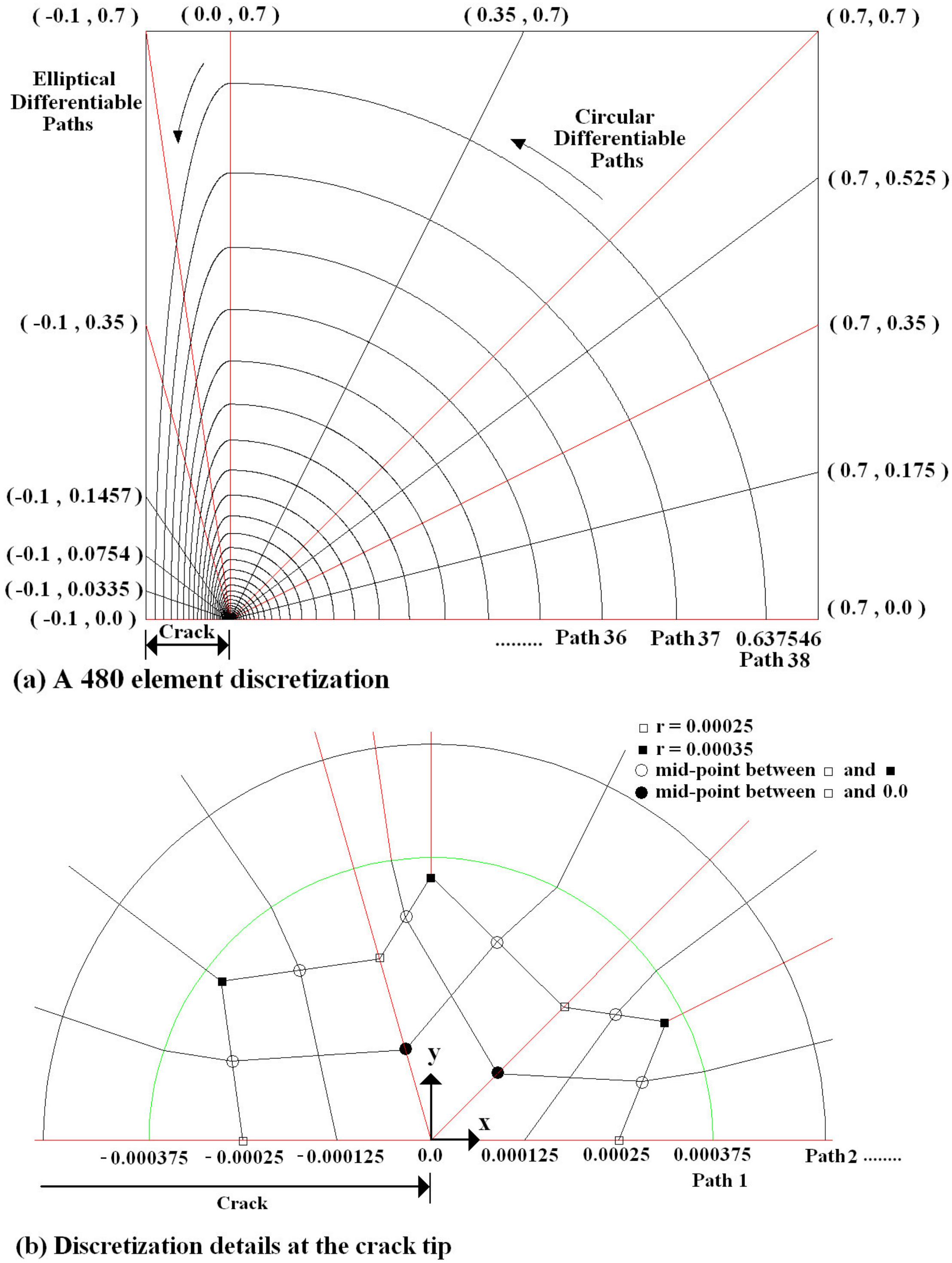

Figure 4.12: A 480 element graded discretization of quarter domain: non circular differentiable J-integral paths (a=0.1)

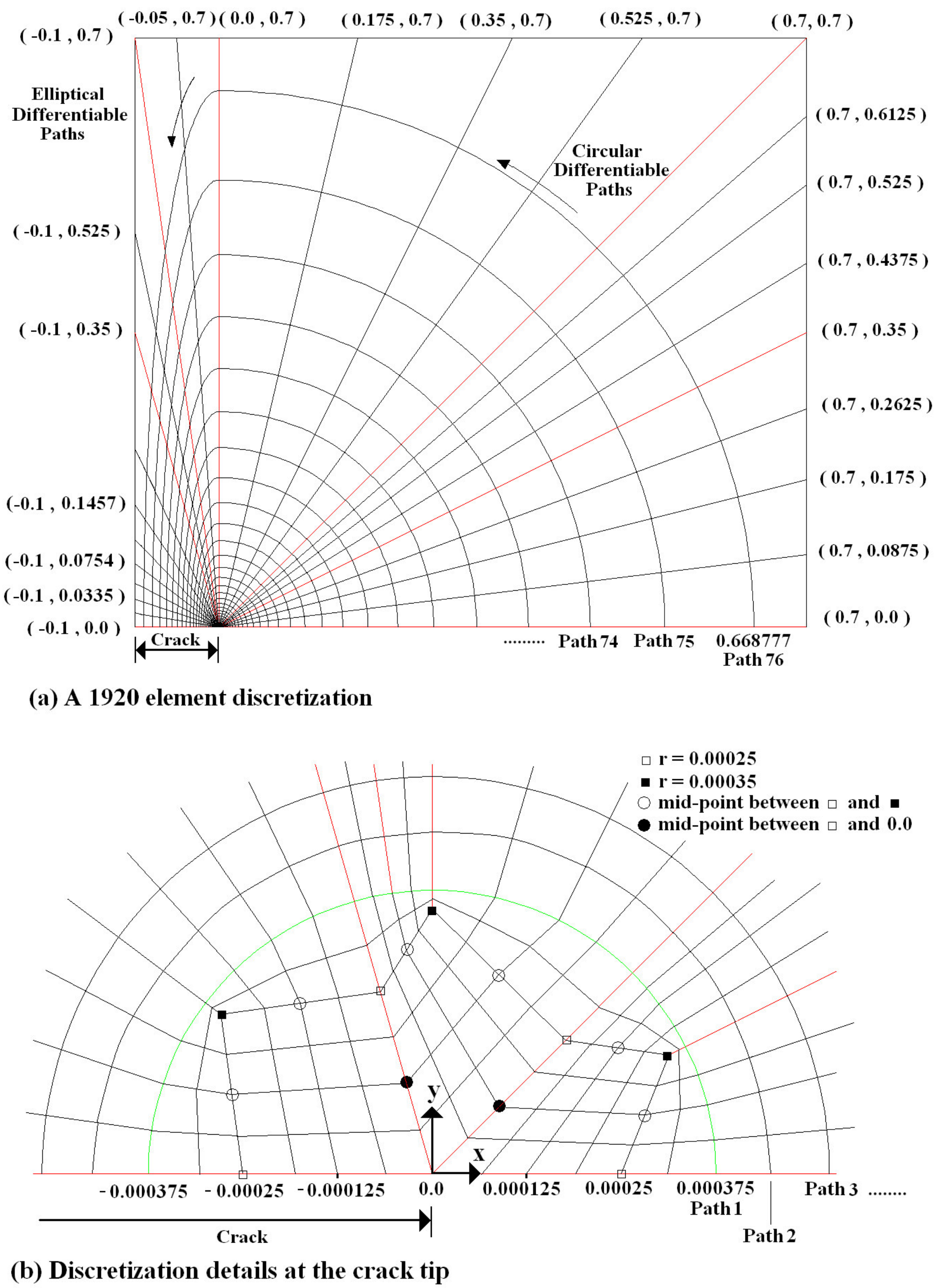

Figure 4.13: A 1920 element graded discretization of quarter domain: non circular differentiable J-integral paths (a=0.1)

Table 4.13: Influence of differentiable but non circular paths: A 480 Element mesh (a=0.1, b/a=8, h/a=7): using Gal/WF: C^{11} solutions and p=5 (Figure 4.12)

Path	Radius Semimajor Axis	Semiminor Axis	$J^f/2 : \Gamma_1$ path	A_J	C^f
1	0.000375	0.000375	1.244631E-07	1.334E-08	1.0278
2	0.000525	0.000516	1.244629E-07	1.265E-08	1.0278
3	0.000705	0.000674	1.244603E-07	1.259E-08	1.0278
4	0.000921	0.000853	1.244598E-07	1.259E-08	1.0278
5	0.001180	0.001054	1.244597E-07	1.259E-08	1.0278
6	0.001491	0.001280	1.244597E-07	1.259E-08	1.0278
7	0.001864	0.001535	1.244597E-07	1.259E-08	1.0278
8	0.002312	0.001822	1.244597E-07	1.259E-08	1.0278
9	0.002850	0.002145	1.244597E-07	1.259E-08	1.0278
10	0.003495	0.002508	1.244597E-07	1.259E-08	1.0278
11	0.004269	0.002918	1.244597E-07	1.259E-08	1.0278
12	0.005198	0.003379	1.244597E-07	1.259E-08	1.0278
13	0.006312	0.003898	1.244597E-07	1.259E-08	1.0278
14	0.007649	0.004483	1.244597E-07	1.259E-08	1.0278
15	0.009254	0.005141	1.244597E-07	1.258E-08	1.0278
16	0.011180	0.005882	1.244597E-07	1.258E-08	1.0278
17	0.013491	0.006717	1.244597E-07	1.258E-08	1.0278
18	0.016265	0.007657	1.244597E-07	1.258E-08	1.0278
19	0.019593	0.008715	1.244597E-07	1.258E-08	1.0278
20	0.023586	0.009907	1.244597E-07	1.258E-08	1.0278
21	0.028378	0.011249	1.244597E-07	1.257E-08	1.0278
22	0.034129	0.012760	1.244597E-07	1.257E-08	1.0278
23	0.041030	0.014461	1.244596E-07	1.257E-08	1.0278
24	0.049311	0.016376	1.244596E-07	1.257E-08	1.0278
25	0.059248	0.018533	1.244595E-07	1.257E-08	1.0278
26	0.071172	0.020962	1.244595E-07	1.257E-08	1.0278
27	0.085482	0.023697	1.244595E-07	1.256E-08	1.0278
28	0.102653	0.026776	1.244595E-07	1.256E-08	1.0278
29	0.123258	0.030243	1.244595E-07	1.256E-08	1.0278
30	0.147985	0.034147	1.244595E-07	1.255E-08	1.0278
31	0.177657	0.038543	1.244596E-07	1.255E-08	1.0278
32	0.213264	0.043493	1.244597E-07	1.254E-08	1.0278
33	0.255991	0.049067	1.244597E-07	1.254E-08	1.0278
34	0.307265	0.055343	1.244595E-07	1.254E-08	1.0278
35	0.368793	0.062409	1.244591E-07	1.254E-08	1.0278
36	0.442626	0.070366	1.244587E-07	1.254E-08	1.0278
37	0.531226	0.079326	1.244586E-07	1.255E-08	1.0278
38	0.637547	0.089415	1.244584E-07	1.257E-08	1.0278

Table 4.14a: Influence of differentiable but non circular paths (1 – 38): A 1920 Element mesh (a=0.1, b/a=8 h/a=7): using Gal/WF: C^{11} solutions and p=5 (Figure 4.13)

Path	Radius Semimajor Axis	Semiminor Axis	$J^f/2$: Γ_1 path	A_J	C^f
1	0.000375	0.000375	1.244573E-07	1.240E-08	1.0278
2	0.000450	0.000445	1.244569E-07	1.239E-08	1.0278
3	0.000525	0.000516	1.244570E-07	1.238E-08	1.0278
4	0.000615	0.000595	1.244570E-07	1.238E-08	1.0278
5	0.000705	0.000674	1.244570E-07	1.238E-08	1.0278
6	0.000813	0.000763	1.244570E-07	1.238E-08	1.0278
7	0.000921	0.000853	1.244570E-07	1.238E-08	1.0278
8	0.001051	0.000953	1.244570E-07	1.238E-08	1.0278
9	0.001180	0.001054	1.244570E-07	1.238E-08	1.0278
10	0.001336	0.001167	1.244570E-07	1.238E-08	1.0278
11	0.001491	0.001280	1.244570E-07	1.238E-08	1.0278
12	0.001678	0.001407	1.244570E-07	1.238E-08	1.0278
13	0.001864	0.001535	1.244570E-07	1.238E-08	1.0278
14	0.002088	0.001678	1.244570E-07	1.238E-08	1.0278
15	0.002312	0.001822	1.244570E-07	1.238E-08	1.0278
16	0.002581	0.001983	1.244570E-07	1.238E-08	1.0278
17	0.002850	0.002145	1.244570E-07	1.238E-08	1.0278
18	0.003172	0.002326	1.244570E-07	1.238E-08	1.0278
19	0.003495	0.002508	1.244570E-07	1.238E-08	1.0278
20	0.003882	0.002713	1.244570E-07	1.238E-08	1.0278
21	0.004269	0.002918	1.244570E-07	1.238E-08	1.0278
22	0.004733	0.003148	1.244570E-07	1.238E-08	1.0278
23	0.005198	0.003379	1.244570E-07	1.238E-08	1.0278
24	0.005755	0.003639	1.244570E-07	1.238E-08	1.0278
25	0.006312	0.003898	1.244570E-07	1.238E-08	1.0278
26	0.006981	0.004190	1.244570E-07	1.238E-08	1.0278
27	0.007649	0.004483	1.244570E-07	1.238E-08	1.0278
28	0.008452	0.004812	1.244570E-07	1.238E-08	1.0278
29	0.009254	0.005141	1.244570E-07	1.238E-08	1.0278
30	0.010217	0.005512	1.244570E-07	1.238E-08	1.0278
31	0.011180	0.005882	1.244570E-07	1.238E-08	1.0278
32	0.012336	0.006300	1.244570E-07	1.238E-08	1.0278
33	0.013491	0.006717	1.244570E-07	1.238E-08	1.0278
34	0.014878	0.007187	1.244570E-07	1.238E-08	1.0278
35	0.016265	0.007657	1.244570E-07	1.238E-08	1.0278
36	0.017929	0.008186	1.244570E-07	1.238E-08	1.0278
37	0.019593	0.008715	1.244570E-07	1.238E-08	1.0278
38	0.021589	0.009311	1.244570E-07	1.238E-08	1.0278

Table 4.14b: Influence of differentiable but non circular paths (39 – 76): A 1920 Element mesh (a=0.1, b/a=8, h/a=7): using Gal/WF: C [11] solutions and *p*=5 (Figure 4.13)

Path	Radius Semimajor Axis	Semiminor Axis	$J^f/2 : \Gamma_1$ path	A_J	C^f
39	0.023586	0.009907	1.244570E-07	1.238E-08	1.0278
40	0.025982	0.010578	1.244570E-07	1.238E-08	1.0278
41	0.028378	0.011249	1.244570E-07	1.238E-08	1.0278
42	0.031254	0.012004	1.244570E-07	1.238E-08	1.0278
43	0.034129	0.012760	1.244570E-07	1.238E-08	1.0278
44	0.037579	0.013610	1.244570E-07	1.238E-08	1.0278
45	0.041030	0.014461	1.244570E-07	1.238E-08	1.0278
46	0.045170	0.015418	1.244570E-07	1.238E-08	1.0278
47	0.049311	0.016376	1.244570E-07	1.238E-08	1.0278
48	0.054279	0.017455	1.244570E-07	1.238E-08	1.0278
49	0.059248	0.018533	1.244570E-07	1.238E-08	1.0278
50	0.065210	0.019747	1.244570E-07	1.238E-08	1.0278
51	0.071172	0.020962	1.244570E-07	1.238E-08	1.0278
52	0.078327	0.022329	1.244570E-07	1.238E-08	1.0278
53	0.085482	0.023697	1.244570E-07	1.238E-08	1.0278
54	0.094067	0.025236	1.244570E-07	1.238E-08	1.0278
55	0.102653	0.026776	1.244570E-07	1.238E-08	1.0278
56	0.112956	0.028509	1.244570E-07	1.238E-08	1.0278
57	0.123258	0.030243	1.244570E-07	1.238E-08	1.0278
58	0.135622	0.032195	1.244570E-07	1.238E-08	1.0278
59	0.147985	0.034147	1.244570E-07	1.238E-08	1.0278
60	0.162821	0.036345	1.244570E-07	1.238E-08	1.0278
61	0.177657	0.038543	1.244570E-07	1.238E-08	1.0278
62	0.195460	0.041018	1.244570E-07	1.238E-08	1.0278
63	0.213264	0.043493	1.244570E-07	1.238E-08	1.0278
64	0.234628	0.046280	1.244570E-07	1.238E-08	1.0278
65	0.255991	0.049067	1.244570E-07	1.238E-08	1.0278
66	0.281628	0.052205	1.244570E-07	1.238E-08	1.0278
67	0.307265	0.055343	1.244570E-07	1.238E-08	1.0278
68	0.338029	0.058876	1.244570E-07	1.238E-08	1.0278
69	0.368793	0.062409	1.244570E-07	1.238E-08	1.0278
70	0.405709	0.066639	1.244570E-07	1.238E-08	1.0278
71	0.442626	0.070366	1.244570E-07	1.238E-08	1.0278
72	0.486926	0.074846	1.244570E-07	1.238E-08	1.0278
73	0.531226	0.079326	1.244569E-07	1.238E-08	1.0278
74	0.584387	0.084370	1.244569E-07	1.238E-08	1.0278
75	0.637547	0.089415	1.244569E-07	1.238E-08	1.0278
76	0.668773	0.094707	1.244569E-07	1.238E-08	1.0278

Table 4.15: A 180 Element mesh (a=0.4, b/a=8, h/a=7) in region of near the crack tip: using Gal/WF: *C* [11] solutions and *p*=5 (discretization similar to Figure 4.6)

Path	Radius	$J^f/2 : \Gamma_1$ path	A_J	C^f
1	0.000375	4.98396E-07	8.505E-08	1.0284
2	0.000598	4.98070E-07	8.435E-08	1.0281
3	0.000994	4.98053E-07	8.406E-08	1.0281
4	0.001699	4.98054E-07	8.396E-08	1.0281
5	0.002953	4.98056E-07	8.388E-08	1.0281
6	0.005187	4.98057E-07	8.380E-08	1.0281
7	0.009163	4.98058E-07	8.373E-08	1.0281
8	0.016240	4.98058E-07	8.366E-08	1.0281
9	0.028837	4.98058E-07	8.360E-08	1.0281
10	0.051260	4.98058E-07	8.354E-08	1.0281
11	0.091172	4.98057E-07	8.349E-08	1.0281
12	0.162217	4.98052E-07	8.349E-08	1.0281
13	0.287102	4.98014E-07	8.372E-08	1.0280

4.10 Case (g); Integral Form: LSP using weak form of GDEs; Influence of the Solution of Higher Classes on J-integral Computations

In this study we investigate the influence of higher order global differentiability on J-integral computations using LSP with weak form of GDEs. We consider $a = 0.4$, $b/a = 35$ $(h = 14.0)$ and $b/a = 16$ $(b = 4.8)$. The domain is close to infinite compared to the size of the crack. We consider a discretization strategy similar to that shown in Figure 4.6. The zone at the crack tip is modeled using 180 element graded mesh shown in Figure 4.3 and the remainder of the domain is modeled using a coarse mesh. We investigate the following classes of solutions and *p*-levels:

$C^{00}(\bar{\Omega}^e)$; *p*-level of 3, 5, 7

$C^{11}(\bar{\Omega}^e)$; *p*-level of 3, 5, 7

$C^{22}(\bar{\Omega}^e)$; *p*-level of 5, 7

$C^{33}(\bar{\Omega}^e)$; *p*-level of 7

Integral paths, path radius, J^f, K_I^f, A_J and C^f are summarized in tables 4.16(a) – 4.16(d). We make the following observations and remarks.

(1) Since h/a and b/a are very large, we can consider the center crack to be in a infinite medium, and a 180 element mesh in the crack zone has proven to be excellent, we expect $C^f \cong 1$ in all studies.

(2) For all cases we note that $C^f = 1.00--$ indicating exceptional accuracy of all computed results for various orders of global differentiability listed above.

(3) Closer examination of C^f reveals improvement in second and fourth decimal places for :

(a) increasing *p*-level for $C^{00}(\bar{\Omega}^e)$, $C^{11}(\bar{\Omega}^e)$ and $C^{22}(\bar{\Omega}^e)$ classes of solutions

(b) increasing order of global differentiability

(4) A_J well below $O(10^{-8})$ confirm path independence of J-integral in computations.

(5) While it might appear (examining C^f) that there is no apparent gain in going to higher classes, this is not so. We note that $C^{00} \rightarrow C^{11} \rightarrow C^{22} \rightarrow C^{33}$ results in progressively reduced total degrees of freedom. Thus, a comparable accuracy is obtained with progressively higher classes in spite of substantial reduction in total degrees of freedom.

Table 4.16a: Influence of higher order global differentiability for b/a=16, h/a=35 and a=0.4: A 180 element mesh in region of near the crack tip (Figure 4.6) using LSP using weak form of GDEs: C^{00} solutions

	C^{00} p=3	dofs = 122,958				C^{00} p=5	dofs = 341,130				C^{00} p=7	dofs = 668,262			
Path	$J^f/2 : \Gamma_1$ path	A_J	K_I^f	% Error based on K_I	C^f	$J^f/2 : \Gamma_1$ path	A_J	K_I^f	% Error based on K_I	C^f	$J^f/2 : \Gamma_1$ path	A_J	K_I^f	% Error based on K_I	C^f
1	4.03150E-07		1.0369E-03	7.5062	0.9249	4.67736E-07		1.1168E-03	0.3724	0.9963	4.91646E-07		1.1450E-03	-2.1423	1.0214
2	4.18116E-07		1.0559E-03	5.8050	0.9419	4.69073E-07		1.1184E-03	0.2301	0.9977	4.73503E-07		1.1237E-03	-0.2399	1.0024
3	4.38950E-07		1.0819E-03	3.4868	0.9651	4.71041E-07		1.1208E-03	0.0210	0.9998	4.72545E-07		1.1226E-03	-0.1385	1.0014
4	4.55368E-07		1.1020E-03	1.6984	0.9830	4.71979E-07		1.1219E-03	-0.0785	1.0008	4.72828E-07		1.1229E-03	-0.1685	1.0017
5	4.63652E-07		1.1119E-03	0.8083	0.9919	4.72465E-07		1.1225E-03	-0.1301	1.0013	4.73008E-07		1.1231E-03	-0.1876	1.0019
6	4.67404E-07	not	1.1164E-03	0.4077	0.9959	4.72745E-07	not	1.1228E-03	-0.1597	1.0016	4.73115E-07	not	1.1232E-03	-0.1989	1.0020
7	4.69610E-07	possible	1.1191E-03	0.1730	0.9983	4.72947E-07	possible	1.1230E-03	-0.1811	1.0018	4.73179E-07	possible	1.1233E-03	-0.2056	1.0021
8	4.71783E-07		1.1216E-03	-0.0577	1.0006	4.73130E-07		1.1232E-03	-0.2005	1.0020	4.73216E-07		1.1233E-03	-0.2096	1.0021
9	4.74020E-07		1.1243E-03	-0.2947	1.0029	4.73261E-07		1.1234E-03	-0.2144	1.0021	4.73237E-07		1.1234E-03	-0.2118	1.0021
10	4.75432E-07		1.1260E-03	-0.4439	1.0044	4.73320E-07		1.1235E-03	-0.2206	1.0022	4.73248E-07		1.1234E-03	-0.2130	1.0021
11	4.75759E-07		1.1264E-03	-0.4785	1.0048	4.73334E-07		1.1235E-03	-0.2221	1.0022	4.73256E-07		1.1234E-03	-0.2138	1.0021
12	4.75510E-07		1.1261E-03	-0.4522	1.0045	4.73381E-07		1.1235E-03	-0.2270	1.0023	4.73275E-07		1.1234E-03	-0.2158	1.0022
13	4.76925E-07		1.1277E-03	-0.6015	1.0060	4.73591E-07		1.1238E-03	-0.2492	1.0025	4.73403E-07		1.1236E-03	-0.2293	1.0023

Table 4.16b: Influence of higher order global differentiability for b/a=16, h/a=35 and a=0.4: A 180 element mesh in region of near the crack tip (Figure 4.6) using LSP using weak form of GDEs: C^{11} solutions

	C^{11} p=3	% Reduction in dofs from C^{00} = 21.84				C^{11} p=5	% Reduction in dofs from C^{00} = 7.87				C^{11} p=7	% Reduction in dofs from C^{00} = 4.02			
Path	$J^f/2 : \Gamma_1$ path	A_J	K_I^f	% Error based on K_I	C^f	$J^f/2 : \Gamma_1$ path	A_J	K_I^f	% Error based on K_I	C^f	$J^f/2 : \Gamma_1$ path	A_J	K_I^f	% Error based on K_I	C^f
1	3.69225E-07	3.935E-08	9.9227E-04	11.4833	0.8852	4.63043E-07	-1.519E-07	1.1112E-03	0.8734	0.9913	4.68756E-07	-1.014E-07	1.1180E-03	0.2638	0.9974
2	3.89792E-07	-5.197E-09	1.0195E-03	9.0515	0.9095	4.66020E-07	-1.509E-07	1.1148E-03	0.5552	0.9944	4.70101E-07	-1.059E-07	1.1196E-03	0.1208	0.9988
3	4.12520E-07	-3.218E-08	1.0488E-03	6.4375	0.9356	4.68789E-07	-1.533E-07	1.1181E-03	0.2603	0.9974	4.71380E-07	-1.068E-07	1.1212E-03	-0.0150	1.0001
4	4.32534E-07	-5.337E-08	1.0740E-03	4.1947	0.9581	4.70651E-07	-1.554E-07	1.1203E-03	0.0624	0.9994	4.72219E-07	-1.076E-07	1.1222E-03	-0.1040	1.0010
5	4.46079E-07	-6.769E-08	1.0907E-03	2.7061	0.9729	4.71841E-07	-1.565E-07	1.1217E-03	-0.0638	1.0006	4.72720E-07	-1.080E-07	1.1228E-03	-0.1570	1.0016
6	4.54277E-07	-7.881E-08	1.1006E-03	1.8162	0.9818	4.72585E-07	-1.570E-07	1.1226E-03	-0.1427	1.0014	4.73010E-07	-1.083E-07	1.1231E-03	-0.1877	1.0019
7	4.61364E-07	-9.096E-08	1.1092E-03	1.0533	0.9895	4.72999E-07	-1.572E-07	1.1231E-03	-0.1866	1.0019	4.73173E-07	-1.084E-07	1.1233E-03	-0.2050	1.0021
8	4.66885E-07	-1.014E-07	1.1158E-03	0.4631	0.9954	4.73177E-07	-1.575E-07	1.1233E-03	-0.2055	1.0021	4.73263E-07	-1.085E-07	1.1234E-03	-0.2145	1.0021
9	4.69421E-07	-1.086E-07	1.1188E-03	0.1931	0.9981	4.73253E-07	-1.577E-07	1.1234E-03	-0.2135	1.0021	4.73311E-07	-1.085E-07	1.1235E-03	-0.2197	1.0022
10	4.70277E-07	-1.147E-07	1.1199E-03	0.1021	0.9990	4.73300E-07	-1.579E-07	1.1234E-03	-0.2184	1.0022	4.73338E-07	-1.086E-07	1.1235E-03	-0.2225	1.0022
11	4.70954E-07	-1.204E-07	1.1207E-03	0.0302	0.9997	4.73335E-07	-1.581E-07	1.1235E-03	-0.2221	1.0022	4.73352E-07	-1.086E-07	1.1235E-03	-0.2240	1.0022
12	4.69778E-07	-1.237E-07	1.1193E-03	0.1551	0.9984	4.73308E-07	-1.581E-07	1.1235E-03	-0.2192	1.0022	4.73358E-07	-1.086E-07	1.1235E-03	-0.2246	1.0022
13	4.72277E-07	-1.290E-07	1.1222E-03	-0.1101	1.0011	4.73463E-07	-1.579E-07	1.1236E-03	-0.2357	1.0024	4.73373E-07	-1.086E-07	1.1235E-03	-0.2262	1.0023

Table 4.16c: Influence of higher order global differentiability for b/a=16, h/a=35 and a=0.4: A 180 element mesh in region of near the crack tip (Figure 4.6) using LSP using weak form of GDEs: C^{22} solutions

	C^{22} p=5 % Reduction in dofs from C^{00} = 27.50 from C^{11} = 21.31					C^{22} p=7 % Reduction in dofs from C^{00} = 14.04 from C^{11} = 10.44				
Path	$J^f/2$: Γ_1 path	A_J	K_I^f	% Error based on K_I	C^f	$J^f/2$: Γ_1 path	A_J	K_I^f	% Error based on K_I	C^f
1	4.46307E-07	-3.221E-07	1.0909E-03	2.6813	0.9732	4.66883E-07	-3.324E-07	1.1158E-03	0.4633	0.9954
2	4.56142E-07	-3.143E-07	1.1029E-03	1.6149	0.9839	4.67000E-07	-3.154E-07	1.1159E-03	0.4508	0.9955
3	4.63285E-07	-3.234E-07	1.1115E-03	0.8476	0.9915	4.68930E-07	-3.196E-07	1.1182E-03	0.2453	0.9975
4	4.67297E-07	-3.271E-07	1.1163E-03	0.4191	0.9958	4.70784E-07	-3.211E-07	1.1205E-03	0.0483	0.9995
5	4.69731E-07	-3.296E-07	1.1192E-03	0.1602	0.9984	4.71878E-07	-3.221E-07	1.1218E-03	-0.0678	1.0007
6	4.71116E-07	-3.306E-07	1.1209E-03	0.0131	0.9999	4.72508E-07	-3.226E-07	1.1225E-03	-0.1345	1.0013
7	4.71963E-07	-3.312E-07	1.1219E-03	-0.0768	1.0008	4.72863E-07	-3.229E-07	1.1229E-03	-0.1722	1.0017
8	4.72448E-07	-3.316E-07	1.1224E-03	-0.1282	1.0013	4.73062E-07	-3.231E-07	1.1232E-03	-0.1932	1.0019
9	4.72716E-07	-3.319E-07	1.1228E-03	-0.1566	1.0016	4.73171E-07	-3.231E-07	1.1233E-03	-0.2047	1.0020
10	4.72869E-07	-3.322E-07	1.1229E-03	-0.1728	1.0017	4.73230E-07	-3.232E-07	1.1234E-03	-0.2110	1.0021
11	4.72971E-07	-3.325E-07	1.1231E-03	-0.1836	1.0018	4.73262E-07	-3.232E-07	1.1234E-03	-0.2144	1.0021
12	4.73043E-07	-3.323E-07	1.1231E-03	-0.1913	1.0019	4.73279E-07	-3.232E-07	1.1234E-03	-0.2163	1.0022
13	4.73082E-07	-3.322E-07	1.1232E-03	-0.1954	1.0020	4.73290E-07	-3.232E-07	1.1234E-03	-0.2174	1.0022

Table 4.16d: Influence of higher order global differentiability for b/a=16, h/a=35 and a=0.4: A 180 element mesh in region of near the crack tip (Figure 4.6) using LSP using weak form of GDEs: C^{33} solutions

	C^{33} p=7 % Reduction in dofs from C^{00} = 30.08 from C^{11} = 27.15 from C^{22} = 18.66				
Path	$J^f/2$: Γ_1 path	A_J	K_I^f	% Error based on K_I	C^f
1	4.49835E-07	-2.231E-07	1.0952E-03	2.2974	0.9770
2	4.58767E-07	-2.346E-07	1.1061E-03	1.3322	0.9867
3	4.64560E-07	-2.396E-07	1.1130E-03	0.7112	0.9929
4	4.68201E-07	-2.425E-07	1.1174E-03	0.3228	0.9968
5	4.70357E-07	-2.444E-07	1.1199E-03	0.0936	0.9991
6	4.71605E-07	-2.455E-07	1.1214E-03	-0.0389	1.0004
7	4.72310E-07	-2.462E-07	1.1223E-03	-0.1135	1.0011
8	4.72700E-07	-2.465E-07	1.1227E-03	-0.1549	1.0015
9	4.72915E-07	-2.467E-07	1.1230E-03	-0.1777	1.0018
10	4.73031E-07	-2.467E-07	1.1231E-03	-0.1900	1.0019
11	4.73095E-07	-2.468E-07	1.1232E-03	-0.1968	1.0020
12	4.73135E-07	-2.469E-07	1.1233E-03	-0.2010	1.0020
13	4.73204E-07	-2.476E-07	1.1233E-03	-0.2083	1.0021

Chapter 5

Summary and Conclusions

In this chapter we summarize the work presented in this thesis and draw some conclusions.

Summary

(1) The numerical computations of J-integral are presented for linear elastic fracture mechanics in *h,p,k* framework using finite element formulations based on Galerkin method with weak form and least squares method. The center crack panel in plane strain with uniaxial tension (mode I fracture) is used as a model problem.

(2) For linear elasticity, the differential operators in the mathematical models (strong form of GDEs) are self-adjoint and hence both the Galerkin method with weak form and the least squares method yield unconditionally stable computational processes.

(3) In the present work we do not employ quarter point or singular elements or any other special means at the crack tip. The studies presented here are straight forward computations with graded meshes. A significant strength of the work is that J-integral values for path radius as small as 0.000375 (dimensionless) from the crack tip are as accurate as those away from it (half crack lengths of 0.1, 0.4 and 1.2 were considered). For all paths chosen and listed in the tables there is very insignificant variation in the values of the J-integral from one path to the other.

(4) Stress intensity factors and correction factors obtained from the numerical studies presented here compare very well with those reported in the literature [46].

Conclusions

(1) The use of *h,p,k* framework in which *k* is the order of the approximation space permits global differentiability of order (*k*-1) (i.e. higher order global differentiability) in the design of the computations. The higher order global differentiability is necessitated due to physics, calculus of continuous and differentiable functions and the higher order global differentiability characteristics of the theoretical solutions. Minimally conforming spaces are discussed and it is demonstrated that minimum order of continuity must correspond to the highest orders of the derivatives of the dependent variables in the GDEs and the integral forms in order for the integrals to be Riemann.

(2) A derivation of the J-integral is presented (based on Rice) and it is shown that path independence of the J-integral in the computational processes requires that the GDEs be satisfied in the pointwise sense for each element in the area bounded by Γ, the J-integral path. If this condition is not met by the numerical solution, then path independence of J-integral cannot be ensured. With the local approximations of class C^{00} used currently, these computations are not possible. When local approximations are of class C^{11} or higher (as in the present work) A_J can be computed accurately. All our numerical studies show A_J to be $O(10^{-8})$ or lower confirming that GDEs are satisfied accurately by the computed numerical solution and hence, ensuring the path independence of the J-integral in the computations.

(3) It is shown that the J-integral path Γ must be continuous and differentiable,

otherwise $d\Gamma$ along the path is not defined at the points of discontinuity. Numerical studies are presented to illustrate the damage done to the J-integral computations if the path Γ is non-differentiable. Progressively increased lack of differentiability yields progressively deteriorated J-integral values.

(4) The continuity of the integrand in the J-integral along the path Γ as well as normal to the path Γ is essential for uniqueness of a path and for accurate values of J-integral. This can be ensured either by using local approximation of minimally conforming class or by ensuring weak convergence of the solutions of lower classes.

(5) Solution of the higher classes shows benefit. Similar accuracy as the converged solution of lower class is achieved with solution of higher classes but for much reduced dofs as demonstrated in the numerical studies using least squares formulation.

In conclusion, accurate computations of J-integral are straight forward in *h,p,k* framework using Galerkin method with weak form or least square processes provided: (i) The approximation spaces are minimally conforming. (ii) The J-integral path is continuous and differentiable. (iii) The integrand in the J-integral is continuous along the path Γ as well as normal to the path Γ, and (iv) GDEs are satisfied accurately in the pointwise sense for each element in the region bounded by the J-integral path Γ, otherwise path independence of the J-integral is lost. All these requirements are really dictated by the physics and calculus of continuous and differentiable functions. The methodology presented here requires no special treatments at the crack tip.

References

1. H. L. Ewarlds and R. J. H. Wanhill, "Fracture Mechanics", Edward Arnold Ltd., London, (1984).

2. J. M. Barsom and S. T. Rolfe, "Fracture and Fatigue Control in Structures", Third Edition, ASTM, Philadelphia, (1999).

3. M. H. Aliabadi and D. P. Rooke, "Numerical Fracture Mechanics", Computational Mechanics, Boston, (1990).

4. G. R. Irwin, "Analysis of Stress and Strains Near the End of a Crack Transversing a Plate", Journal of Applied Mechanics, Vol. 24, (1957).

5. A. R. Infraffea, P. A. Wawrzynek, "Finite Element Methods for Linear Elastic Fracture Mechanics", Elsevier Science Ltd., Oxford, England, (2003).

6. S. K. Chan, I. S. Tuba and W. K. Wilson, "On the Finite Element Method in Linear Fracture Mechanics", Engineering Fracture Mechanics, Vol. 2 Pergamon Press. Vol. 2, pp.1-17 (1970).

7. M. Berkovic, "Determination of Stress Intensity Factors using Finite Element Method", Structural Integrity and Life, Vol. 4, No 2, pp. 57-62 (2004).

8. D. M. Parks, "A stiffness Derivative Finite Element Technique for Determination of elastic crack tip stress intensity factors", International Journal of Fracture, Vol. 10, pp. 487-502 (1974).

9. T.K. Hellen, “On the Method of Virtual Crack Extensions”, International Journal for Numerical Methods in Engineering, Vol. 9, pp 187-207 (1975).

10. A. A. Wells, “Unstable Crack Propagation in metals, Cleavage and Fast Fracture”, Proceedings of the Crack Propagation Symposium, Vol. 1, pp. 210-230, Cranfield (1961).

11. P.C. Paris and G. C. Sih, “Stress Analysis of Cracks”, Fracture Toughness Testing and Its Applications, ASTM STP 381, pp. 30-83 (1965).

12. T. K. Hellen, “Numerical Methods in Fracture Mechanics”, Numerical Methods in Fracture Mechanics, Vol. 1, pp. 401-415, Swansea (1980).

13. J. C. Conway, “Finite Element Techniques Applied to Cracks Interacting with Selected Singularities”, Journal of the American Ceramic Society, Vol. 58, Issue 9-10, pp. 402-405 (1975).

14. A. Sedmak, “Finite Element Evaluation of Fracture Mechanics Parameters using Rapid Mesh Refinement”, Advances in Fracture Research (Fracture 84), Vol. 6, pp. 1095-1106 (1984).

15. T. K. Hellen, “Finite element techniques in fracture mechanics”, International Journal in Numerical Methods in Engineering, Vol. 9, pp.187-202 (1973).

16. F. Z. Li, C. F. Shih and A. Needleman, “A comparison of methods for calculating energy release rates”, Engineering Fracture Mechanics, Vol. 21, Issue 2, pp. 405-421 (1985).

17. L. Banks-Skills and D. Sherman, "On the computation of stress intensity factors for three-dimensional geometries by means of the stiffness derivative and J-integral methods", International Journal of Fracture, Vol. 53, Issue 1, pp. 1-20 (1992).

18. R. S. Barsoum, "On the use of Isoparametric Finite Elements in Linear Fracture Mechanics", International Journal for Numerical Methods in Engineering, Vol. 10, Issue 1, pp. 23-37 (1976).

19. R. S. Barsoum, "Triangular Quarter-point Elements as Elastic and Perfectly-Plastic Crack Tip Elements", International Journal for Numerical Methods in Engineering, Vol. 11, Issue 1, pp. 85-98 (1977).

20. D. M. Tracey. "Finite Elements for Determination of crack Tip Elastic Stress Intensity Factors", Engineering Fracture Mechanics, Vol. 3, Issue 3, pp. 255-265 (1971).

21. R. D. Henshell and K. G. Shaw, "Crack Tip Elements are Unnecessary", International Journal for Numerical Methods in Engineering, Vol. 9, pp. 405-507 (1975).

22. H. D. Hibbitt, "Some properties of Singular Isoparametric Elements", International Journal for Numerical Methods in Engineering, Vol. 11, Issue 1, pp. 180-184 (1977).

23. W. K. Wilson, "Some Crack Tip Finite Elements for Plane Elasticity", Stress Analysis and Growth of Cracks: Proceedings of the 1971 National Symposium on Fracture Mechanics: Part I, ASTM STP 513, pp. 90-105 (1972).

24. J. J. Oglesby and O. Lamackey, "An Evaluation of Finite Element Methods for the Computation of Elastic Stress Intensity Factors." NSRDC Rep Nº 3751 (1972).

25. S. E. Benzley, "Representation of Singularities with Isoparametric Finite Elements", International Journal of Numerical Methods in Engineering, Vol. 8, Issue 3, pp. 537-545 (1974).

26. P. Tong, T. H. H. Pian and S. J. Lasry, "A Hybrid-element Approach to Crack Problems in Plane Elasticity", International Journal of Numerical Methods in Engineering, Vol. 7, pp. 297-308 (1973).

27. L. A. Ying, "A Note on the singularity and the strain energy of singular elements", International Journal of Numerical Methods in Engineering, Vol. 18, pp. 31-39 (1982).

28. L. Banks-Sills and Y. Bortman, "Reappraisal of the quarter-point quadrilateral element in linear fracture mechanics", International Journal of Fracture, Vol. 25, Issue 3, pp. 169-180 (1984).

29. L. Banks-Skills and O. Einav, "On singular, nine-noded, distorted, isoparametric elements in linear elastic fracture mechanics", Computers & Structures, Vol. 27. pp. 445-449 (1987).

30. R. B. Haber and M. K. Koh, "Explicit expressions for energy-release rates using virtual crack extensions", International Journal of Numerical Methods in Engineering, Vol. 21, pp. 301-278, (1985).

31. J. R. Rice, "A Path Independent Integral and the Approximate Analysis of Strain Concentration by Notches and Cracks", Journal of Applied Mechanics, Vol. 35, pp. 379-386, (1968).

32. M. L. Williams, "Stress Singularities Resulting from Various Boundary Conditions in Angular Corners of Plates in Extension", Journal of Applied Mechanics, Vol. 19, pp. 526-528, (1952).

33. A. Rajwani, "*k*-Version of the Finite Element Method and Singular Boundary Value Problems: Linear Elastic Fracture Mechanics", M.S. Thesis, The University of Kansas, Lawrence, Kansas, (2003).

34. L. V. Prasad Pondugala, "Stochastic J-integral and Reliability of Composite Laminates on a Computational Methodology combining Experimental Investigation, Stochastic Finite Element Analysis and Maximum Entropy Method" M.S. Thesis, Concordia University, Montreal, Quebec, Canada, (2000).

35. M. Isida, "Effect of Width and Length on Stress Intensity Factors of Internally Cracked Plates under Various Boundary Conditions", International Journal of Fracture, Vol. 7, pp. 301-316, (1971).

36. L. Banks-Sills and D. Sherman, "Comparison of Methods for Calculating Stress Intensity Factors with Quarter-Point Elements" International Journal of Fracture, Vol. 32, pp. 127-140, (1986).

37. D. R. J. Owen, and A. J. Fawkes, "Engineering Fracture Mechanics: Numerical Methods and Applications", Pineridge Press Ltd, Swansea, UK (1983).

38. J. R. Rice, "Mathematical Analysis in the Mechanics of Fracture", Chapter 3 of Fracture: An Advanced Treatise (Vol. 2, Mathematical Fundamentals) (e.d. H. Liebowitz), Academic Press, N.Y., pp. 191-311, (1968).

39. R.H. Gallagher, "Survey and Evaluation of the Finite Element Method in Fracture Mechanics Analysis", 1st International Conference on Structural Mechanics in Reactor Technology, Vol. 6 pt. L, pp. 637-653, Berlin (1971).

40. B.A. Szabo and A. K. Mehta, "*p*-Convergent Finite Element Approximations in Fracture Mechanics.", International Journal of Numerical Methods in Engineering, Vol. 12, pp. 551-560 (1978).

41. M. F. Kanninen and C. H. Popelar, "Advanced Fracture Mechanics", Oxford University Press, Oxford, (1985).

42. T. L. Anderson,. "Fracture Mechanics", Second edition, CRC Press, Boca Raton, (1995).

43. Z.-H. Jin and C. T. Sun, "On J-integral and Potential Energy Variation", International Journal of Fracture, Vol. 126, pp. L19-L24, (2004).

44. H. Tada, P. C. Paris and G. R. Irwin, "The Stress Analysis of Cracks Handbook", Third edition, ASME Press, New York, (2000).

45. W. F. Brown Jr. and J. E. Srawley, "Plane Strain Crack Toughness Testing of High Strength Metallic Materials", ASTM STP Nº 410, Philadelphia, Pa. (1966).

46. M. Isida, "Stress Intensity Factors for the Tension of an Eccentrically Cracked Strip", Journal of Applied Mechanics, Vol. 33, pp. 674-675 (1965).

47. M. Isida, "Effect of Width and Length on Stress Intensity Factors of Internally Cracked Plates Under Various Boundary Conditions", International Journal of Fracture Mechanics, Vol. 7, pp. 301-316, (1971).

48. K.S. Surana, A. R. Ahmadi and J. N. Reddy, "The *k*-Version of Finite Element Method for Self-adjoint Operators in BVP", Int. J. Comp. Eng. Sci, Vol. 3, Nº 2, pp 155-218 (2002).

49. K. S. Surana, A. R. Ahmadi and J. N. Reddy, "The *k*-Version of Finite Element Method for Non-self-adjoint Operators in BVP", Int. J. Comp. Eng. Sci, Vol. 4, Nº 4, pp 737-812 (2003).

50. K. S. Surana, A. R. Ahmadi and J. N. Reddy, "The *k*-Version of Finite Element Method for Non-linear Operators in BVP", Int. J. Comp. Eng. Sci, Vol. 5, Nº 1, pp 133-207 (2004).

51. M. Gelfand, S. V. Formin, "Calculus of Variations", Dover Publications, New York (2000).

52. G. Mikhlin, "Variational Methods in Mathematical Physics", Pergamon press, New York (1964).

53. J. N. Reddy, "Applied Functional Analysis and Variational Methods in Engineering", McGraw Hill Company (1986).

54. K. S. Surana, L. R. Anthoni, S. Allu, J. N. Reddy and P. W. Tenpas, "Strong and Weak Form of the Governing Differential Equations in Least Squares Finite Element Processes in *h,p,k* Framework, CMESM, in print (2007).